

POLITECNICO DI TORINO

Master degree course in Biomedical Engineering

Master Degree Thesis

Reproducible segmentation of white matter tractograms using artificial intelligence and spatial fuzzy sets



Supervisors:

Prof. Gabriella Balestra

Prof. Isabelle Bloch

Prof. Pietro Gori

Candidate:

Alessandro Di Girolamo

Academic year 2018/2019

Summary

Tractography is the only in-vivo technique that allows the extraction of white matter fibers from the brain in a non-invasive way. It is used as a support in neurosurgeries and as research tool to study structural connectivity in both healthy and pathological subjects. It generates, from diffusion MRI volumes, millions of 3D polylines that are estimates of the path followed by real axons. One important clinical application is the automatic segmentation of precise and anatomically well-defined white matter tracts from whole-brain tractograms, but this task is particularly difficult to accomplish since the large number of streamlines makes the computational costs very high and the anatomical tracts definitions found in literature are usually vague or imprecise. The purpose of this master thesis is to model, in a reproducible way, the tracts anatomical definitions using fuzzy logic and to extract them from whole-brain tractograms of multiple subjects with the help of clustering techniques. The whole process have been implemented on a desktop computer with normal characteristics paying particular attention on memory and time issues, so that it can be ideally used by an external operator without the need of a high performance machine and in a reasonable time.

This thesis, firstly introduces the dataset used to generate the tractograms and the importance of tractography as a novel support in nowadays research and clinical applications. It then explains the state of the art segmentation techniques that can be used to extract individual fiber bundles. It briefly describes the tool used to model the anatomical definitions and proceeds with the explanation of the algorithm created for tracts segmentation, whose aim is to lead the fuzzy set approach from a proof of concept state to a validated technique. Finally, the results are presented together with the ones obtained using the state-of-the-art techniques to assess the validity of the outputs and to show the improvements achieved.

Acknowledgements

I would like to first thank my thesis advisors. Prof. Gabriella Balestra, at Politecnico di Torino, for her great willingness and for the passion she passed to me during her courses. Prof. Isabelle Bloch, at Télécom ParisTech, for her professionalism, for her trust and for the opportunity she gave to me to do this extremely enriching experience. Prof. Pietro Gori, for his mentoring and his support during all the duration of the master thesis. His guidance has been fundamental for the development of the project.

I would also like to thank my mum and my dad for all their support and the efforts they did during these years. Their precious moral convictions and their values were deeply important to me, at work as well as in life. Un immenso grazie anche ai nonni, per i loro sacrifici e la loro resistenza. Il loro affetto e i sogni riposti in me sono stati la motivazione più forte di tutte.

An inevitable thank goes to Silvia, who showed me the way and who always believed in me. She gave me the strenght to achieve any goal. The adventure that we built across Turin, Milan, Lisbon, Besançon and Paris has been one of the best thing of my life. Thank you.

Finally, I would like to thank all my friends, in Italy and abroad. Another master thesis would be necessary to tell their deeds, so please be satisfied with these few lines. Your help stopped me from becoming crazy, maybe.

Alessandro Di Girolamo

Contents

I	Introduction	1
1	Background	2
1.1	Diffusion	3
1.2	Diffusion-weighted imaging (DWI)	4
1.2.1	Acquisition sequence and DWI image generation	5
1.3	Diffusion Tensor Imaging (DTI)	8
1.3.1	Fractional Anisotropy (FA)	8
1.4	Tractography	10
1.4.1	Crossing fibers issue	11
1.4.2	Constrained Spherical Deconvolution (CSD)	11
2	Dataset and applications	14
2.1	Specifications of the dataset	14
2.2	Tractography applications	15
II	State Of The Art	18
3	Segmentation Methods	19
3.1	Manual Segmentation: virtual dissection	19
3.2	Supervised Learning methods	20
3.2.1	Clustering	20
3.2.2	TractSeg	23
3.3	Parcellation Methods	25
3.3.1	White Matter Query Language (WMQL)	25
3.4	Hybrid Approaches	27
3.5	Discussion	28
III	FuzzyTracts	29
4	FuzzyTracts: a tool for fuzzy spaces creation	30
4.1	Fuzzy sets theory	30
4.2	FuzzyTract	32
4.2.1	Writing a definition	34
4.3	Discussion	35

IV	Contribution	36
5	Tracts segmentation	37
5.1	Use of TractSeg bundles as reference tracts	38
5.1.1	Data extraction	38
5.2	Angle tuning	41
5.3	Segmentation Pipeline	42
5.4	Step 1: Best fuzzy space selection	42
5.4.1	Error map	43
5.4.2	Delta Metric	45
5.5	Steps 2 and 3: tracts extraction	47
5.5.1	Dice score correction: the convex hull approach	48
5.6	Between bundles	51
5.7	Post-processing	53
5.7.1	Principal direction and tortuosity	53
6	Tracts modelling	55
6.1	Arcuate Fasciculus (AF)	55
6.2	Anterior Thalamic Radiation (ATR)	56
6.3	Cyngulate Fasciculus (CG)	56
6.4	Corticospinal Tract (CST)	57
6.5	Fronto-pontine Tract (FPT)	57
6.6	Inferior Cerebellar Peduncle Fasciculus (ICP)	58
6.7	Inferior Longitudinal Fasciculus (ILF)	58
6.8	Superior Longitudinal Fasciculus (SLF)	58
6.8.1	Superior Longitudinal Fasciculus I (SLF I)	58
6.8.2	Superior Longitudinal Fasciculus II (SLF II)	59
6.8.3	Superior Longitudinal Fasciculus III (SLF III)	59
6.9	Summary tables	59
7	FiberExtractor	64
7.1	Tracts extraction: fuzzy score simplification	64
7.2	Tracts merging and VTK to OBJ conversion	66
7.3	Implementation of a 3DSlicer extension	67
V	Results and discussion	69
8	Results	70
8.1	Important relations	70
8.2	Training and test	74
8.3	Fuzzy vs WMQL	75
8.4	Future developments	77
8.5	Conclusions	78

List of Figures

1.1	White matter fiber architecture from the Human Connectome Project archives	2
1.2	Diffusion motions: (a) Isotropic (circular) diffusion, (b) Anisotropic (elliptical) diffusion	3
1.3	Isotropic and anisotropic diffusion in brain. In grey matter (GM) the diffusion is lower than in CSF because they are present random barriers that lower the diffusion coefficient	4
1.4	A DWI sequence that shows stroke in brain tissue (Image taken from ucl.ac.uk).	5
1.5	PGSE sequence with gradient pulse parameters (Image taken from mriquestions.com).	5
1.6	Effect of DGs on spin. Note that since the gradient is applied in horizontal direction, the method is sensitive only to diffusion of water molecules in horizontal direction, while it is not sensitive to water molecules diffusion in vertical direction (Image taken from [6]).	6
1.7	DWI images obtained with different b-values (Image taken from Radiopaedia.org).	6
1.8	Creation of a trace DW image as combination of images obtained applying the gradient pulses ($b = 1000s/mm^2$) in each of the three directions (Image taken from [8]).	7
1.9	Diffusion ellipsoid representation (right) of axon fibers (left) (Image taken from [11]).	9
1.10	(A) FA map, (B) Color-encoded principal diffusion direction: red:left-right, green: anteroposterior, blue: superior-inferior (Image taken from [11]).	9
1.11	Fiber tracking using FACT algorithm. Fibers path is terminated when in ends in a low anisotropy region like gray matter (Image taken from [13]).	10
1.12	Diffusion tensor as seen for no fiber crossing (left), fiber crossing in two different orientations (center) and in three different orientations (right)	11
1.13	We consider here a single voxel containing two different fiber populations with two different orientations (θ, ϕ) and volume fractions. The dotted lines are the fibers orientation while the continuous lines are the signal attenuations. Their sum can be expressed as the convolution between the response function, thus the signal attenuation measured for one single fiber population, and the FOD (Image taken from [16]).	12

1.14	Left: FA map of a slice. Middle: coronal slice with colored code according to the major eigenvector of the diffusion tensor. Right: FOD of the voxel indicated by the arrow (negative lobes have been excluded) (Image taken from [16]).	13
2.1	Difference between an image with 2 mm isotropic voxels, 60 directions and the HCP 1.25 mm isotropic voxels image. The two images have been acquired from different subjects (Image taken from [20]).	15
2.2	Preoperative planning of a tumor removal using tractography: (A) axial MRI view, (B) sagittal MRI view, (C) tumor sitting on the CST, (D) tumor (red arrow) sitting on the CST (yellow arrow) (Image taken from [30]).	17
3.1	Relations between multiple ROIs. (a) All streamlines crossing the first ROI are selected, (b) Only the stramlines that cross both ROIs are selected, (c) The NOT relation is used to exclude some streamlines from the previous case, (d) Using CUT, only the segmentes of the streamlines between the two ROIs are selected (Image taken from [31]).	20
3.2	The similarity values obtained from top eigenvectors are represented as point and used to create the clusters. Each cluster contains the streamlines of a particular bundle (Image taken from [37]).	21
3.3	A visual example of hierarchical clustering	22
3.4	Architecture of TractSeg neural network inspired by the U-Net (Image taken from [43]).	23
3.5	Steps for binary mask generation of a CST tract (Image taken from [43]).	24
3.6	Example of brain gyri parcellation atlas obtained with FreeSurfer. At each segmentation it is associated a label and an identification number (Image taken from <i>freesurger.net</i>).	25
3.7	Examples of use of anatomical terms, relative position terms and logical operation in WMQL. (i) is the final query that defines the Uncinate Fasciculus (Image taken from [34]).	27
4.1	Crisp logic does not provide adequate information on objects A and B positions. Objects A and B are to the right of reference R but they are also to some extent above it.	31
4.2	A single slice of a fuzzy space evaluated from the definition "anterior of amygdala": (a) Fuzzy space evaluated giving a value to the aperture patameter, (b) Fuzzy space evaluated with a small aperture patameter.	32
4.3	Definition of the angle β_{min}	33

4.4	Anatomical definition of a tract written in query language. The tract (black) called “Bundle” is defined with respect to some reference structures (green). In particular, this imaginary tract is located to the left of the Amygdala and under the Thalamus, where the words “left” and “inferior” (red) correspond to some spatial relations. The two spatial relations are then linked together by the logical connective “and” (blue), that will output the intersection between the two fuzzy regions representing the relations, thus resulting in a fuzzy space where the voxels with higher membership degree will be the ones in left-under oblique direction. Note that it is also possible to specify the degree of aperture of a cone (orange), arbitrarily excluding some regions not useful to the definition.	34
4.5	Fuzzy space obtained with an AND relation (a) and an OR relation (b). The used AND relation is <i>left(LeftAmygdala) and inferior(LeftAmygdala)</i> , the used OR relation is <i>left(LeftAmygdala) or inferior(LeftAmygdala)</i> . 35	35
5.1	Decussation of corticospinal tract (CST) at the medulla level. The oblique crossin of this tract does not affect data extraction since whole-tractogram streamlines stops at the level of peduncles	40
5.2	Reference tract and fuzzy space overlap. (a) TractSeg reference cingulate bundle, (b) Section of the fuzzy space obtained from literature definition. The voxels with highest membership degrees are brighter than the others. Imposing a threshold, we want to extract only the streamlines that are in these whiter voxels (and thus that correspond to the definition), (c) Overlap between (a) and (b). The brighter voxels are the ones crossed by the reference bundle.	43
5.3	Visual representation of the error map. The left matrix represents the voxelization of a bundle, with value 1 in voxels crossed by the streamlines (blue) and 0 anywhere else. The matrix in the middle is the representation of a fuzzy space whose fuzzy values have been normalized between 0 and 1. Their difference in absolute value gives the error map: a matrix that has, in voxels crossed by streamlines, low values for good fuzzy spaces and increasing values for worst fuzzy sets.	44
5.4	The CST, shown on the left, has been clusterized using quickbundle whose result is a certain number of centroids, shown in the middle. Each cluster is represented with a different color in the right picture	46
5.5	Convex hull in 2D (a) and 3D (b)	49
5.6	3D convex hull time complexity (a) compared to dice score improvements (b). Data refers to the SLF II bundle composed by 10980 streamlines but the same result has been obtained with other tracts. We can see that, if we use more the 15 points per streamline, the computation time increases while there are no improvings on the dice score.	50
5.7	Limitation of the convex hull approach. Down in the image it is shown the ideal result, up in the picture there is the real one	50
5.8	SLF I (blue), SLF II (red) and SLF III (green) from TractSeg	51
5.9	(a) step 2, (b) step 3, (c) step 4	52

5.10	Complexity of between bundles relation using all streamlines (a) and only centroids (b)	52
5.11	ILF uncleaned (a) and cleaned (b) streamlines using principal direction	54
6.1	All the 10 segmented tracts	63
7.1	Extraction of the left hemisphere Arcuate Fasciculus. From the tractogram (a), we compute its centroids (b), we preserve the corresponding streamlines that respect the current threshold (c) and we extract the fiber tract (d).	65
7.2	Side views of the 10 left hemisphere segmented tracts	66
7.3	3D rendering of the 10 tracts	67
7.4	Screenshot of the functional part of the implemented 3DSlicer plug-in.	68
8.1	Limitation of the convex hull approach in dice calculation: the technique gives the same dice score for both sets of streamlines. The problem has been solved creating fuzzy spaces with U shapes for concave fibers. In this way we are sure that, even if the masks are accidentally filled, they only contains the streamlines shown in (a) and not the ones shown in (b).	71
8.2	Left SLF I in TractSeg reference bundle (a), extracted with our method (b) and using WMQL (c).	77

List of Tables

6.1	Tracts definitions (Part I)	60
6.2	Tracts definitions (Part II)	61
6.3	Tracts definitions (Part III)	62
8.1	Table showing the resulting dice score when we remove a certain relation from the original anatomical definition of a tract (Part I) . . .	71
8.2	Table showing the resulting dice score when we remove a certain relation from the original anatomical definition of a tract (Part II) . . .	72
8.3	Table showing the resulting dice score when we remove a certain relation from the original anatomical definition of a tract (Part III) . .	73
8.4	Mean and standard deviation for threshold and dice score of the training and test set	75
8.5	Disce scores obtained using our method and WMQL	76

Part I

Introduction

Chapter 1

Background

The human brain consists of approximately 86 billion neurons connected one another by a dense and incredible network of axons and dendrites. These transmission lines are believed to extend for about 850.000 km in each of us, more than twice the distance between the Earth and the Moon! They are responsible of something like 100 trillion connections between neurons and they allow the storage of nearly 1100 terabytes of information (a normal desktop computer stores just 1 terabyte of data). All of this is contained in barely more than 1500 grams of matter, that is the 2% of our body's weight.

Until recently, the study of axonal anatomy was limited to invasive techniques, but the advent of diffusion magnetic resonance imaging (dMRI) made it possible to analyze neural anatomical connections with in-vivo non-invasive technologies. The idea was to detect the movement of water inside axons to rebuild their pathway, a technique known as tractography. Nowadays scanners are not yet powerful to detect individual axons but they are useful to provide an *estimation* of the trajectories of the big tracts. This allows a better comprehension of structural and functional connections inside the brain and opens to the study of already known pathologies from a different point of view, as well as a development in preoperative planning for neurosurgeries.

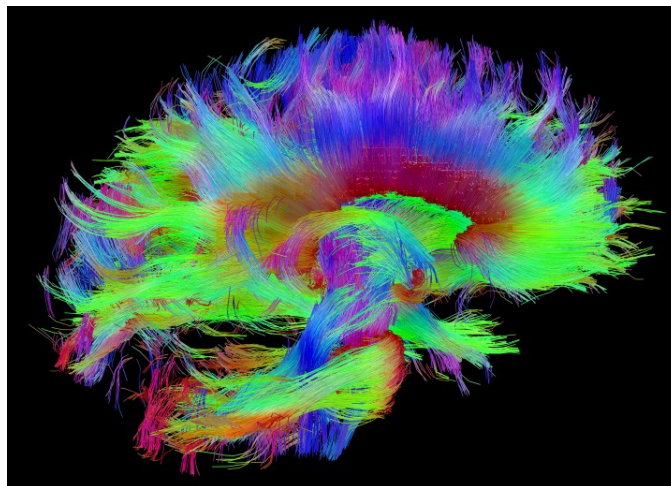


Figure 1.1: White matter fiber architecture from the Human Connectome Project archives

1.1 Diffusion

Water molecules in human body undergo random microscopic movements due to thermal energy. This motion is known as Brownian motion, or simply, Diffusion. Einstein published a paper in 1905 [1] in which he showed that the displacement, or more accurately expressed, the root-mean-square displacement of a molecule in *one direction*, is given by (1.1).

$$d_{rms} = \sqrt{2Dt} \quad (1.1)$$

D is called diffusion coefficient. It measures the flux of particles through a surface during a certain period of time and has units of mm^2/s . As it is shown in (1.2), D is directly proportional to the absolute temperature T and to the Boltzmann coefficient k but inversely proportional to the particles radii r and the medium viscosity η .

$$D = \frac{kT}{6\pi r\eta} \quad (1.2)$$

The diffusion coefficient for pure water in brain tissue at body temperature is about $1 \times 10^{-3} mm^2/s$ [2]. This means that a water particle, to diffuse a distance $x_{rms} = 1\mu m$, takes approximately $1ms$ and to diffuse a distance $x_{rms} = 10\mu m$ takes about $100ms$.

In general, they exist two types of diffusion (Figure 1.2): isotropic diffusion and anisotropic diffusion. The isotropic diffusion (circular diffusion) is the motion of molecules in an unrestricted space, where each direction has an equal probability to be run and the diffusion is the same in all directions. It is characterized by a single scalar diffusion coefficient D . Anisotropic diffusion (elliptic diffusion) is the motion of molecules in a constrained space, characterized by a preferred diffusion direction. It cannot be described by a single number since the diffusion rate is different for each direction. It is necessary a 3×3 matrix called diffusion tensor whose elements describe the diffusion rates along different directions (See Section ??)

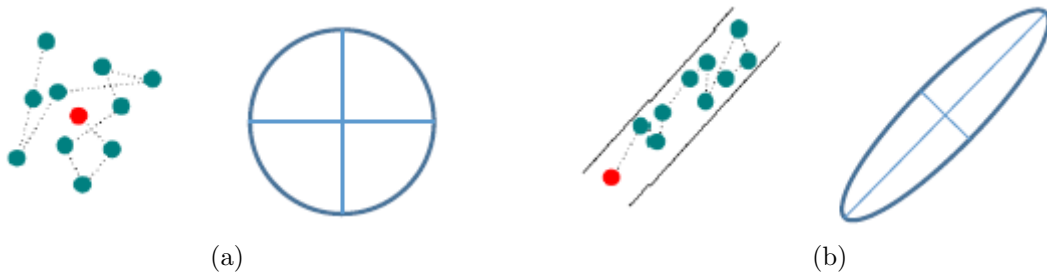


Figure 1.2: Diffusion motions: (a) Isotropic (circular) diffusion, (b) Anisotropic (elliptical) diffusion

In human brain, diffusion of water molecules in grey matter and cerebrospinal fluid (CSF) is roughly isotropic, while in white matter it is highly anisotropic since axons have a parallel orientation (Figure 1.3).

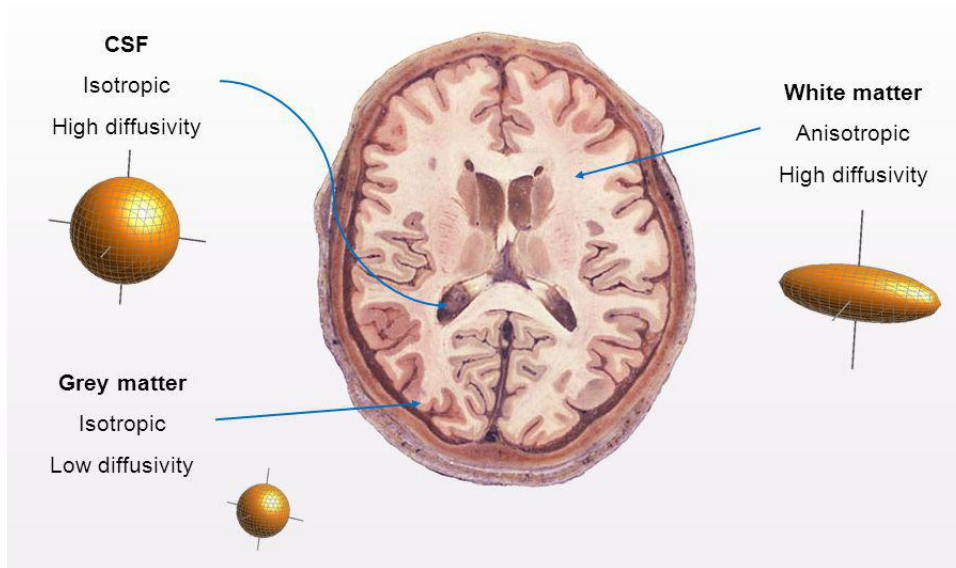


Figure 1.3: Isotropic and anisotropic diffusion in brain. In grey matter (GM) the diffusion is lower than in CSF because they are present random barriers that lower the diffusion coefficient

1.2 Diffusion-weighted imaging (DWI)

Diffusion-weighted imaging (DWI) is a magnetic resonance (MR) technique that exploits diffusion of water molecules in brain for the creation of an image. It was first invented in 1965 but its use in clinical MR scanners is dated second half of 1980. The image contrast generated in a DWI image is based on differences in the magnitude of diffusion of water particles according to the crossed region and allows the detection of different kinds of brain matter (i.e. white and gray matter, as well as the cerebro-spinal fluid (CSF)).

In DWI, the type of diffusion being investigated is water self-diffusion, namely the thermal motion of water molecules in a medium that itself consists mostly of water [3]. Its peculiarity and, as we will see its weak point, is that it accounts only for isotropic diffusion, not considering the anisotropic one. It is based on just one diffusion coefficient.

The reason that in past led to the development of DWI is that many pathologies in brain are related to altered diffusion of water in tissues. This alteration from the normal condition is detected just looking at the DWI images: differences from normal diffusion values are visualized as darker or brighter regions. In particular, in restricted diffusion (brighter image) water molecules travel a shorter distance than expected due to the reduced extracellular space, while in facilitated diffusion (darker image), water diffuses greater distances than in the healthy tissue because the extracellular space is widened. Restricted diffusion is for example a sign of stroke (Figure 1.4) while facilitated diffusion can be caused by a vasogenic edema.

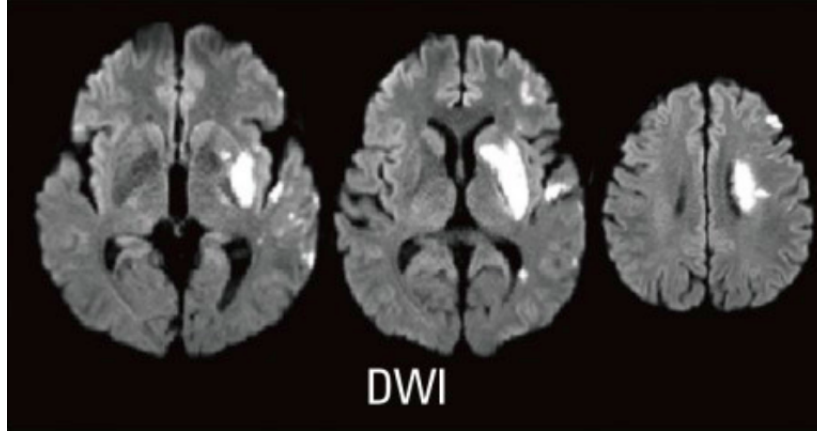


Figure 1.4: A DWI sequence that shows stroke in brain tissue (Image taken from ucl.ac.uk).

1.2.1 Acquisition sequence and DWI image generation

In DWI, a particular sequence (Figure 1.5) called pulsed gradient spin echo (PGSE) created by Stejskal and Tanner in 1965 [4] is used to detect water motion. It consists in applying two “diffusion gradients” (DG) before and after the 180° spin-echo (SE) radio-frequency (RF) pulse.

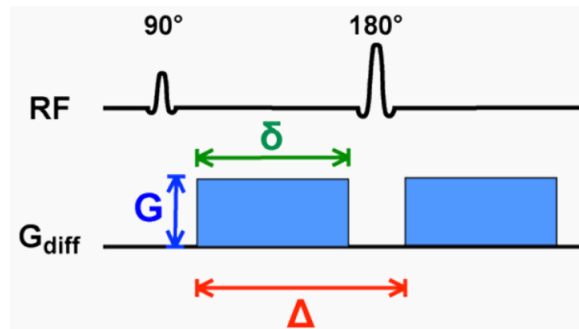


Figure 1.5: PGSE sequence with gradient pulse parameters (Image taken from mriquestions.com).

In particular, the pair of DGs is used respectively to dephase and rephase (Figure 1.6) water molecules spins and to induce a signal loss in case of water motion [5]. The first gradient dephases the spins of water molecules of a quantity which depends on their position along the gradient axis. If water molecules have not moved, the application of the second gradient (which has opposite polarity to the first one) is able to completely refocus their phases bringing them back to the starting condition. However, if molecules have moved, their change in position makes them experience a gradient intensity which is different from the intensity they had experienced during the first gradient. In this case spins are not rephased, leading to signal attenuation.

The measured signal is given by (1.3).

$$S = S_0 e^{-bD} \quad (1.3)$$

b is called b-value and is responsible for the diffusion weighting. It has units of s/mm^2 , the opposite of D . The b-value depends on the strength G , duration δ and

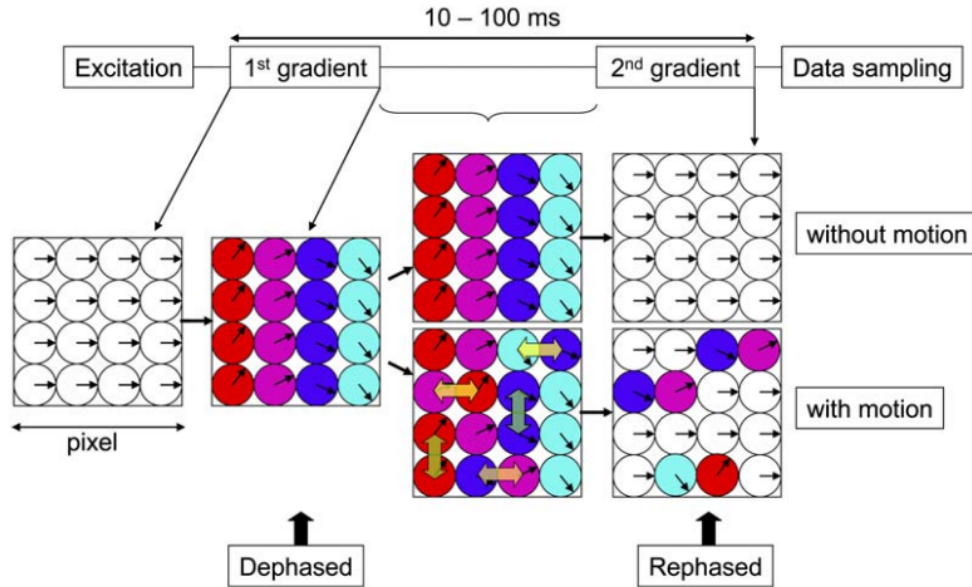


Figure 1.6: Effect of DGs on spin. Note that since the gradient is applied in horizontal direction, the method is sensitive only to diffusion of water molecules in horizontal direction, while it is not sensitive to water molecules diffusion in vertical direction (Image taken from [6]).

time interval Δ between the onsets of the gradient pulse (Figure 1.5), therefore it can be modified by the operator directly acting on the gradient. Increasing the b-value accentuates the weighting towards diffusion¹, making water flow more visible in the image, but at the same time it increases the noise level (Figure 1.7). Typical b-values available on nowadays MRI scanners range from 0 to approximately $4000s/mm^2$ but clinically we usually do not overcome $1000s/mm^2$.

S_0 is the signal obtained without using the diffusion gradients (thus obtained with $b = 0$). It give us an image called "b₀ image".

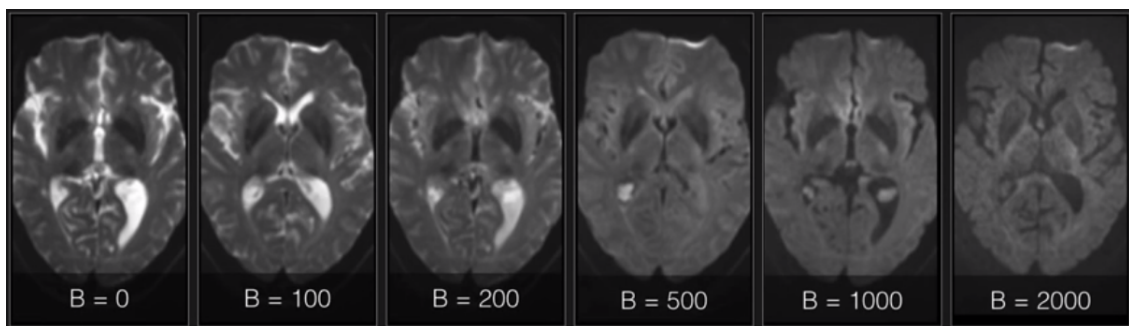


Figure 1.7: DWI images obtained with different b-values (Image taken from Radiopaedia.org).

In reality, water molecules move in brain not just in an isotropic manner but,

¹It should be noted that, in Figure 1.7, CSF brightness decays when we move to higher b-values while white matter (WM) stays more or less the same across different b-values. This happens because in CSF water molecules are freer to move while in WM they are constrained by axons. Increasing the b-values means also to increase the time of observation and in that time water molecules leave more easily CSF voxels while they remain trapped in WM voxels by axons.

in white matter tracts, they are constrained by the fibers walls and are obliged to follow their paths, causing an anisotropic diffusion. However, according to (1.2.1), a single DWI image is obtained measuring the signal loss that results from the application of a diffusion gradient in just one direction. This means that, if the direction of the diffusion gradient matches the principal direction of a white matter tract, the signal is suppressed, since no water particle translation can be detected (for example in Figure 1.6 the vertical water particles translation cannot be detected since the gradient is applied only in horizontal direction). This loss of information can be compensated applying diffusion gradients along three orthogonal directions and combining the information provided by each of the measured signal losses [7]. This way of combining isotropic DWI images is a partial solution to account also for anisotropic diffusion. Signals obtained from diffusion gradients applied in x, y and z direction are listed in (1.4).

$$S_x = S_0 e^{-bADC_x} \quad S_y = S_0 e^{-bADC_y} \quad S_z = S_0 e^{-bADC_z} \quad (1.4)$$

The three signals are then used to create (1.5) a single DWI image (Figure 1.10). Since the resulting diffusion coefficient is given by the average of the diffusion coefficients in each direction, it takes the name of Apparend Diffusion Coefficient (ADC).

$$S = \sqrt[3]{S_x S_y S_z} = S_0 e^{-b(D_{xx} + D_{yy} + D_{zz})/3} = S_0 e^{-bD_{trace}/3} = S_0 e^{-b*ADC} \quad (1.5)$$

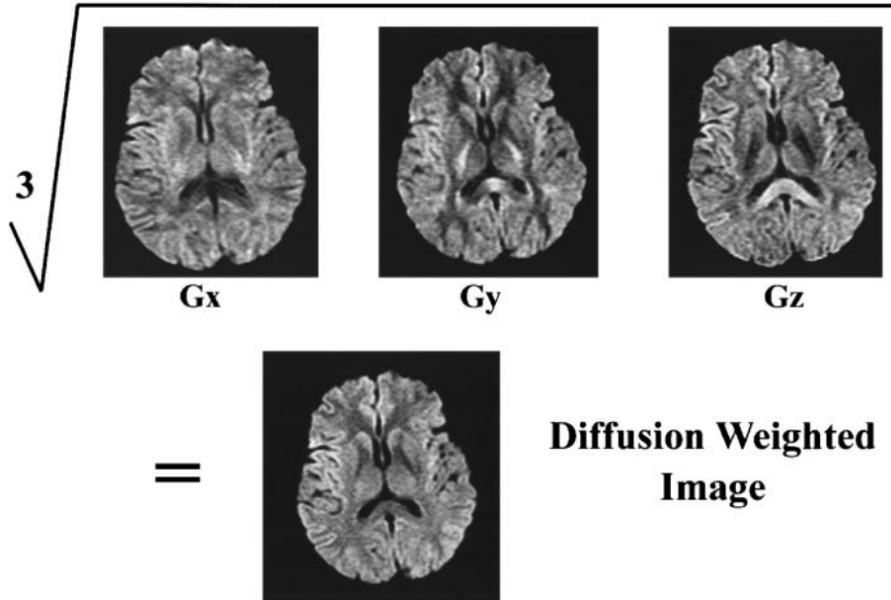


Figure 1.8: Creation of a trace DW image as combination of images obtained applying the gradient pulses ($b = 1000s/mm^2$) in each of the three directions (Image taken from [8]).

1.3 Diffusion Tensor Imaging (DTI)

As we have seen, DWI is an imaging technique that relies on multiple application of diffusion gradients to account for both isotropic and anisotropic diffusion. The resulting diffusion coefficient is a scalar value obtained as the average of the diffusion coefficients for each applied gradient but it is not sufficient to describe the real anisotropic movements. To do that, a new technique called Diffusion Tensor Imaging (DTI) was proposed in 1994.

The idea is that we can exploit anisotropy in axonal organization to visualize white matter tracts anatomy. Indeed water movement is aligned with axons rather than across them since the parallel diffusion is facilitated, a phenomenon that can be represented as a diffusion ellipsoid. Moreover, since diffusion can be measured in different directions, measuring enough directions allows to calculate for each voxel which is the dominant direction and generate maps of white matter tracts.

The diffusion coefficient in anisotropic materials is no more a single scalar value as it was for DWI, but a 3×3 diffusion tensor (1.6) that describes diffusion of water molecules in multiple directions.

$$\mathbf{D} = \begin{bmatrix} D_{xx} & D_{xy} & D_{xz} \\ D_{yx} & D_{yy} & D_{yz} \\ D_{zx} & D_{zy} & D_{zz} \end{bmatrix} \quad (1.6)$$

It is a symmetric matrix ($D_{xy} = D_{yx}$, $D_{xz} = D_{zx}$, $D_{yz} = D_{zy}$) in which the diagonal elements (D_{xx} , D_{yy} , D_{zz}) are the diffusion coefficients along the x, y and z direction respectively, while the remaining terms represent the correlation between these three directions. It comes that the tensor \mathbf{D} is calculated for each pixel from the measurement along six independent coordinate directions plus a seventh measurement obtained without applying the diffusion gradients [9]. This means that a DTI image is obtained from six gradient application in different direction (plus one b_0 image).

1.3.1 Fractional Anisotropy (FA)

From a geometrical point of view, the diffusion tensor is a 3D ellipsoid whose shape tell us which is the dominant direction of water molecules diffusion (Figure 1.9). The shape of the diffusion ellipsoid is obtained looking at the eigenvectors and eigenvalues of the the diffusion tensor. They can be computed diagonalizing [10] the diffusion tensor. The orientation of its three principal axes is defined by three eigenvectors (ϵ_1 , ϵ_2 , ϵ_3) while their length depends on the corresponding eigenvalues (λ_1 , λ_2 , λ_3) that tell which is the magnitude of diffusivity in that directions.

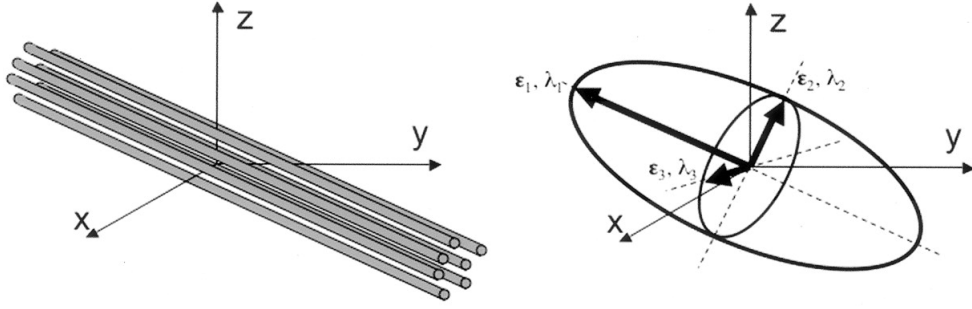


Figure 1.9: Diffusion ellipsoid representation (right) of axon fibers (left) (Image taken from [11]).

Eigenvalues permit to calculate a scalar value (1.7) that tells us which is the predominant diffusion direction inside each voxel. It is called Fractional Anisotropy (FA) and ranges between 0 and 1, where 0 identifies a perfect sphere while 1 identifies an ellipsoid of elongated shape.

$$FA = \sqrt{\frac{3}{2}} \sqrt{\frac{(\lambda_1 - \bar{\lambda})^2 + (\lambda_2 - \bar{\lambda})^2 + (\lambda_3 - \bar{\lambda})^2}{\lambda_1^2 + \lambda_2^2 + \lambda_3^2}} \quad (1.7)$$

$\bar{\lambda}$ is the mean of the three eigenvalues. The direction of predominant diffusivity inside a voxel is generally represented using RGB convention, with color brightness modulated by FA [11]. Combining the directional map given by DTI and the FA values we obtain the white tracts anatomy and their orientation (Figure 1.7).

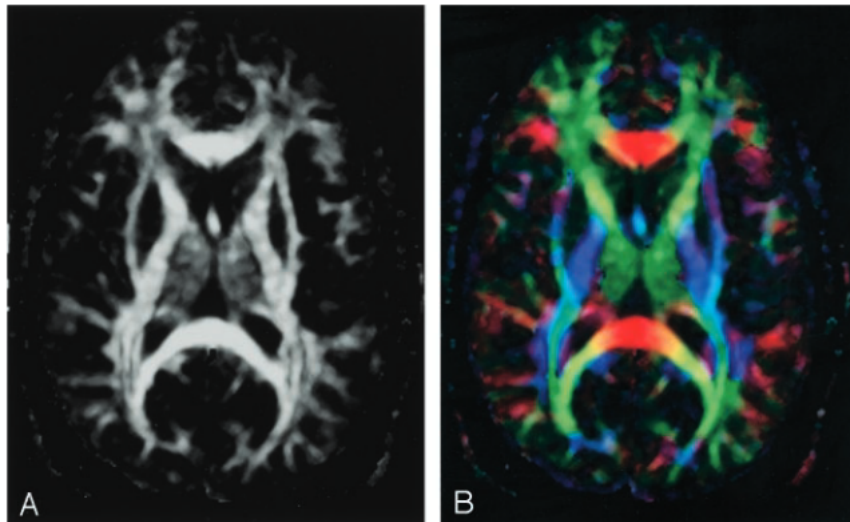


Figure 1.10: (A) FA map, (B) Color-encoded principal diffusion direction: red:left-right, green: anteroposterior, blue: superior-inferior (Image taken from [11]).

Since FA tells us how strong is the directional diffusion, it is also a good marker to determine WM integrity and to study his related pathologies.

1.4 Tractography

Currently, the most commonly used method for white matter fiber tractography is the diffusion tensor model. Its main assumption is that the dominant direction of axonal fibers inside a brain voxel is parallel to the primary eigenvector of the diffusion tensor. Thus, knowing the primary eigenvector inside a voxel will give us the direction of the fiber inside that voxel. Connecting the voxels one on other gives us the estimates of the fiber pathway. In particular, they exist two kinds of reconstructing techniques: deterministic and probabilistic. Deterministic methods are based on the principal direction inside the voxels: once the initial voxels have been randomly selected (initial seeds), the fibers pathways are reconstructed joining the principal directions of consecutive voxels. Voxels are connected according to the principal direction inside them. This family of algorithms is called deterministic because the fiber direction inside each voxel is only one and is determined by the principal direction inside the voxels. On the contrary, in the probabilistic model, multiple directions are chosen inside each voxel. When the seeds have been launched, a solid angle is defined around the principal direction of the seeds voxels. Then, multiple random directions are selected inside the angle cone and propagated to neighbor voxels to create the fibers pathways. Probabilistic algorithms are computationally more expensive than deterministic algorithms but produce better results.

An example of deterministic algorithm used in clinical application is the reconstruction technique named Fiber Assignment by Continuous Tracking (FACT). It allows streamlines course reconstruction starting from some seeds voxels. The initial direction of the fiber is determined by the dominant direction in this first voxel. Then, when the trajectory reaches the edge of the voxel, it is changed to match the dominant direction of the contiguous voxel, and so on to build the entire pathway. The reconstruction ends when the angle between two contiguous directions overcome a certain threshold or when the FA values between contiguous voxels change dramatically. Indeed, since the gray matter has an FA between 0.05 and 0.15 [12], when the FA of a contiguous voxel falls into this interval, the propagation is interrupted 1.11.

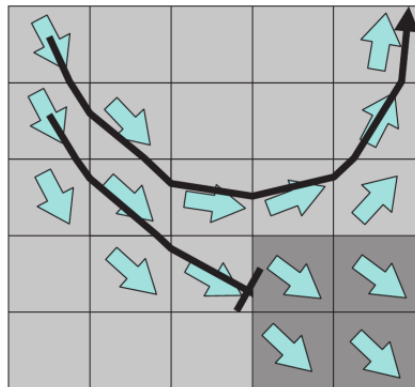


Figure 1.11: Fiber tracking using FACT algorithm. Fibers path is terminated when it ends in a low anisotropy region like gray matter (Image taken from [13]).

FACT is called “continuous tracking” because, to propagate the trajectory, the discrete (integer) voxel coordinates are converted to continuous (floating point) coordinates, so that accuracy reconstruction is improved.

An initial issue is that the axes of the diffusion ellipsoid do not have polarity, thus in every voxel, starting from the one selected by the user, there are two possible directions of propagation. The algorithm solve this problem by always choosing the direction which forms an obtuse angle between the direction of the current voxel and the direction of the contiguous one. In case they form a 90° angle, the propagation is terminated.

1.4.1 Crossing fibers issue

DTI estimates the principal direction of water diffusion inside a voxel. However, in voxels containing multiple fibers going in different directions, the cited method may give a result which differs from reality. If within a voxel there are no crossing fibers, the measured signal is the expected one and we obtain a classical diffusion ellipsoid. However, if there are two different orientations, the DTI technique gives as a result a "pancake" (or oblate) shaped ellipsoid, while if there are three different orientations, it gives a sphere, like if there is isotropic diffusion instead of the anisotropic behaviour (Figure 1.12).

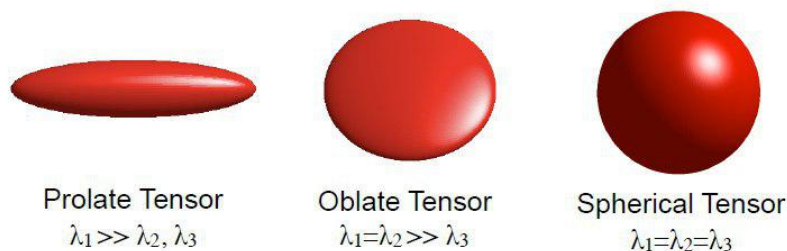


Figure 1.12: Diffusion tensor as seen for no fiber crossing (left), fiber crossing in two different orientations (center) and in three different orientations (right)

This happens because DTI resolution, which ranges from 1 to $3mm$, does not match with the diameter of white fibers which ranges between 1 and $30\mu m$ [14].

To the current clinical image resolutions, it has been estimated that up to 90% of voxels show this issue, resulting in a possible incorrect tracts pathway estimation [15]. In order to fix it, Tournier [16] proposed in 2004 a new method based on spherical deconvolution that can be used to estimate the distribution of fiber orientations present within each image voxel. This method is implemented in a software called MRtrix [17], [13].

1.4.2 Constrained Spherical Deconvolution (CSD)

Tournier's technique has two main assumptions. The first one is based on the physics of displacement of water molecules, for which during a typical dMRI acquisition the average displacement of water particles is of the order of $10 \mu m$. In this way, it is possible to assume that during the experiment, water particles do not pass from one bundle to the other, but mostly remain in the bundle of origin. Thus, the total attenuation signal measured can be seen as the sum of the independent signals coming from different regions. The second main assumption is that the diffusion characteristics of all fiber populations found in the brain are identical,

making their diffusion profiles differ just for their orientation. Let's denote $R(\theta)$ the response function of a single coherently oriented fiber population, where θ is the elevation angle. $R(\theta)$ describes the signal attenuation measured for one single fiber population. Thanks to the previous assumptions, the overall signal $S(\theta, \phi)$ obtained from several distinct fiber populations is given by the sum of the response functions of each population. It is weighted by the volume fractions f_i of each fiber population and the response functions are also rotated by an operator A_i so that they are aligned along their respective orientations (1.8). ϕ is the azimuth angle.

$$S(\theta, \phi) = \sum_i f_i A_i R(\theta) \quad (1.8)$$

This can be expressed as the convolution between the response function $R(\theta)$ and a fiber orientation density function (FOD) $F(\theta, \phi)$, which gives the fraction of fibers oriented along the direction (θ, ϕ) , thus describing the fibers orientations present in the voxel (1.13).

$$S(\theta, \phi) = F(\theta, \phi) \otimes R(\theta) \quad (1.9)$$

The FOD is just the sum, for each fiber population present in the sample, of the Dirac delta functions pointing along the direction of each population and weighted by their respective volume fractions (Figure 1.13).

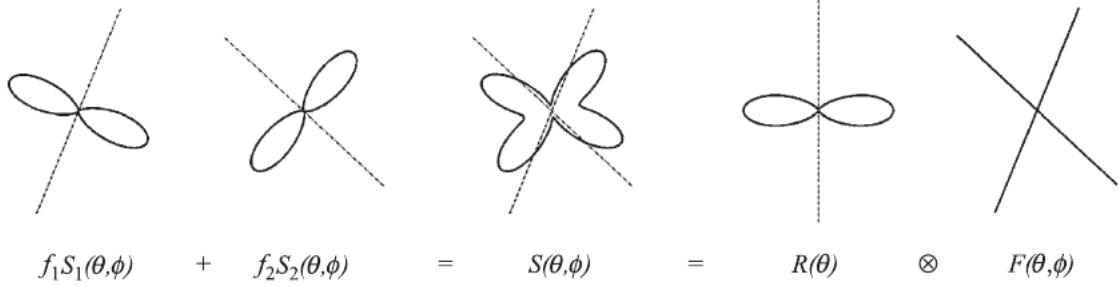


Figure 1.13: We consider here a single voxel containing two different fiber populations with two different orientations (θ, ϕ) and volume fractions. The dotted lines are the fibers orientation while the continuous lines are the signal attenuations. Their sum can be expressed as the convolution between the response function, thus the signal attenuation measured for one single fiber population, and the FOD (Image taken from [16]).

So, if the response function $R(\theta)$ is known, it is sufficient to perform the inverse operation, a spherical deconvolution, to obtain the FOD and to extract the fiber orientations in each voxel. The response function can be estimated directly from the diffusion data looking at the regions that contain a single fiber population, that is looking at the regions that show the highest diffusion anisotropy.

For each voxel, the FOD is visualized as a set of lobes corresponding to the fiber orientations in that voxel, in which the size of lobes is proportional to the volume fraction of fibers with that orientation (Figure 1.14).

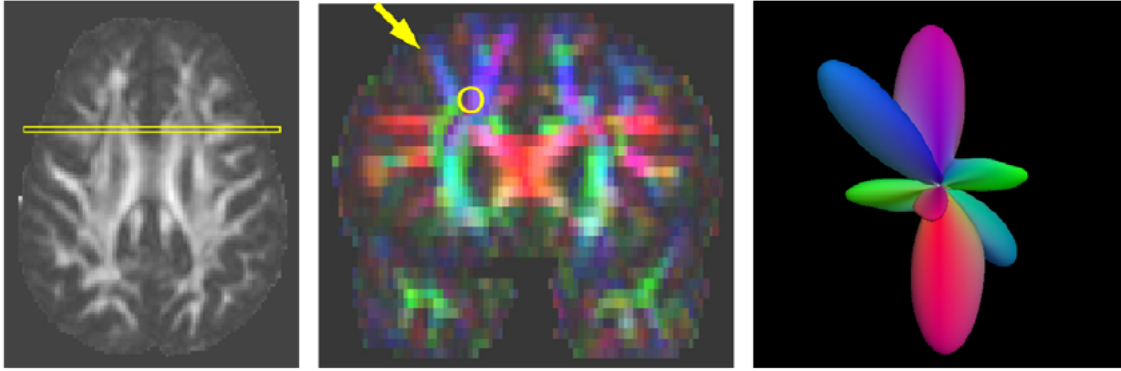


Figure 1.14: Left: FA map of a slice. Middle: coronal slice with colored code according to the major eigenvector of the diffusion tensor. Right: FOD of the voxel indicated by the arrow (negative lobes have been excluded) (Image taken from [16]).

In 2007, Tournier enhanced the robustness of his technique introducing a constraint [17] according to which all negative lobes in FOD had to be excluded, since they have nonphysical meaning. This permitted to decrease noise and to increase the algorithm performances. The method takes the name of constrained spherical deconvolution (CSD).

Chapter 2

Dataset and applications

2.1 Specifications of the dataset

The acquisition protocols of high quality diffusion images to use for tractograms generation usually requires long times. In general, 6 directions of application of the gradient pulses are sufficient to obtain a DTI tensor, but in practice we need to acquire images on many more directions to obtain an accurate tractogram. For this reason, acquisitions for tractograms generation is done just in particular cases and with specific radiological protocols that may vary from hospital to hospital.

The missing of a large diffusion images dataset led in the last years to the development of an ambitious project named Human Connectome Project (HCP), whose aim was to acquire MR images of very high quality with particular scanning protocols. The scanning protocols were specifically created to provide images of the highest possible quality and dramatically differ from usual clinical acquisition protocols, especially in terms of time. One need only think that the dMRI session for each subject was 1 h [18]. Overall, images of the brain of 1200 healthy subjects aging between 22-35 were acquired in a 5 years-period to allow the study of functional and structural connections in brain.

The long times needed to acquire HCP diffusion images are due to the fact that 270 non-collinear directions distributed equally over 3 shells defined with b-values of 1000, 2000 and 3000 s/mm^2 are used [19] for a 3T scanner. This allows to have the highest possible accuracy, also spotting complex fiber configurations. Moreover, voxels of the diffusion image are isotropic with 1.25mm dimensions. In clinics, even when a tractography is needed, the number of used DWI images is far from the ones used in HCP to get the tensor and images have a lower resolution (Figure 2.1).

Even if the HCP quality is considerably high, current MR scanners resolution is too low to detect water traslations in single axons: MRI voxels are typically of the scale of mm and can contain up to hundreds of thousands of axons [21], whose diameter ranges from 1 to 30 μm . In HCP, the 1.25mm voxels dimension is still not enough to visualize individual axons, since white matter contains approximately 300,000 axons per mm^2 cross-sectional area [18]. Tractography thus provides just an *estimation* of the bundles big trajectories and, even if its potential is high, it should not be considered as a strict representation of reality.

The high quality HCP diffusion images publicly available online constitute our starting point for tractograms generation.

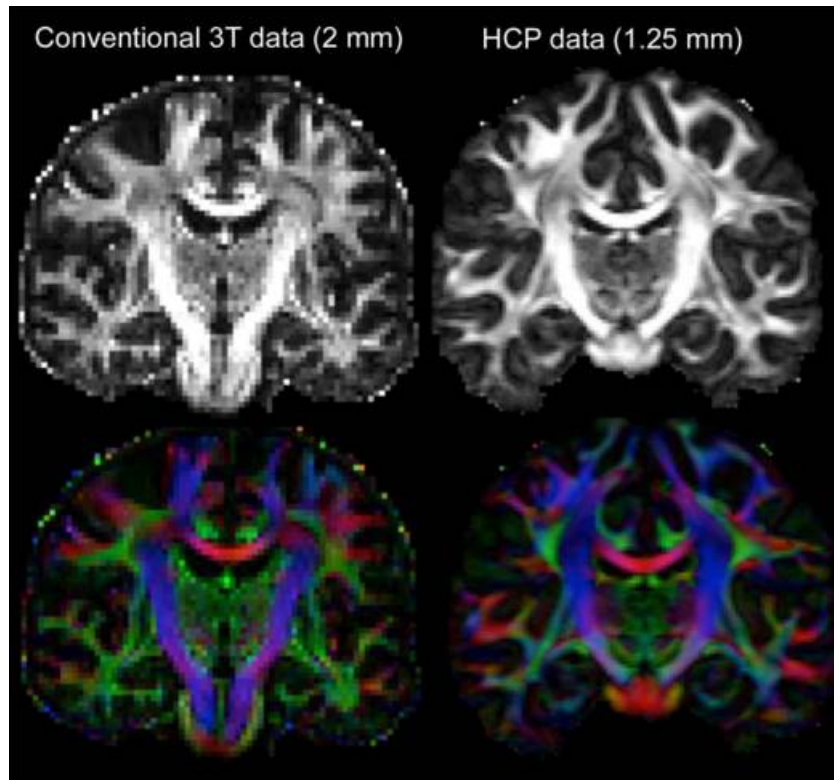


Figure 2.1: Difference between an image with 2 mm isotropic voxels, 60 directions and the HCP 1.25 mm isotropic voxels image. The two images have been acquired from different subjects (Image taken from [20]).

2.2 Tractography applications

Tractography provides an estimation of the trajectories of sets of axons. We call these trajectories, streamlines, or fibers. One single tractogram contains millions of streamlines and is the representation of white matter connections in brain. In literature, streamlines are grouped in bundles, also called tracts, according to their functionality or structure. They are the connection lines that allow us to speak, to move, to see but also to feel. The interest in tractography arises from the fact that it is the only in-vivo non-invasive technique that makes it possible to generate a 3D model of brain connections and, especially, to extract and visualize individual fiber bundles. Tracts can be then analyzed for research or clinical purposes, revealing characteristics or abnormalities that cannot be obtained with conventional MR images.

For example, the streamlines responsible for voluntary control of body and limbs are grouped in the so called corticospinal tract (CST). A lesion to this motor pathway may lead to paralysis of the corresponding side of the body. It is thus of great importance to know where this tract is located and to visualize it, so that it is possible to minimize or even avoid lesions during neurosurgeries or to understand the implications of a certain pathology on its anatomy. The segmentation of individual bundles is thus crucial in both the research and the clinical field.

Concerning research, the study of a particular tract can broaden the understanding of the pathophysiology of a certain brain disease but also help in the identification

of new biomarkers that can be used, for example, to assess the presence or the stage of an illness. Indeed, brain pathologies may be manifested as connection abnormalities and can be detected analyzing the individual tracts. The most studied illnesses are epilepsy, schizophrenia and Alzheimer. For example, as regards epilepsy, [22] suggests that abnormalities in uncinate fasciculus (UF), inferior longitudinal fasciculus (ILF), superior longitudinal fasciculus (SLF) and cingulum (CG) may be observed in pathological subjects. Focusing instead on schizophrenia [23] analyzed the integrity of frontotemporal and interhemispheric white matter bundles, finding alterations in the left UF and right CG of patients under 55 years old. A bilateral disruption in fornix (FX) integrity was observed by [24], while [25] found alterations in right arcuate fasciculus (AF). The individual fiber bundles obtained from tractography may also lead to question previously obtained results. For example, the apathy that arises in subjects affected by Alzheimer was previously associated with structural changes in anterior thalamic radiation fibers (ATR), however both [26] and [27] found that ATR was spared in pathological subjects.

For clinical purposes, tractography potentials can be fully appreciated in neurosurgeries. It can indeed be used to improve the preoperative evaluation, to plan and to target the intraoperative neuronavigation, as well as to predict the procedural risks and postprocedural outcomes of a neurosurgical operation [28]. It can help in detection of sensible tracts whose surgical resection should be avoided when possible. It can also be used as a support during implantable devices like deep brain stimulation electrodes. A clinical application of tractography is for example the surgical removal of brain tumors. Since they grossly displace fiber tracts, having an estimation of bundles pathway and the entity of their displacement may help neurosurgeons in planning an operation to preserve important brain functions like language, motion, vision or sensations [29]. In Figure 2.2, the manual segmentation of a 4-cm cystic lesion in the right frontal lobe is visualized together with the brain tractogram. The tumor sits within the CST. The surgical plan, that previously aimed to enter the lesion anteriorly, was modified after it was shown thanks to tractography that it would have led to the resection of CST streamlines, jeopardizing motor functions. Instead, a right frontal access was planned. The patient had no neurological change over a long-term follow-up [30].

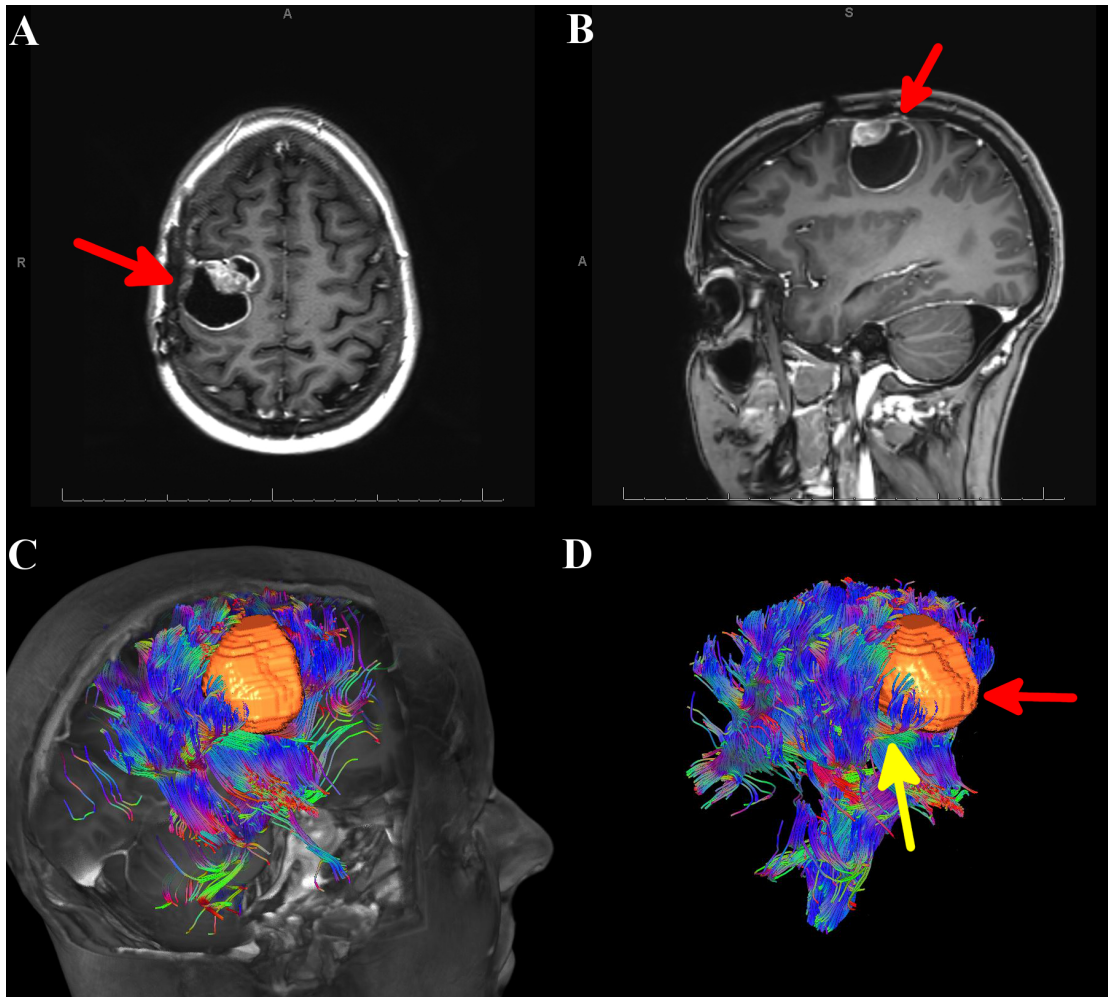


Figure 2.2: Preoperative planning of a tumor removal using tractography: (A) axial MRI view, (B) sagittal MRI view, (C) tumor sitting on the CST, (D) tumor (red arrow) sitting on the CST (yellow arrow) (Image taken from [30]).

Part II

State Of The Art

Chapter 3

Segmentation Methods

The individual course of white matter fiber tracts is an important key for analysis of white matter characteristics in healthy and diseased brains. However, even if DTI-based tractography provides an estimation of the streamlines path inside brain, it does not directly permit to extract the pathway of a specific fiber bundle. To perform such an uneasy task, various segmentation methods that can be divided into four main categories have been developed: manual segmentation, parcellation techniques, supervised learning approaches and hybrid methods.

3.1 Manual Segmentation: virtual dissection

Virtual dissection is a manual segmentation method that strongly relies on the operator knowledge of which areas of the brain are connected by a particular fiber bundle. It consists in manually selecting on the dMRI volume some set of voxels that the user believes to be crossed by the desired fiber tract. These set of voxels define regions called Regions of Interest (ROIs) and constitute the constraint used to isolate a particular set of streamlines from a whole brain tractogram. For example, one might want all streamlines crossing that particular ROI to be considered as part of the wanted tract or, on the contrary, to exclude each streamline entering that ROI. Whatever the ROI created, the process then consists in visually checking the subset of streamlines selected and to eventually modify by hand the drawn region to include/exclude a different number of streamlines so that the resulting fiber tract is closer to reality.

It is also possible to draw multiple ROIs and to combine them using some spatial connectors: AND, CUT and NOT (See Figure 3.1). The AND relation permits to consider fibers that penetrate both ROIs, while NOT allows to exclude some subset of unwanted fibers penetrating one of the ROIs, and CUT is similar to AND but limits the desired region to the one between the two ROIs [31]. One should in general try to minimize the number of drawn ROIs and connectors used, since practice has shown that an extensive use of them is usually counterproductive and worsens the result that can be achieved using a small number of regions.

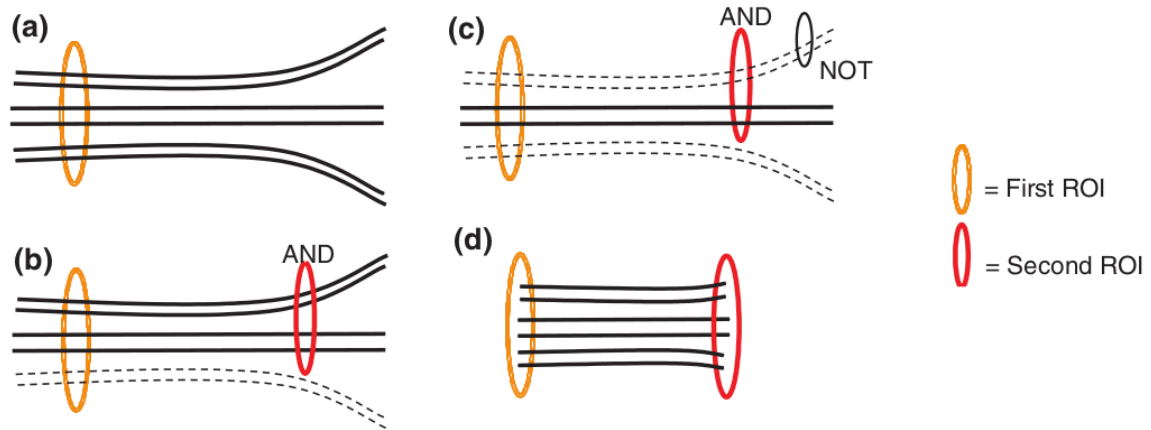


Figure 3.1: Relations between multiple ROIs. (a) All streamlines crossing the first ROI are selected, (b) Only the streamlines that cross both ROIs are selected, (c) The NOT relation is used to exclude some streamlines from the previous case, (d) Using CUT, only the segments of the streamlines between the two ROIs are selected (Image taken from [31]).

The user has the total freedom to choose the ROIs and the spatial connectors he prefers, but he can also decide to rely on some pre-built protocols based on brain anatomy. Guidelines have been developed to facilitate the choice of ROIs and to enhance the level of reproducibility, since they can be used with small modifications across different subjects and by different operators, but they are available only for the main tracts [32].

Whatever the choice of the user, manual segmentation method dramatically relies on his anatomical knowledge of the brain. We need indeed to remember that a diffusion image does not show the path of an individual bundle and the user has to know it a-priori in order to build an adequate ROI, making this approach suitable only for medical personnel. However, being the bundles definitions in literature quite vague, especially for what concerns the extent of their edges, even when a tract is extracted by a professional we cannot be sure on the entity of its accuracy. Moreover virtual dissection has little reproducibility, since it is user-dependent and even small changes to one ROI lead to very different results. Finally, among all the limitations, this approach is also tedious and the manual search for an adequate ROI is highly time consuming. For this reason, even if it is the most commonly employed technique in clinics, it is quite unusable for research purposes where we have to manage data sets constituted by many subjects.

3.2 Supervised Learning methods

3.2.1 Clustering

Clustering segmentation methods do not rely on brain anatomy but they build a fiber tract joining together streamlines that have similar geometrical properties. Clustering techniques differ by the distance metric and the cluster method chosen. Many different pairwise fiber distances and similarity measures were developed.

One of the earliest fiber clustering approach has been developed by [35], in which

two fibers are considered similar when they have comparable length, similar shape, and are separated by a small distance. In particular, shape similarity and closeness are calculated by the mean Euclidean distance while the length comparability is measured by a ratio of fiber lengths. The most similar fibers are then chosen thanks to a threshold: a cluster around a fiber is constructed by neighbouring fibers whose similarity to that fiber is the greatest.

In early times, spectral and hierarchical clustering were the most used clustering techniques [36]. Spectral clustering is a method that group data on the basis of its similarity to other data exploiting graph theory. The goal is to build a matrix, called affinity matrix, that is representative of the relationships between the input data and to divide them in a number k of clusters according to the eigenvectors of that matrix. An example of k -way spectral clustering used in tractography can be found in [37], in which the authors group streamlines on the basis of their shape and location. They use the pair-wise average distance between streamlines to build the affinity matrix, in which for each streamline it is computed the distance from all the others. Eigenvectors and eigenvalues are then extracted and the top eigenvectors are used to calculate the most important shape similarity for each streamline. This similarity information can be visualized as a point (Figure 3.2), thus a node of the graph. K -way spectral clustering is then used to generate the clusters and group the streamlines to form different bundles. The main limitation, intrinsic to spectral clustering, is that the number of clusters k that we expect to find needs to be defined a priori. Another example can be found in [38], where the affinity matrix is build using as similarity measure between streamlines the number of times two fibers share the same voxel. The six largest eigenvalues and their corresponding eigenvectors are calculated and then clusterized using k -means to find the bundles.

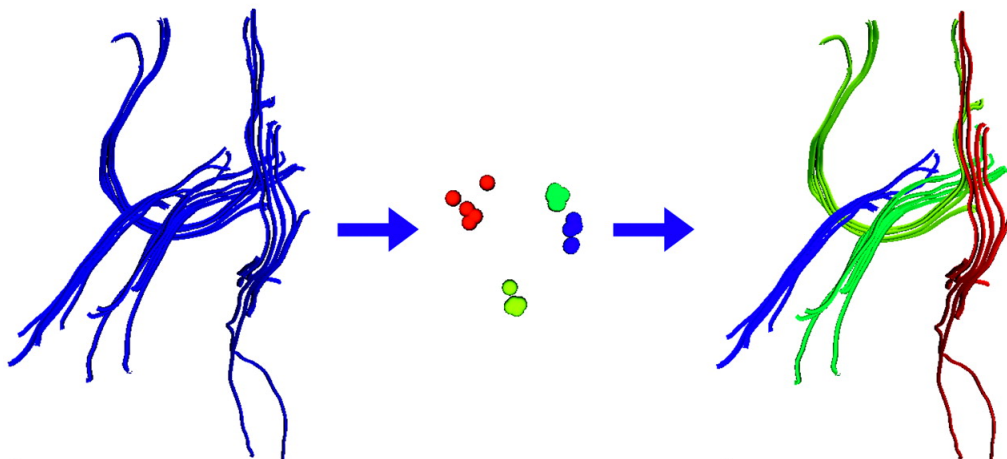


Figure 3.2: The similarity values obtained from top eigenvectors are represented as point and used to create the clusters. Each cluster contains the streamlines of a particular bundle (Image taken from [37]).

Another technique used in early times is hierarchical clustering, a technique that, as the name suggests, aims to build a hierarchy of clusters. There exist two kind of hierarchical clustering: agglomerative and divisive. Agglomerative hierarchical clustering initially considers each data point as an individual cluster and then, at each iteration, merges together similar clusters. The process continues until there is only one cluster left. Results are then represented as a tree (or dendrogram), in

which the root is the unique cluster that includes all the others, the branches are the merged clusters and the leaves are the clusters with only one sample (Figure 3.3). Deciding the cut point in a way that maximizes inter-cluster distance and minimizes intra-cluster distance allows to obtain a proper number of clusters. During the process the clusters are merged together according to a certain metric that it is for example the maximum, minimum or mean distance between the elements of each cluster but there exist many other types. Divisive hierarchical clustering is less used and is the opposite of agglomerative hierarchical clustering. It initially considers all the data points as a unique cluster and then it progressively splits them until each data point represents a cluster. The hierarchical tree can be suddenly cut on the wanted level. The main disadvantage of hierarchical clustering is that it is highly time consuming, thus it is not suitable for multi-subject tractogram analysis. One example of agglomerative hierarchical clustering can be found in [39], in which the authors tried different metrics like closest point distance, mean distance of closest distances and Hausdorff distance to build clusters. In [40] the authors used a self-made distance to, starting from a singleton cluster, iteratively merge the current two nearest clusters until reaching an inter-cluster distance equal to $2.5mm$.

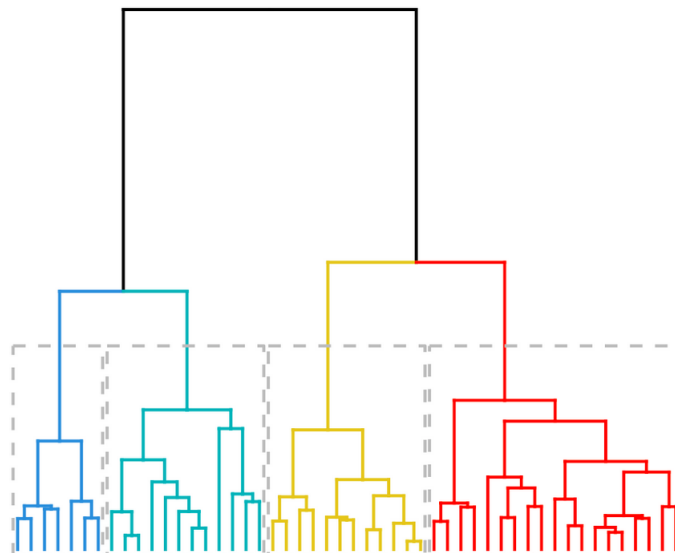


Figure 3.3: A visual example of hierarchical clustering

Segmentation methods have then evolved to allow the study of multiple subjects thanks to the development of the clustering algorithms and the creation of atlas. For instance, in [41] a tractography atlas was constructed and used to find proper clusters. More precisely, the atlas is build identifying common clusters across subjects using spectral clusterig and giving expert anatomical labeling. The desired clusters from new subjects are then automatically found expressing the tracks as points, calculating a similarity measure and looking at the closest existing atlas clusters. The development of clustering techniques allowed also to use tractograms with a high number of streamlines. For example the method developed by [42] permits to computes pair-wise distances of around 450.000 streamlines without incur in memory issues. The authors first randomize the streamlines order, then they divide them in a certain number of subsets and compute the hierarchical clustering of each subset according to the pair-wise distance between streamlines. They subsequently calcu-

late a mean tract for each cluster of each subset and compute the pair-wise distance between the mean tracts. Using this distance, every cluster, which is represented by a mean tract, is assigned to the nearest cluster. The process ends when all clusters have been assigned.

Many different techniques have been created. They minimize user interaction increasing accuracy with respect to manual segmentation, but almost all of them rely on pairwise distances calculation and this makes algorithms very time consuming. Moreover, clustering techniques are based on hyperparameters that have to be fixed by the user and their change produces completely different results. They have no direct medical meaning and their setting may be difficult for those who do not have a mathematical background.

3.2.2 TractSeg

TractSeg [43] is a convolutional neural network (CNN) approach which aims to obtain fiber tracts circumventing the intermediate step of streamlines generation. It provides bundles segmentation directly using the input images. In particular, 72 tract segmentations were obtained from a dataset of the Human Connectome Project (HCP) composed by 105 subjects.

The architecture of the neural network is similar to the one of the U-Net [44] created in 2015, which consists in a downsampling (contracting) path, and an up-sampling (expansive) path. We basically reduce the image dimensions and compute the feature extraction in the descending path and then we do the inverse in the symmetric ascending path (which is the reason for the U-shape name), thus we up-sample and we give the precise localization of an object according to the extracted features.

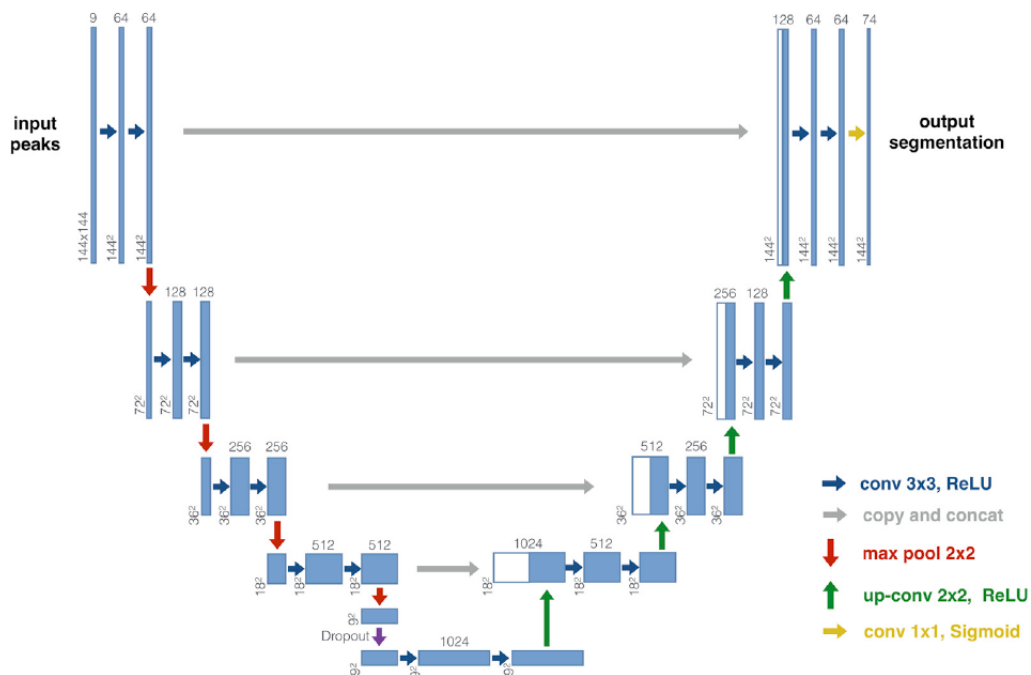


Figure 3.4: Architecture of TractSeg neural network inspired by the U-Net (Image taken from [43]).

In TractSeg neural network architecture (Figure 3.4), the inputs are 2D images in the three orientations (axial, coronal and sagittal) that contain for each voxel the three principal fiber directions computed using the CSD in MRtrix. The neural network is ran three times, one per each orientation. We obtain as output a 3D image that contains for each voxel the probabilities of finding each of the 72 tracts. Probabilities are finally converted to a binary segmentation using a 0.5 threshold. During inference of the CNN, three predictions per voxel per tract are extracted. These predictions can be optionally passed to a second CNN to obtain an optimal result. Indeed, this second CNN generates other three predictions per voxel that are finally merged using the mean. As said, giving the predictions to a second CNN is optional and a reliable result can be obtained just merging the predictions obtained from the first CNN.

What is of particular interest in TractSeg is the reference that, in their turn, the authors have used to asses the validity of the output tracts. As we have said, there is no ground truth today, so they generated one in their own. Especially, they created a reference binary segmentation for each of the 72 tracts for each of the 105 subjects, using a semi-automatic process that includes a final manual quality clean-up (Figure 3.5). The reference creation consists in 5 steps:

1. Generation of a whole brain tractography consisting of 10 million streamlines using MRtrix;
2. Initial tract extraction using tract definitions with respect to a parcellation atlas;
3. Filtering of fibers: removal of clusters of small dimensions, removal of streamlines with unconsistent geometries with respect to the tract, removal of streamlines that enters some manually defined exclusion ROIs;
4. Manually clean-up: undo of the filterings that removed valid streamlines and manually removal of unwanted fibers;
5. Binary mask generation: conversion of streamlines to binary masks, removing small unconnected regions.

Tracts extracted using TractSeg are then compared to the reference binary mask of a particular tract to quantitatively evaluate their similarity.

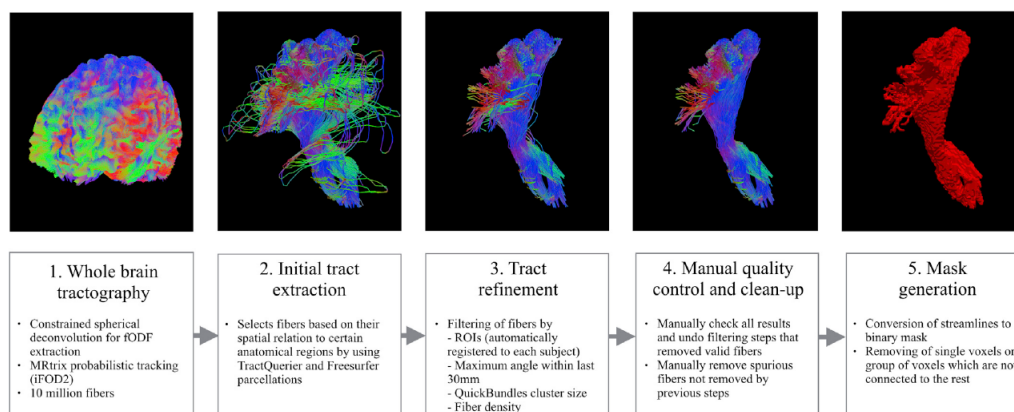


Figure 3.5: Steps for binary mask generation of a CST tract (Image taken from [43]).

The main limitations of TractSeg is that it uses a pre-trained model. If we want to train the model using different inputs and to have results of the same quality, we have to perform the pre-processing steps that lead to the creation of the binary masks by our own. It could be especially hard for what concerns the manual cleaning and it would be a very long procedure in case we would like to repeat it for all tracts of a single subject. One could also question whether the final cleaned tracts reflect the actual anatomical tracts since they seem too perfect.

3.3 Parcellation Methods

Similarly to manual segmentation, in parcellation techniques we use some regions to establish an inclusion/exclusion relation that allows to extract the wanted fiber bundle from the tractogram. However, using this technique we do not have to manually draw the ROI but we exploit the parcellations of cortical and subcortical regions of the brain. These are pre-defined structures that have been segmented from the T1 volumes using an appropriate software like Freesurfer [33] and that are stored in an atlas (Figure 3.6). Parcellation-based techniques are thus useful to overcome manual segmentation limitations, however their result strongly depends on the parcellation quality. For example, for pathological subjects (e.g. with tumors) it is usually difficult to extract the correct parcellation. Moreover, also for healthy subjects, some structures necessary for tracts segmentation cannot be extracted and some important spatial relations cannot thus be used.



Figure 3.6: Example of brain gyri parcellation atlas obtained with FreeSurfer. At each segmentation it is associated a label and an identification number (Image taken from *freesurfer.net*).

3.3.1 White Matter Query Language (WMQL)

WMQL [34] borrows as an alternative to manual segmentation and clustering methods. Manual segmentation is indeed suitable for single subject studies but it lacks of accuracy, reproducibility and is heavily user-dependent. Clustering methods are fully

automatic and are used to improve accuracy, joining together streamlines according to the similarity of their paths, but they are very high time consuming. WMQL is instead based on a near-to-English textual computer language, where it is the user who defines the path of the tract he wants to extract, with the help of some spatial relations and an atlas containing all principal main structures. The operator writes the anatomical definition of a tract in textual form, using brain parcellations as reference structures, which is then transferred to a tool capable of automatically identify the white matter tracts from dMRI volumes. To do that, parcellations of the brain are labeled and stored in a separate file and they are accessed according to the spatial relations chosen by the user.

The peculiarity of this technique is that it is very simple to use since it relies on a textual language which is very close to the one we use everyday, allowing also non-engineers to easily code the anatomical definitions. Another main advantage is that the definitions can be used to extract white matter anatomy across subjects and not just from a single person. Moreover, since definitions are human-readable they can be modified according to the newest discoveries. This technique is thus applicable to a relatively large group of people but it also maintains a certain degree of flexibility that can be exploited to analyze specific cases.

The anatomical definition are constructed combining three different kind of terms:

1. Anatomical terms: they say if a tract traverses or ends in a certain region (e.g. `endpoints_in(postcentral)`);
2. Relative position terms: to indicate the position of a tract with respect to an anatomical structure used as reference (e.g. `anterior_of(amygdala)`);
3. Logical operations: to establish a relationship between the previous two terms (e.g. `endpoints_in(postcentral)` and `anterior_of(amygdala)`).

The result is a query that contains all the information to extract the desired tract (Figure 3.7). Once an anatomical definition has been written, it is applied to a whole-tractogram and the streamlines which respect the definition are extracted to build the wanted fiber tract.

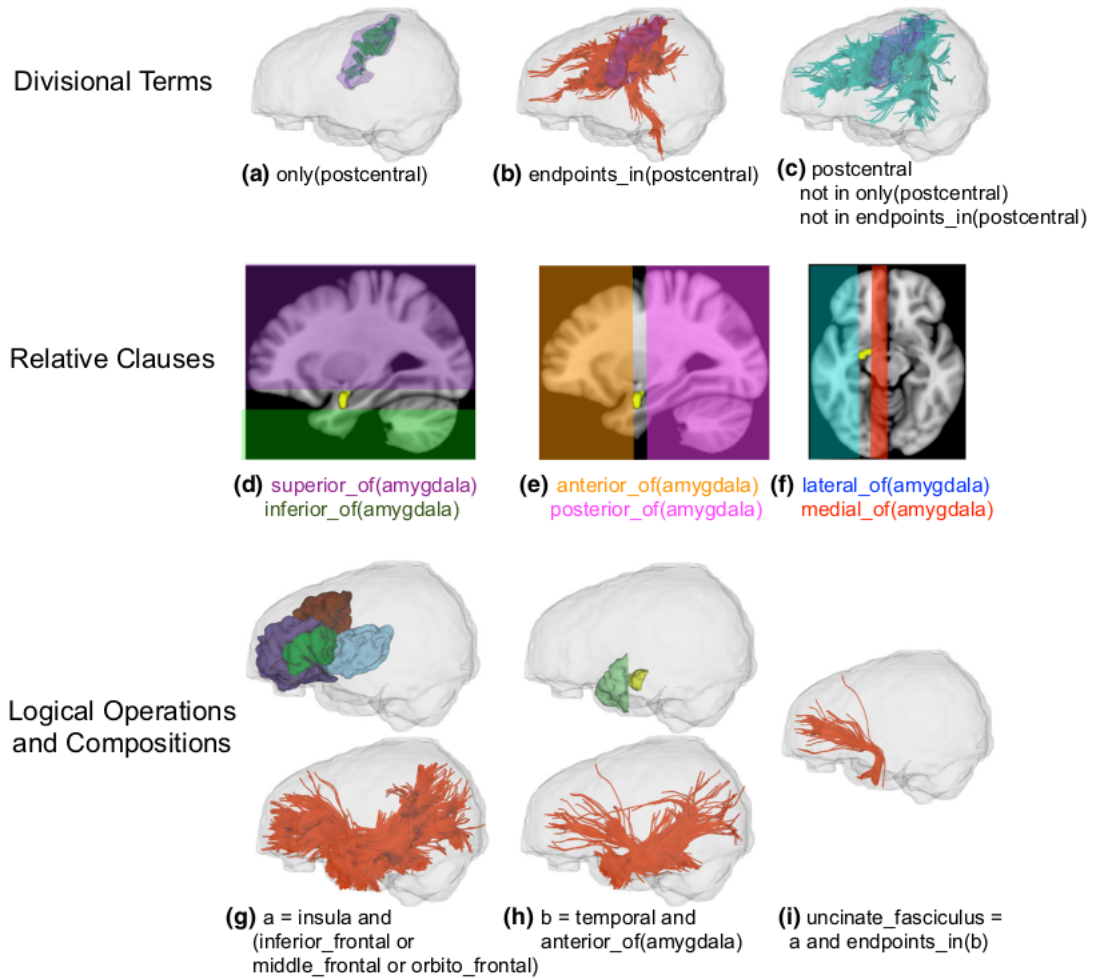


Figure 3.7: Examples of use of anatomical terms, relative position terms and logical operation in WMQL. (i) is the final query that defines the Uncinate Fasciculus (Image taken from [34]).

WMQL, as the others parcellation techniques, makes bundle extraction to be more reproducible than manual segmentation but retains the accuracy issues caused by the imprecision of anatomical definitions. The use of relations between parcellations allows to create bounding boxes that encompass the tracts pathways but their rigidity does not account for the vagueness that affects bundles edges. On the contrary, we propose a technique based on fuzzy logic which models the intrinsic vagueness of the definitions and let the user choose the result he considers to be the most accurate.

3.4 Hybrid Approaches

The idea behind the development of hybrid approaches is to combine the information of different kinds of segmentations to obtain an accuracy that is higher to the one of the individual methods. Generally, an hybrid method exploits the segmentations of a parcellation atlas to impose a constraint on the streamlines that have to be extracted and then it uses a clustering technique to identify the different fiber bundles. In this way it is possible to combine the anatomical information provided

by the parcellation-based techniques with the geometrical knowledge exploited in clustering-based segmentations. As an example, in [45], a gray matter parcellation atlas is used to label streamlines according to the anatomical regions where their terminations are located. Streamlines with the same label are then grouped to form the fiber tracts. However, since DTI resolution is quite low, it is possible that inconsistent paths are created during tractogram generation. In order to remove these outliers a clustering technique is used. Clustering has also the aim of splitting the initial bundles and regroup streamlines according to their similarity, since the previous process may attribute a streamline to an incorrect bundle. Indeed, two pair-wise similarity distances (mean distance and Hausdorff distance) are computed. The first step is to compute the mean distance between streamlines of a same fiber bundle and to clusterize them according to a threshold. These sub-clusters of a bundle can be then grouped to a neighbour bundle, or grouped to other sub-clusters to form a proper bundle or even be rejected, according to similarity between the closest bundle. At the end of the process, rejected sub-clusters have to be manually checked by an expert.

In general, in the development of an hybrid technique one has to note that, whilst it is possible to combine the structural and functional information of other techniques, it may suffer of the drawbacks of the different methods.

3.5 Discussion

The segmentation methods are all subjected to different challenges like lack of accuracy and difficulties in reproducibility but the main limitation is the lack of a *ground truth*. It does not exist a reference tract atlas whose bundles are considered a faithful reproduction of reality. This is also because tracts structure slightly changes across subjects and it is different according to subjects ages. When a bundle is extracted it is thus not possible to quantitatively evaluate its closeness to reality and the only method that allows to assess the validity of a result is the advice of medical experts. Moreover, tracts anatomical definitions are still vague or imprecise and only qualitative evaluations are possible. In particular, bundles edges are not well defined in literature and lead to an intrinsic inaccuracy in fibers extraction. Current existing tract segmentation techniques are not flexible and only provide a single result that does not account for the vagueness of the anatomical definitions. We aim to create a novel segmentation technique, based on fuzzy set theory, that is able to model imprecision giving better results and leaving the user the possibility to choose between different outputs.

Part III
Fuzzy Tracts

Chapter 4

FuzzyTracts: a tool for fuzzy spaces creation

This chapter serves as connection between the state of the art and the next contribution chapter. It explains the use of fuzzy sets theory in our work. The main idea is to define fuzzy subsets of the 3D space that model spatial relations and that can be combined to model anatomical definitions. This chapter also focuses on the description of an already existing algorithm, called FuzzyTract, which is at the base of this master thesis.

4.1 Fuzzy sets theory

In this master thesis, fuzzy set theory is used as tool to model the intrinsic vagueness of human language with regard to spatial relationships between objects. We remember that the aim of the work is to find the fiber tracts of the brain. These are defined in literature, especially in dissection papers, as a set of relations with adjacent brain structures. Thus, creating a fuzzy model of the spatial relations may allows us to extract the wanted fiber bundles that are dipped in a one million fibers tractogram.

The information on where an object is located with respect to another has fundamental implications in fiber tracts detection. In everyday talk, we use expressions like “to the left of”, “under and many others spatial relations to describe the position of something with respect to a reference point. Even if these words are intrinsically not accurate, they give an intuitive idea of the position we are describing, permitting us to easily locate the wanted object. The intrinsic imprecision of these concepts can be used in fuzzy sets theory to describe the relative positions of objects and can be exploited to find some fiber tracts with respect to a reference brain structure (e.g. amygdala). Moreover, fuzzy sets theory allows us to overcome the “all-or-nothing” definitions proper to crispy logic that usually lead to unsatisfactory results (Figure 4.1).

The idea [46], [47], [48] is to represent image regions as spatial fuzzy sets, thus as sets of points that have a degree of satisfaction of a relation. This degree of satisfaction is the degree of membership to the spatial fuzzy sets representing the relation. In this way, looking at the previous figure, it is for example possible to say that objects A and B have a degree of satisfaction of the relation “to the right

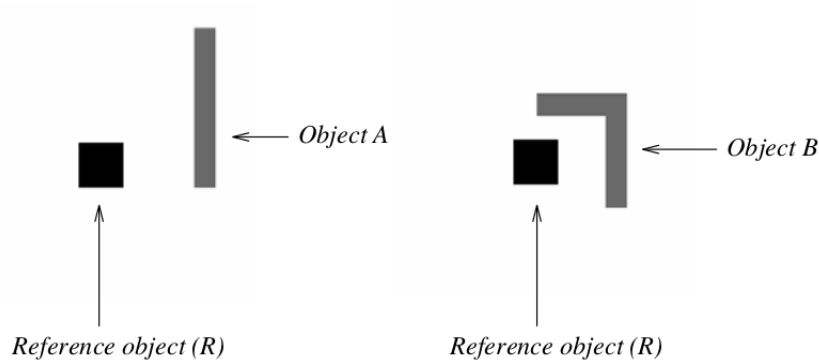


Figure 4.1: Crisp logic does not provide adequate information on objects A and B positions. Objects A and B are to the right of reference R but they are also to some extent above it.

of” but also of the relation “above”, allowing a good description of their position in space. Spatial fuzzy sets are indeed used to evaluate a certain rule and establish if the desired object is located in the wanted space and “how much” it respects the cited rule. Let us consider a reference object R and an object A for which we want to evaluate the relative position with respect to R . We need to follow two steps:

1. Define a fuzzy “landscape” around R . This means giving to each point present in the space around R a membership value that express the degree to which it satisfies the spatial relation we are examining. For example, we want to know “how much” the points around R respect the rule “to the right of R ”. The points which are exactly at the right of the reference object will have the higher degree of membership while the degree decreases more and more for points which respect less and less the rule;
2. Compare the object A to the fuzzy landscape of R . In this way we can understand if the object is located in the area where the membership values of the landscape are the highest, so if A is in the desired direction.

In our work, the object A will be the tract we are searching for, while the reference object R will be the parcellation structure we are using to evaluate the spatial relation (e.g. Amygdala). We want to combine multiple spatial relations and use them to create the anatomical definition of a tract.

The first step, the creation of a tool capable of generating a fuzzy region of the 3D space, is implemented in an already existing algorithm called FuzzyTract [49]. The second step, the creation of the anatomical definitions, the corresponding fuzzy sets and the extraction of the resulting streamlines is the purpose of this master thesis.

4.2 FuzzyTract

In the 3D space, a direction is defined by two angles α_1 and α_2 ; by combining them it is possible to describe the main six directions in space: “right_of”, “left_of”, “inferior_of”, “superior_of”, “anterior_of”, “posterior_of” and all the oblique directions that result from their combination. These directions are defined with respect to the reference structures present in the brain atlas. Once the direction to evaluate has been chosen, the fuzzy landscape is computed: a fuzzy value is given at each voxel according to the angle between the line that goes from the voxel to the middle point of the image and the vector that describes the wanted direction, whose origin is in the middle point of the image as well. This defines the structuring element ν , providing the semantic of the relation, and then used to compute the membership function μ_{alpha} as $\delta_\nu(R)$ where δ denotes a morphological dilation. Fuzzy values range between 0 and 255 (scaling of the $[0, 1]$ interval of membership values) to give a visual representation on gray-scale colors of the landscape: voxels in the same direction as the relation vector will have values closer to 255 (white RGB) while voxels more and more distant from the vector will have decreasing values that will bring the color closer to dark gray. Voxels on the opposite direction of the vector will have the lowest values and will appear as black in the image. In this way the color of a voxel represents the degree of membership that it has with the wanted direction, thus voxels with high degree of membership will be white while voxels with small degree of membership will be darker, as more as they are farther from the desired direction. The region which the highest membership takes the form of a cone (Figure 4.2 a).

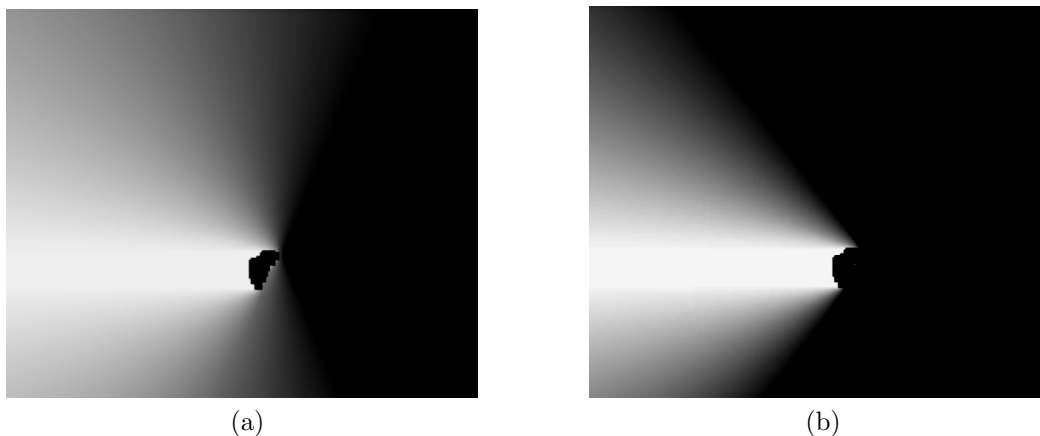


Figure 4.2: A single slice of a fuzzy space evaluated from the definition “anterior of amygdala”: (a) Fuzzy space evaluated giving a value to the aperture parameter, (b) Fuzzy space evaluated with a small aperture parameter.

The user has the possibility to vary the width of the cone thanks to an “aperture” parameter that he can arbitrarily set. In this way, the “speed” at which the membership degree increases or decreases moving away from the wanted direction can be changed. For example, increasing the aperture would give a faster variation speed and thus a larger white area (Figure 4.2 b). This is useful when we want to be a bit more precise when writing an anatomical definition. To understand how does the aperture parameter work, let us see its impact on the membership function.

The membership function $\mu_\alpha(R)$ at a point P of the image depends on the minimum angle β_{min} formed between the direction α (with respect to the reference object R) and the segment joining P with a point Q of the reference structure R (Figure 4.3). It can be represented as a linear function:

$$\mu_\alpha(R)(P) = f(\beta_{min}(P)) = \max(0, 1 - \frac{2\beta_{min}}{\pi} * (1 - \frac{k}{2\pi})) \quad (4.1)$$

and this is equal to $\delta_\nu(R)(P)$.

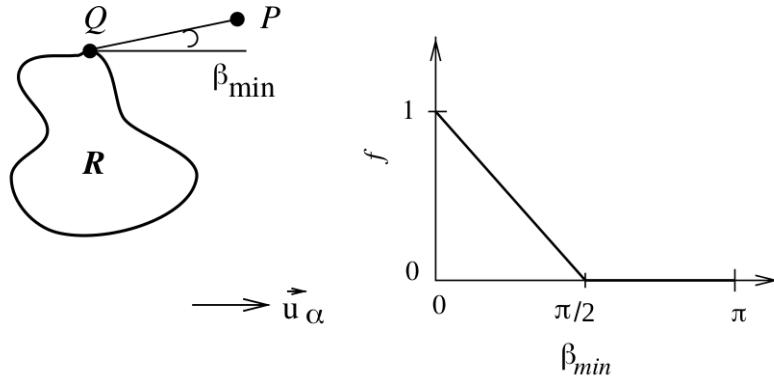


Figure 4.3: Definition of the angle β_{min} .

We can see that the more the angle β_{min} becomes big, the more the membership function becomes small. In this way, the points P of the image which respect less the wanted spatial relation with the reference object will have a smaller membership degree (a darker color).

The aperture parameter k , forces all points P that form angles bigger than k , to have the lowest membership degree. Thus, all points P for which $\beta_{min} > k$, will have a black color in the resulting space. If no aperture parameter is imposed, the algorithm sets it to be $k = 2\pi$.

Considering the reference object R , only the external points give useful information for β_{min} computation. The computation of distances between a point P of the space and the internal points of the reference structure would only slow down the process without adding any further information. For this reason, only the boundary points are extracted from the reference structure and used for the angle calculation. To do that, the reference structure is first extracted from the atlas in form of a binary mask. A dilation of the mask is performed using as structuring element a $3 \times 3 \times 3$ cube and then it is compared with the original one to extract only the boundary voxels of the structure, thanks to an erosion. Then the angle computation begins.

The two inputs we need to provide to the algorithm are: a labeled list of brain segmented structures and a parcellation atlas. In the labeled list, with each structure name, an identification number is associated. The parcellation atlas is a map of the brain major subdivisions, generated for example using Freesurfer [33]. When we create a fuzzy space using the name of a particular subdivision, the algorithm searches for its corresponding number in the labeled list and, from the parcellation atlas, it selects the 3D segmentation whose label corresponds to that number and evaluates the wanted fuzzy space.

This novel technique, being based on a near-to-english language, retains all the benefits of intuition and flexibility proper of common human language. The fuzzy set theory provides a model for the vagueness of concepts that does not exist in any other tract segmentation method and that constitutes the power of this approach. At the same time, the use of a parcellation atlas allows the user to try multiple ways to create an anatomical definition, a feature that is not possible to exploit in automatic methods like classical clustering techniques or machine learning approaches like TractSeg.

4.2.1 Writing a definition

The anatomical definitions of tracts found in literature are written by the user in form of a query language, using the atlas parcellations as reference structures and logical connectives AND, OR and NOT to link the different spatial relations (Figure 4.4).

Bundle = left_of(LeftAmygdala) and under_of(LeftThalamus, aperture=0.8)

Figure 4.4: Anatomical definition of a tract written in query language. The tract (black) called “Bundle” is defined with respect to some reference structures (green). In particular, this imaginary tract is located to the left of the Amygdala and under the Thalamus, where the words “left” and “inferior” (red) correspond to some spatial relations. The two spatial relations are then linked together by the logical connective “and” (blue), that will output the intersection between the two fuzzy regions representing the relations, thus resulting in a fuzzy space where the voxels with higher membership degree will be the ones in left-under oblique direction. Note that it is also possible to specify the degree of aperture of a cone (orange), arbitrarily excluding some regions not useful to the definition.

The algorithm first reads the whole definition given as input by the user and then splits it in correspondence of the logical connectives, to evaluate the spatial relations one at a time. The evaluation of each spatial relation produces as output one fuzzy space per relation. Individual fuzzy spaces are finally merged together to give one final output, in a way that depends on the logical connectives used. It is to note that the logical connectives AND and OR assume here a different meaning with respect to the one cited in manual segmentation methods to create the ROIs, while NOT operator has a similar explanation. Operators are, as we were saying, not only used to establish a relation between different regions, but they rule the way fuzzy sets are combined together. The AND operator computes the minimum between two sets, corresponding to fuzzy set intersection, the OR operator computes the maximum between two sets, corresponding to fuzzy set union, while NOT performs the complement of an individual fuzzy set, which is like creating an exclusion region in manual segmentation. When writing an anatomical definition one has to consider these aspects of fuzzy set operations, since evaluating the same anatomical definition using different logical connectives will give completely different results (Figure 4.5).

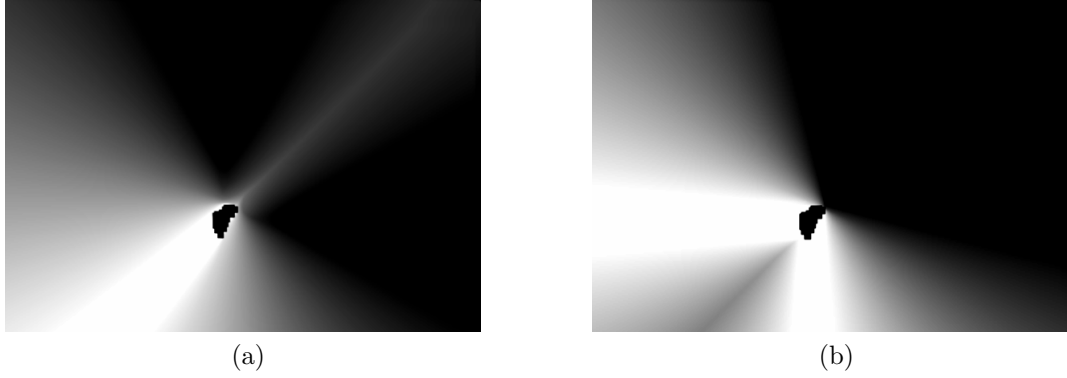


Figure 4.5: Fuzzy space obtained with an AND relation (a) and an OR relation (b). The used AND relation is $left(LeftAmygdala)$ and $inferior(LeftAmygdala)$, the used OR relation is $left(LeftAmygdala)$ or $inferior(LeftAmygdala)$.

4.3 Discussion

As seen in the state of the art, there exist different segmentation techniques and each of them suffers from different drawbacks. Manual segmentation is far from being reproducible, is tedious, highly time consuming and the accuracy from a qualitative point of view can fall down just using a slightly different ROI. Parcellation approaches enhance reproducibility but raise accuracy issues since they allow creating only rigid bounding boxes. Supervised learning methods rely on hyperparameters that have to be set by the user but do not have medical meaning and are difficult to be understood by non-engineering personnel. We aim to create a novel technique that is reproducible and improves accuracy thanks to the use of fuzzy logic. We believe that modeling the imprecision that affects bundle definitions can produce better results.

Part IV
Contribution

Chapter 5

Tracts segmentation

This chapter contains the contributions made to the segmentation of white matter tracts by means of fuzzy sets theory. The aim is to extract individual fiber bundles from a one million fibers tractogram exploiting the concepts introduced in FuzzyTract, bringing this novel approach from a proof of concept state [50] to a validated technique.

The first part of the work was to analyze medical literature to find appropriate tracts definitions and to translate them in query language. When some important parcellations were not present in the atlas, combinations of segmented structures or different definitions were used. The definitions were then evaluated using FuzzyTract to create the corresponding fuzzy spaces.

The second step was to exploit the generated fuzzy spaces to extract the individual tracts from a brain tractogram. For this purpose, TractSeg bundles have been used as reference tracts to find an appropriate extraction threshold. A comparison between our results and the ones obtained with different techniques have been performed to assess the validity of the outputs.

Finally, some functionalities were added to FuzzyTract. It has also been created a tool capable of extracting multiple tracts at the same time and to merge them in a unique final model of the brain, where each tract is represented with a different color. A 3DSlicer plug-in was also implemented.

5.1 Use of TractSeg bundles as reference tracts

As we have said, it does not currently exist a brain tracts atlas that we can exploit as reference. Moreover, anatomical definitions are usually vague or imprecise and we cannot be sure that the obtained result is quantitatively close to reality. Therefore, the questions are how to extract a fiber tract and how to know that the obtained fibers are the ones that we were searching for. To answer these questions, we decided to use as reference tracts the ones obtained in TractSeg. In particular, as described in subsection 3.2.2, the best would be to exploit the binary masks they generated to create their own reference system, since they underwent a medical expert examination, but they are not open access. TractSeg authors allow however free access¹ to all tracts that they have obtained for 105 HCP subjects. We underline that, as well as said by TractSeg authors in their paper, their model *does not* represent the ground truth. However, since it is at our knowledge the widest open access fiber tract atlas until now created, we can exploit it as our reference to help bundles extraction and to assess the validity of the results. It shall remain valid that, since these tracts are not the ground truth, the value that we will obtain from a quantitative comparison represents just an indication and must not be interpreted as the real score that we would have obtained making a comparison with an accepted model. The first thing to do, is thus to obtain the same dataset of TractSeg and to generate the corresponding tractograms.

5.1.1 Data extraction

TractSeg used 3T dMRI volumes of 105 subjects chosen from the “HCP Young Adult” dataset publicly available online. In order to make a comparison between their approach and our method based on fuzzy set theory, the diffusion volumes of the same subjects were downloaded and used to create the whole tractograms. Brain tractographies have been generated using MRtrix² and a server with CPU Intel® Xeon® E5-2695 v4 @ 2.10 GHz, 72 cores to achieve our maximum computing performances and to minimize the time to extract the data. The tractogram generation is indeed a crucial point on which depends all the rest of the work. At this step, one should not trade speed for accuracy. The estimation of white matter connection from diffusion volumes is however a highly time and resource consuming process and the use of a classical desktop computer to generate the data for such a large quantity of subjects would have taken several days or also weeks. The use of a server allows to dramatically reduce the required time preserving accuracy.

Once the whole-tractograms have been obtained, they have been split in left-hemisphere tractograms and right-hemisphere tractograms with the purpose to later use them separately to extract the fiber tracts for the two half of the brain. This process has been done as a pre-processing step to lighten the resources consumption of the extraction algorithm that will be described later, but it can be in any case integrated as part of the extraction algorithm itself.

The splitting has been carried out using a binary space as inclusion/exclusion region, with “True” values in the left half of the space and “False” values in the right one. The space has been firstly used as inclusion region to obtain the streamlines of

¹https://zenodo.org/record/1287850#.XX9_Afz0M5k

²<http://www.mrtrix.org/>

the left-hemisphere, where only streamlines that traversed all inclusion region have been accepted. Then, the same space has been used as exclusion region to extract the right-hemisphere, where streamlines that entered the exclude region, thus the region that before was the inclusion region, have been discarded.

Brain anatomy and tracts pathway have to be considered also during the data extraction process, otherwise some fiber bundles risk to be excluded already in this phase, leading to an impossible detection during the extraction process. Indeed, nerve fibers in human brain can be divided into three groups according to their pathway and the areas they connect: association fibers, commissural fibers and projection fibers. Association fibers are the tracts that connect cortical areas within the same hemisphere, commissural fibers are the ones that cross the two hemispheres allowing them to communicate and projection fibers are tracts that connect the cerebral cortex to the lower parts of the brain and the spinal cord. It is to note that in previous whole-tractogram splitting, the commissural fibers (e.g. corpus callosum) have been discarded and do not appear in any of the two half-tractograms, since they do not completely traverse the inclusion region when the space is used for the left half and they enter the exclusion region when the space is used for the right half. However they can be easily recovered simply making a difference between the whole-tractogram, that contains the fibers connecting the two hemispheres, and the two half, that do not contain them.

It is further to note that some projection fibers like the corticospinal tract decussate at the level of the medulla (Figure 5.1). This means that, if we consider for example the corticospinal tract starting in the left-hemisphere, it remains in the left half until it reaches the medulla and here it obliquely crosses from the left part to the right one. This would make the tract to be discarded in both cases of the whole-tractogram splitting. However, this does not happen because the tractograms extracted from the dMRI volumes, inferiorly ends at the peduncles level. This means that we can use the binary space without worrying about decussation and that the tracts that decussate won't be discarded while extracting the two half tractograms.

The final results are three volumes: a left-tractogram, a right-tractogram and a volume which contains the streamlines crossing the two regions.

Since now we used a powerful server to extract the data from dMRI volumes as fast as possible. However the next tracts extraction from the half tractograms have to be made on ordinary devices. The idea is indeed to create an algorithm that can run on everyday computers, since the source code will be made accessible to everyone so that an user can modify an anatomical definition or add a new one. With this purpose in mind, all tests but the tractograms extraction have been carried on a tower station with the following characteristics:

CPU Intel® Xeon® E5-1620 v2 @ 3.70 GHz, 8 cores

RAM 16G

OS Ubuntu 18.04.2 LTS

MRtrix offers the possibility to chose across a wide range of algorithms to perform the operations that lead to the generation of a tractogram. In TractSeg documentation, a MRtrix pipeline to extract whole-brain tractograms has been provided to obtain a 10 million streamlines model per subject, however the required computational time for data extraction was not specified and a test on one single subject

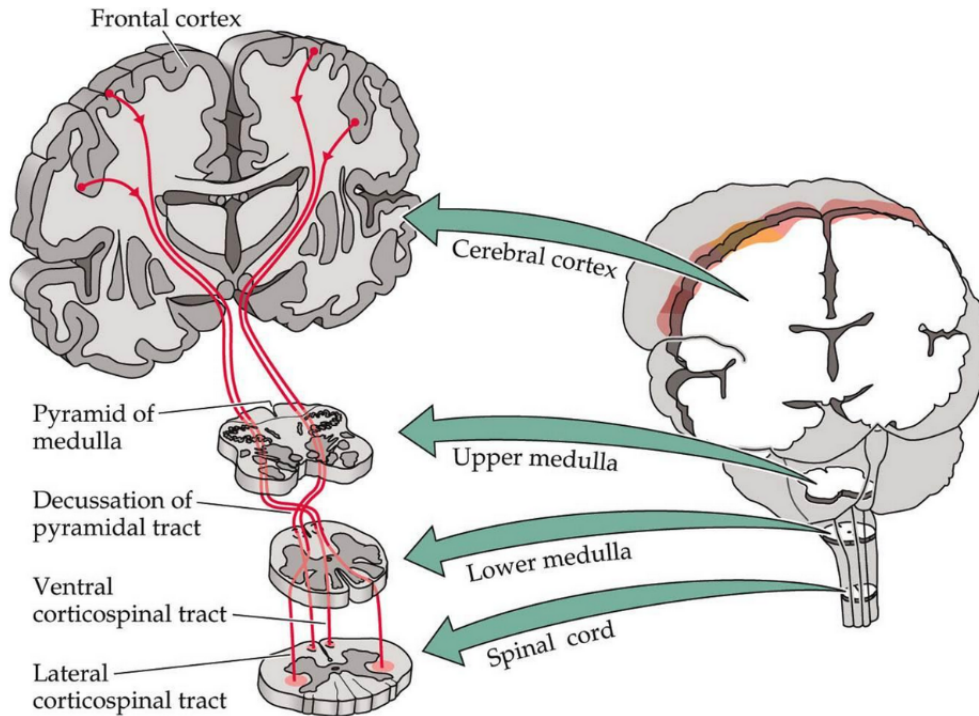


Figure 5.1: Decussation of corticospinal tract (CST) at the medulla level. The oblique crossin of this tract does not affect data extraction since whole-tractogram streamlines stops at the level of peduncles

showed that almost 4 hours were needed to compute the task and to obtain the half tractograms. A total of 17 days would have been necessary to obtain all the data. Moreover, the dimension of the output tractogram for the tested individual was overly big: 33.4 GB for just the left hemisphere tractogram in VTK format or 11.4 in TRK extension! Such huge dimensions would have made any elementary operation extremely time and resource consuming, without even considering that it would have been needed a computer with a huge RAM, consistently exceeding the common nowadays devices commercially available. And even supposing to have such a computer, such an enormous file would have been impossible to be processed in the fiber extraction algorithm without a pre-downsampling step that would have decreased the number of streamlines, making the time used to compute the 10 million fibers tractogram quite useless. For this reason, a new pipeline whose result is a 1 million streamlines model has been proposed. It revealed to take 30 to 40 minutes per subject (including the time to transfer the data from the server to the local machine), giving as output a file of about 3 GBs for the whole-tractogram. Even if these times may seem very long, they are actually normal times when extracting tractograms, considering that it is possible to need many days or also weeks to accomplish the task. MRtrix pipeline optimization was not the goal of this thesis but other solutions can be explored in future, like using the method proposed in [51], that promises to extract whole-brain tractograms made by 4 million streamlines from a 105 subject HCP dataset in just 25 hours. Our pipeline took approximately 2 days (51 hours) to get the data.

The dataset was split in a training set composed of 85 subjects and a test set of 20 subjects. The training set was used to find an appropriate extraction threshold

for each segmented tract. The thresholds were then applied to the subjects of the test set to extract the corresponding bundles.

5.2 Angle tuning

Once the tractograms have been generated using MRtrix, we want to extract individual fiber bundles starting from the anatomical definitions found in literature. In particular, one important parameter that allows to create more precise anatomical definitions is the “aperture” cited in Figure 4.4, which permits to exclude undesired regions that can lead to an imprecise result in fiber extraction. Its use is *optional* and a definition can be evaluated also without setting this parameter, however in certain cases its use may reveal to be useful. But how to know the optimal degree of aperture that allow us to exclude unwanted portions of the space and, at the same time, that minimizes the exclusion of streamlines belonging to the wanted tract? The automatic tuning of “aperture” parameter is the answer.

When writing an anatomical definition, the easiest and fastest way to proceed is to translate the definition found in literature to the query language without setting any aperture parameter. Sometimes however, some fundamental structures that are necessary to create the relations are not present in the atlas and the operator is forced to combine different structures to obtain the wanted one. This leads to a deviation from the original definition that may cause to obtain unexpected results if no correction is applied. Introducing the aperture parameter in the definition allows to be more precise when some structures are missing and to obtain a more precise result.

Other times, it is necessary to write an anatomical definition imposing the aperture parameter to some or all relations. This turns out to be extremely useful for instance when the result obtained with the “fast way” differs from the expected one and it is necessary to modify the definition. Another example is when we have to cope with difficult or long definitions: the combination of the aperture parameters for all the relations must be properly chosen in order to have a reliable result. This is not at all an easy task, especially when we are using more than three structures, and manually tuning each parameter for each relation until the desired result is attained is boring, heavy and highly time consuming for an operator. In all cases, the solution is, first, to automatically tune the aperture parameters to explore all possible combinations and, second, to establish a decision criteria in order to find the combination that gives the best result.

However, it is to remember that every time a definition is evaluated, a fuzzy space is produced and changing just one parameter is equivalent to create a new definition, thus every time we tune a single aperture parameter, we produce another definition. In addition, the time necessary to compute a definition depends on the number of structures but also on their dimension. So the more the number of the used structures, the more the parameters to tune and the greater the time that has to be spent to create the fuzzy set, with a larger time required in case of big structures.

Since the aperture parameter has no medical meaning and some difficulties may be encountered by a non-engineering personnel, a pre-defined range to be tuned may be imposed to each relation, without the need to be changed. The execution time

is however very variable and, as said, depends on the definition. Given a certain number of structures and assuming we want to set an aperture parameter for each of them, the total number of combinations and thus of definition to evaluate is given by (5.1).

$$\text{Num def to evaluate} = \text{num relations}^{\text{length of the range}} \quad (5.1)$$

If for instance we have a definition composed by 3 relations and we want to set an aperture parameter for all of them in a range that is for example $[0.1, 0.4]$, thus exploring 4 different parameters per relation, we will have to evaluate 81 definitions. One can freely decide to use the pre-defined range, but diminishing its length dramatically speeds up the process, minimizing the number of iterations. The final decision on how many parameters to tune and how many relations to use in the definition is left to the user.

Once all the combinations have been evaluated, we end with a certain number of fuzzy spaces, one per combination. We need now to use a criteria that tells us which is the best combination of aperture parameters, thus the best combination that produces a fiber tract as close as possible to the reference one. Different ways have been explored.

5.3 Segmentation Pipeline

The goal is to extract a specific fiber tract from the tractogram of a subject exploiting the similarity with a known reference tract and with the help of a fuzzy space. To do that, we need to furnish three different inputs: one tractogram of the subject for which we want to extract the tract, the known reference tract from TractSeg and the fuzzy space obtained with the evaluation of the definition for that tract. The pipeline can be summarized in:

1. Selection of the best fuzzy space according to a criteria
2. Application of the fuzzy space to all tractogram streamlines
3. Progressive cancellation of selected tractogram streamlines with low membership degree until reaching the best model

5.4 Step 1: Best fuzzy space selection

Once we have evaluated all the combination of parameters, we obtain a certain number of fuzzy spaces. We need now to establish a rule that permits to decide which one is the best fuzzy set. We consider as the best fuzzy set, the space whose voxels with the highest membership degree are the ones crossed by the reference streamlines. That is, if we ideally insert the reference fiber tract into the fuzzy space, we would like to have the highest membership degree exactly in the voxels crossed by the streamlines, with progressively decreasing membership degrees as soon as we move away from the reference tract. In this way, when we apply the fuzzy space to the subject tractogram, as we will see later, we can extract the streamlines that cross the regions where the membership degree is the highest and discard the

others (Figure 5.2). We will obtain a tract as similar as possible to the reference one.

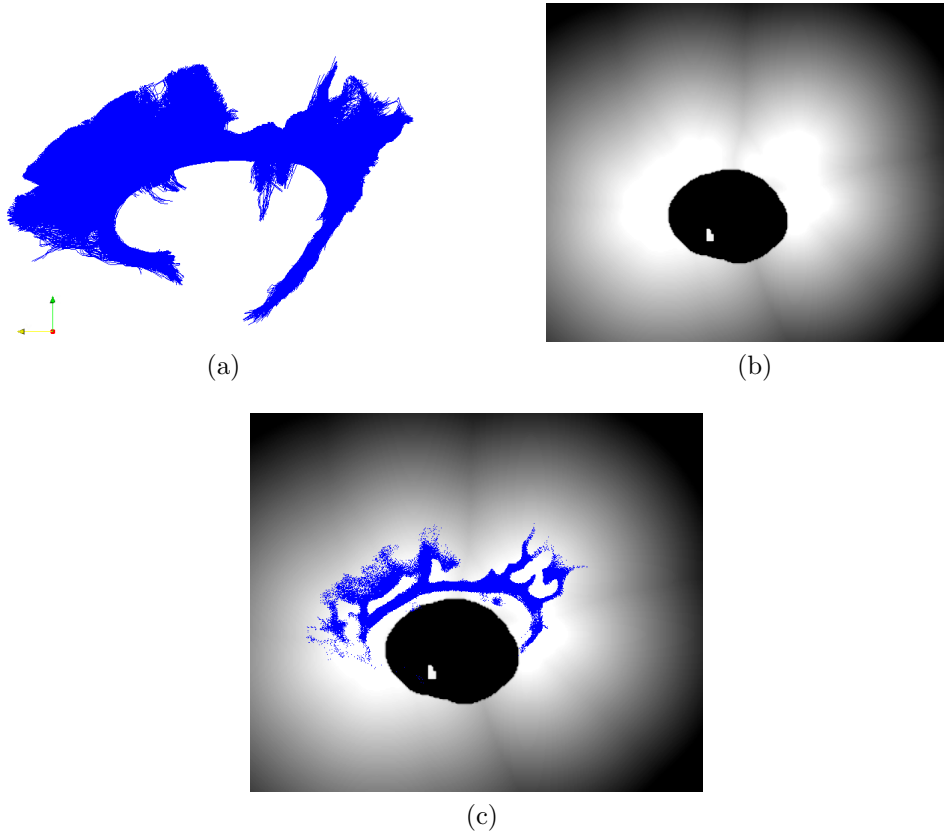


Figure 5.2: Reference tract and fuzzy space overlap. (a) TractSeg reference cingulate bundle, (b) Section of the fuzzy space obtained from literature definition. The voxels with highest membership degrees are brighter than the others. Imposing a threshold, we want to extract only the streamlines that are in these whiter voxels (and thus that correspond to the definition), (c) Overlap between (a) and (b). The brighter voxels are the ones crossed by the reference bundle.

5.4.1 Error map

The first approach we used to select the best fuzzy space relies on the evaluation of an error map. This is generated computing the difference between the space containing the reference streamlines and the normalized fuzzy space. If we write a proper definition, the normalized fuzzy space has higher membership degree in the voxels crossed by the reference streamlines (values close to 1) and lower values in all other voxels. The space containing the reference streamlines is a binary space where the unitary value is given to the voxels crossed by the streamlines. It represents the ideal condition where the membership degree is 1 where there are the streamlines and 0 where they are not present. It follows that, computing the difference between these two spaces, the values inside the error map will be low, possibly close to zero, in correspondence of the voxels crossed by the streamlines while they will be higher in all other voxels. What we would like to have are very small values in the region crossed by the reference tract. The difference allows us to understand "how many" small values we have and thus "how good" is the evaluated definition. The concept

can be understood also looking at Figure 5.2 (c). Each blue dot represents a voxel crossed by a reference streamline and has value 1. The underlying fuzzy space, when normalized, has values ranging from 0 to 1. Voxels with values closer to 1 are brighter than the others. When we compute the difference between the space containing the reference tract and the normalized fuzzy space, we get a new space that has low values if the voxel is crossed by the reference streamline AND has a high membership degree (Figure 5.3).

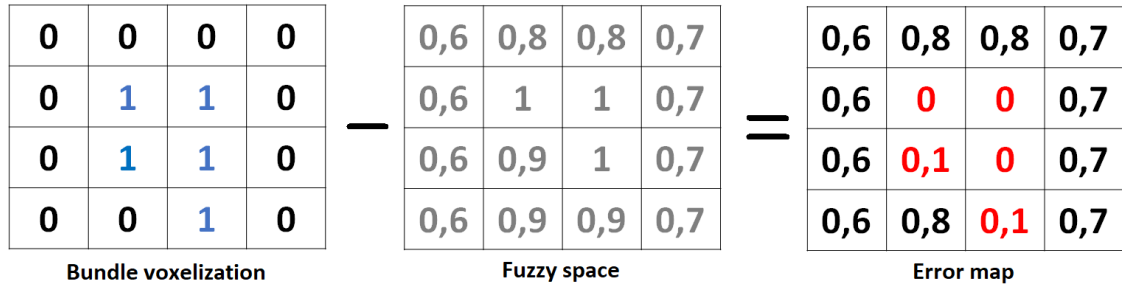


Figure 5.3: Visual representation of the error map. The left matrix represents the voxelization of a bundle, with value 1 in voxels crossed by the streamlines (blue) and 0 anywhere else. The matrix in the middle is the representation of a fuzzy space whose fuzzy values have been normalized between 0 and 1. Their difference in absolute value gives the error map: a matrix that has, in voxels crossed by streamlines, low values for good fuzzy spaces and increasing values for worst fuzzy sets.

In each voxel of the error map there will thus be a value that describes the distance, namely the error, from the ideal condition. To obtain a global score of each error map and to choose the best fuzzy space, we compute the mean between all the values of the error map and we choose the one with the lowest mean. The associated fuzzy space is the fuzzy space that gives the best result.

In other words, we are searching for the fuzzy space which is the closest to the ideal binary condition. This may seem a contradiction, since it may look like that we are trying first to compute a fuzzy space to benefit of its flexibility and to compensate for the drawbacks of a crispy space, and then we are trying to come back to a binary space. Actually, we do not want to reach the binary condition (and it wouldn't be possible) but we just use it as a model to understand which fuzzy space allows us to extract the highest number of streamlines belonging to the wanted tract and to discard the maximum number of unwanted ones. We want to preserve the fuzzy space because it allows us to keep a certain degree of flexibility that can be used when extracting the wanted tract: it arbitrarily permits to increase or decrease the portion of the space where to search for the desired streamlines.

The fact that the space containing the reference streamlines is a binary space is the result of a voxelization process. Indeed, before computing the difference between the two spaces, we have to pass from a .trk or .vtk file where the streamlines are saved as a sequence of 3D voxel coordinates, to a NifTI image where each voxel has a value equal to 1 if it is crossed by a streamline or a value equal to 0 if it is not. Moreover, in order to compute the difference, the NifTI image needs to have the

same dimensions of the fuzzy space. We thus use the affine matrices to pass from voxel to mm coordinates and we then create a space as big as the fuzzy set to attach at the corresponding voxels the proper binary values. The difference can be finally calculated.

The limit of the error map approach is that it is very sensible to outliers. Indeed, if we have a certain number of error values which are much more bigger than the others, the whole average will be shifted to that values, possibly causing the algorithm to discard that fuzzy space. Multiple tests showed that is not uncommon that the algorithm prefers a worst space, but that does not have outliers, with respect to a space that would give better results but that contains outliers. This depends on the definition used and it is detectable only trying manually to use other combination of aperture parameters, thus making the algorithm useless. This approach can be used if we want the algorithm to provide an initial guess of the best fuzzy space but we need to keep in mind that it may exists a better result and a manual tuning of the aperture parameters may be necessary to asses the validity of the result. We thus decided to search for a better solution.

5.4.2 Delta Metric

Clustering

The second method aims to select the best fuzzy space using a clustering technique and analyzing the relationship between the centroids and the fuzzy spaces. Because of the high number of streamlines contained in a tractogram, a process that needs to perform geometrical operations between them, would in any case be high memory and time consuming. Indeed the dimensions of the half-tractogram are around 1.5 GB in .vtk format and it contains around 400.000 streamlines. Processing such a quantity of polylines, when possible, would burden more and more the algorithm as we proceed further with the operations, making the whole process very slow and lowering in general the code performances. As it is common to do when working with large tractographies, we decided to simplify the complexity of the data set reducing the number of streamlines to work with. The first idea to think of could be to apply a simple downsampling, selecting just a certain percentage of streamlines, but as we said before this would make the data extraction useless and, in addition, it could reduce the amount of information useful to extract the desired tract. It would be furthermore necessary to decide which streamlines have to be neglected and why. On the contrary, computing the clusters of the tractogram and extracting its centroids preserves the totality of the information and at the same time it enormously decreases the number of remaining polylines. In literature, there are different clustering algorithms but almost all of them share the same limitation: they are very slow and they often need to calculate pairwise distances between all streamlines, which is very high time and memory consuming. In 2012 however it have been developed a novel clustering algorithm by Garyfallidis [52] which is extremely faster, up to 1000 times with respect to classical algorithms, and which has on average linear time $O(N)$ complexity, with N the number of tracks. We thus decided to use his algorithm named QuickBundle (QB) to perform tractogram clusterization and obtain a few thousand centroids.

The QB average linear time $O(N)$ complexity comes from the fact that it calcu-

lates clusters just one time and it saves only the indexes of the streamlines belonging to the clusters, not the whole streamline, saving time and memory. It is based on a metric called Minimum average Direct-Flip (MDF) described by (5.4.2).

$$\begin{aligned}
 MDF(s_A, s_B) &= \min(d_{direct}, d_{flipped}) \\
 d_{direct}(s_A, s_B) &= \frac{1}{K} \sum_{i=1}^K \|x_i^A - x_i^B\|_2 \\
 d_{flipped}(s_A, s_B) &= \frac{1}{K} \sum_{i=1}^K \|x_i^A - x_{K-i}^B\|_2
 \end{aligned} \tag{5.2}$$

Considering a set of streamlines, the algorithm randomly selects one of them and imposes it to be the first cluster (the first cluster is thus temporarily composed by only one streamline). It then selects another streamline and computes the MDF distance from the first one. If the distance threshold chosen by the user is not overcome, it assigns the selected streamline to the first cluster, otherwise it creates a second cluster that is composed, for the moment, by only this second streamline. It proceeds in this way associating the streamlines to a cluster according to their MDF distance with that cluster.

The peculiarity of QB is that, when a streamline is associated to a cluster, the “virtual track” of the cluster is computed. This is a streamline that does not exist in reality and is placed at the average distance of that cluster fibers, making it considerable representative of that cluster. In this way, a set of streamlines belonging to a cluster can be represented as a single “virtual track”. This heavily speeds up the process, since when the next streamlines is selected, it is sufficient to calculate the distance between the selected streamlines and the “virtual tracks” to associate it to a cluster, and not the distance with all the streamlines composing all clusters. The algorithm continues until all the streamlines have been associated to a cluster (Figure 5.4). A virtual track is the average of all tracks in the cluster and is thus the centroid of the cluster.

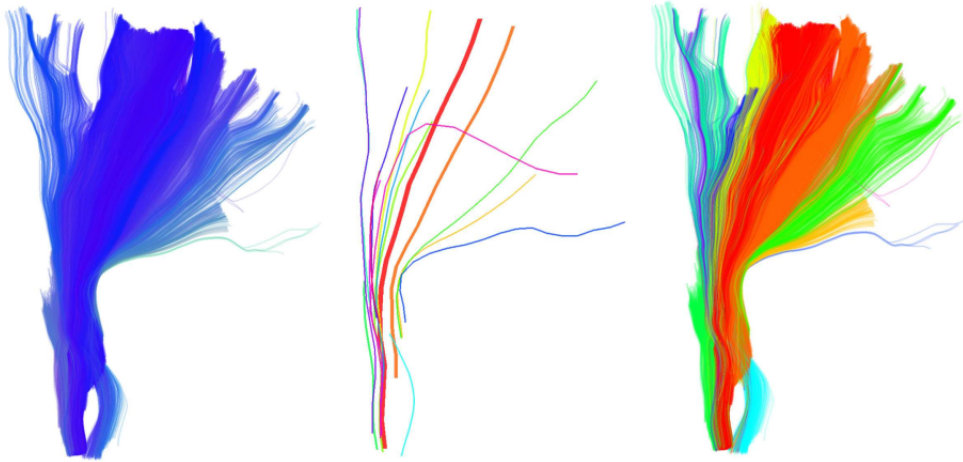


Figure 5.4: The CST, shown on the left, has been clusterized using quickbundle whose result is a certain number of centroids, shown in the middle. Each cluster is represented with a different color in the right picture

It is to note that, by contrast to k-means, we do not have to guess an initial number of clusters but we just need to specify a distance threshold. Moreover, if we were using k-means, at every iteration we would have had to reassign streamlines to clusters, slowing down all the process. In QB there is no recalculation of clusters and it passes through the tracks only once, assigning a streamline to one cluster only.

The only parameters we have to specify in input are the distance threshold and, because of the MDF metric, the number of points to which the streamlines have to be downsampled, since this kind of metric requires that tracks have all the same number of points. Normally [65], 10 mm is considered a very low threshold and 12 points are sufficient to downsample a streamline and permit not to lose the information on its geometry and not to perturb the algorithm linearity (such a perturbation begins to be evident with more than 20 points and at lower thresholds). These constitute for this reason the parameters we provided in input to obtain the clusters and the centroids of both the tractogram and the reference TractSeg tract.

Metric evaluation

Once we have obtained the tractogram centroids, we want to extract the ones whose distance between the reference centroids is the lowest. This is done computing the MDF distance between the reference centroids and ours centroids and selecting, for each reference centroid, which is the one between ours whose distance is the shortest. We end with a certain number of “closest” centroids. All the others are saved into a set and considered as the “farthest” centroids.

We then apply the fuzzy space to each centroid contained in the two groups. Applying a fuzzy space to a centroid means to compute the average membership value of the centroid, according to the values stored in the fuzzy set. This gives to the centroid the average satisfaction degree of the relation describing the tract. In other words, if we consider a single centroid, since it is nothing but a sequence of consecutive voxels, we give to each of its voxels a fuzzy value according to the ones stored in the current fuzzy space. We then compute the mean of all values to obtain a single score per centroid. This score tell us which is the average membership degree of that centroid in the current fuzzy space.

Each centroid of the “closest” and “furthest” group now is described by a fuzzy value. We compute the mean separately for the two groups to have an idea of “how much” they respect the definition. We obviously obtain a high average membership value for the “closest” group and an overall low membership value for the “farthest” group.

We repeat the procedure for all fuzzy spaces and we choose as the best fuzzy space the one for which the distance between the two groups is the biggest. We call this “delta” criteria. This can be seen a clusterization of the centroids in two clusters in which the best space is the one that maximizes the inter-cluster distance.

5.5 Steps 2 and 3: tracts extraction

Once we have chosen the best fuzzy space we need to extract the wanted fiber bundle from the tractogram, with the help of the fuzzy logic. We thus apply the fuzzy space to the tractogram streamlines so that each of them gets a fuzzy value describing their

degree of membership with the fuzzy space. It allows us to decide if it belongs to the wanted tract or if it has to be excluded. When all streamlines of the tractogram got a fuzzy value, we can impose an exclusion threshold to decide which of them form the desired tract and which ones have not to be considered. Again, we want to automatize the process to avoid having to manually try different threshold and we want to establish a decision criteria which returns the best exclusion threshold. The first idea was to apply a general threshold in the range $[0, 1]$, where 0 means that the algorithm has to exclude no streamlines and 1 means that it has to exclude every streamline, with step values of 0.05. We saw however that, depending on the fuzzy space, such a step value might be too wide and might lead to the exclusion or inclusion of too many streamlines. Using a step value of 0.01 is the optimal solution but it means that we have to iterate the process approximately 100 times with all related memory and time consumption problems. To preserve accuracy and reduce computational efforts we need therefore to find a shorter threshold range and reference streamlines come us in aid. Indeed, we apply the fuzzy space to the reference tract so that each of its streamlines gets a fuzzy value and then we compute the mode of all fuzzy values. In this way we know which is the average membership degree of the reference tract to the current definition and we fix a lower bound to the threshold range. We decided it to be of 0.05 steps inferior to the calculated mode, since directly using the mode as lower bound would exclude also some desired streamlines. We didn't use the minimum fuzzy value because in case of outliers it would result in an inaccurate exclusion. The upper bound is set to be 0.05 steps superior to the mode.

At this moment, we have to decide which is the threshold that permits to extract a fiber bundle as close as possible to the reference one. For each threshold, we extract the remaining streamlines and we compute their voxelization to obtain a binary space. We also compute the voxelization of the reference tract to obtain another binary space. Then we want to find a measure of "how much" our binary space is similar to the reference binary space. We used as evaluation metric an index which is one of the most popular measures for evaluating segmentation performance: the dice score D [53]. It is indeed a statistic coefficient used to measure the similarity between two samples and it is calculated from another coefficient called Jaccard index J (5.3). The latter is defined as the dimension of the intersection of two sets divided by the dimension of their union. We choose as the best threshold the one that returns the highest dice score.

$$J(A, B) = \frac{|A \cap B|}{|A \cup B|}$$

$$D = \frac{2J}{1 + J}$$

5.5.1 Dice score correction: the convex hull approach

For what concerns the computation of the dice score, we have to remember that the reference TractSeg bundles have been obtained from a 10 million tractogram while our bundles have been extracted from a 1 million tractogram, and they therefore contain on average one tenth of the streamlines of the reference tracts. This means that, when generating the binary mask, the binary volume of the reference tract

will be more “filled” than the mask obtained from our bundle which will be, on the contrary, characterized by a “holed” pattern. In other words, the fact that our tract is less dense the reference one leads to the generation of a less dense mask with respect to the reference one, even if the obtained streamlines are mostly superimposed to the considered TractSeg bundle.

Since the dice score is calculated superimposing the two masks and exploiting their union and intersection, the “holed” mask lowers the true score that we would have obtained using two filled masks. To solve the problem and to obtain two filled binary masks we computed a 3D convex hull for both the reference tract and our bundle.

For a set of points, a convex hull is the smallest convex set that contains that subset S . In particular, a subset $S \subseteq \mathbb{R}^3$ is convex if for any two points p and q in the set the line segment with endpoints p and q is contained in S . The convex hull of a set of points $P \in \mathbb{R}^3$ is a convex polytope with vertices in P . The example of what convex hull does is represented in 2D in Figure 5.5 (a) and in 3D in Figure 5.5 (b).

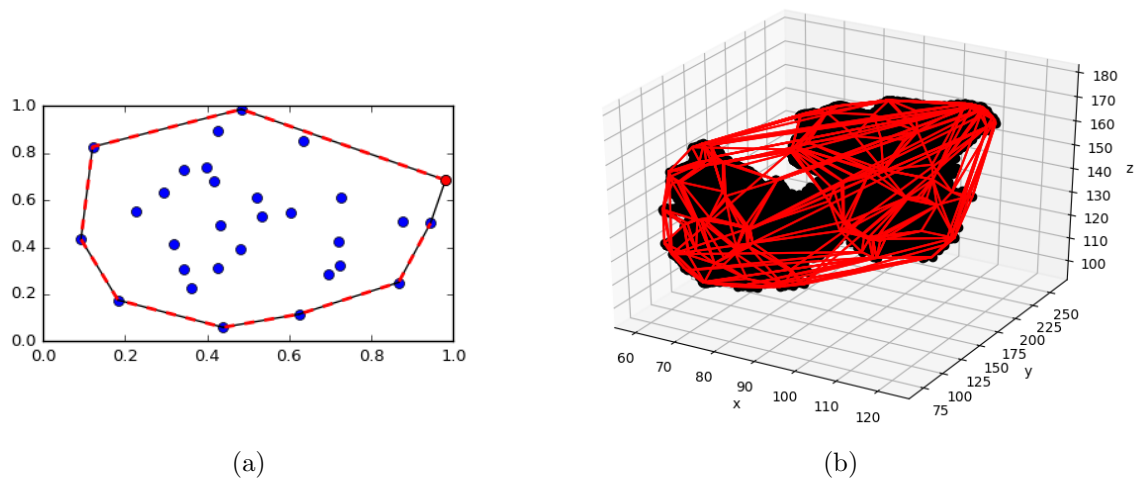


Figure 5.5: Convex hull in 2D (a) and 3D (b)

We downsampled the streamlines points to simplify the polytope computation and evaluated the dice score for the two volumes. We then incremented the number of points to make a comparison with the previous dice scores. As we can see in Figure 5.6, the dice becomes bigger and bigger as we increase the number of points until reaching a plateau at approximately 15 points. From that value on, the computational time increases without giving a better dice score. We thus conclude that 15 points per streamline is a good value to obtain an optimal convex hull.

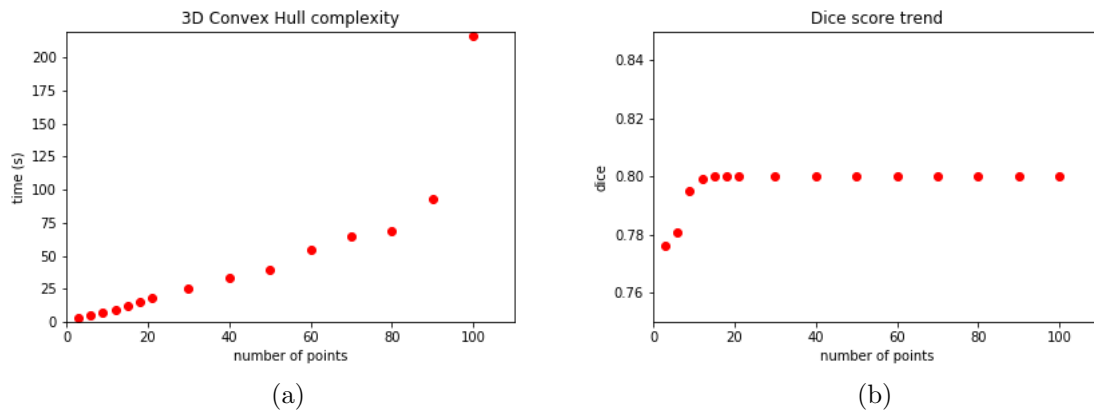


Figure 5.6: 3D convex hull time complexity (a) compared to dice score improvements (b). Data refers to the SLF II bundle composed by 10980 streamlines but the same result has been obtained with other tracts. We can see that, if we use more the 15 points per streamline, the computation time increases while there are no improvements on the dice score.

Moreover, we can see from 5.6 that the process has a linear complexity if we stay in the optimal interval 3 – 80, then the linearity is lost if we increase the number of points.

The limitation of convex hull is that it does not accounts for concave parts in a set of points. That is, if we think of a streamline with a U shape, the function will just connect the two endpoints regardless of the middle point, filling the concavity and losing the information on the streamline shape (Figure 5.7).

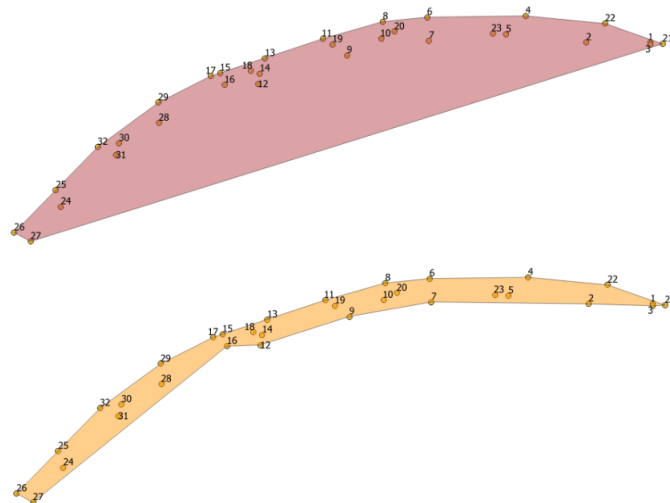


Figure 5.7: Limitation of the convex hull approach. Down in the image it is shown the ideal result, up in the picture there is the real one

5.6 Between bundles

As part of the work we developed a new spatial relation that has been included in FuzzyTract. It is called “between bundles” and, as the name suggests, it gives fuzzy values to a region located between two already computed bundles. The relation can be used alone or together with the others mentioned before to create a fuzzy space. It is particularly useful to replace some missing structures or in case of a bundle whose path is between two others known tracts, as it is for the Superior Longitudinal Fasciculus II (SLF II), which is mostly located between the SLF I and the SLF III (Figure 5.8)

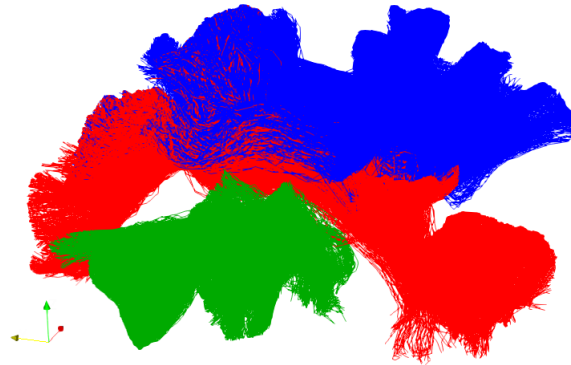


Figure 5.8: SLF I (blue), SLF II (red) and SLF III (green) from TractSeg

In this case we do not have a structure binary mask as it was for previous spatial relations, thus we cannot compute its borders to evaluate the fuzzy cones. What we firstly did was to generate the binary mask with the voxelization process and to then apply the mathematical morphological operations to obtain its borders. However, since tracts are bigger than the parcellations of our atlas, they have much more points and the cones computation resulted to be a too high memory consuming process for which a normal computer RAM was not sufficient.

The second idea was to directly use the streamline points as starting points for the cone computation, without the need of generating a binary mask. In particular, the idea is to:

1. Compute the direction vector between the center of mass of the two bundles;
2. Generate the fuzzy cones for each point of the first bundle and compute their union;
3. Generate the fuzzy cones for each point of the second bundle and compute their union;
4. Compute the intersection between the two fuzzy sets to obtain the final space.

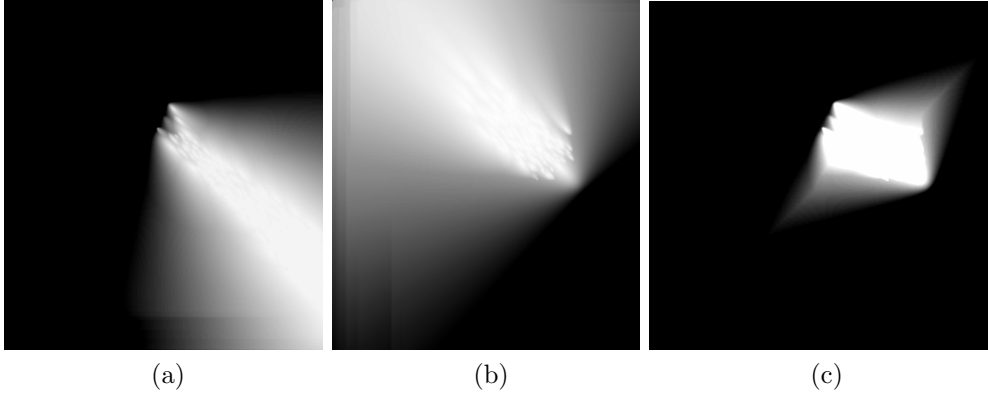


Figure 5.9: (a) step 2, (b) step 3, (c) step 4

Remember that step 1 is necessary to determine the direction for cone computation. Indeed, for instance, one of the cones that goes from the first bundle to the second one has as its vertex one of the points of the streamlines of the first bundle, and it has as direction the parallel to the vector that connects the two centers of mass. This direction determines which voxels will have the highest membership degree.

While we need all the streamlines points to comply with step 1, it would be unnecessarily heavy to maintain all of them for cones computation. For this reason, we applied a downsampling on all streamlines and we used different number of points to find which one was the best to get a good space in a reasonable time. We used the SLF I and SLF III taken from subject 599469 of TractSeg dataset. These tracts are composed respectively by 4531 and 1084 streamlines and have, on average, 25 points each. We downsampled them to a number of points that goes from 3 to 9 and collected the results in Figure 5.10 (a). During downsampling, the extremities of the streamlines remain fixed while the remaining points are chosen between the ones of the streamline so that they form segments of equal length.

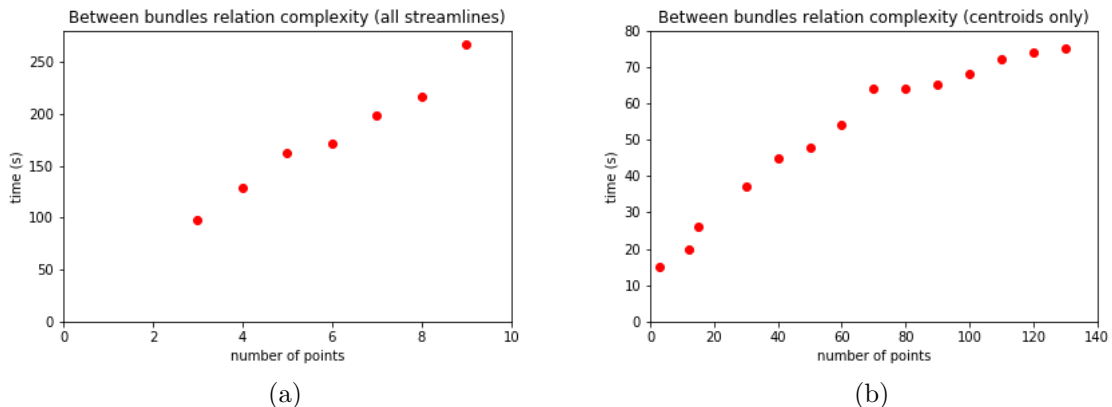


Figure 5.10: Complexity of between bundles relation using all streamlines (a) and only centroids (b)

The results show us that this approach has a complexity of $O(N)$ in the analyzed interval, but it allows up to 9 points per streamline. Above that value the RAM

memory is not sufficient and the algorithm fails to proceed. Moreover we can see that, just with 9 points, the time needed is approximately 5 minutes.

To overcome this limitation, we computed the centroids of each bundle obtaining 16 streamlines for SLF I and 6 for SLF II and then we repeated steps from 2 to 4. As the number of points is 250 times lower and the centroids are adequately representative for the tracts, this solution dramatically improved the computation performance. The downsampling was conducted in a range 3-100 points and showed a complexity of $O(N)$ (Figure 5.10 (b)).

5.7 Post-processing

Fuzzy logic has since now used to obtain a model of the bundle on the basis of a reference one. However, because of its intrinsic flexibility, it might give a tract that contains streamlines that do not belong to the wanted tract. This is the main drawback of using a mean fuzzy value to describe a streamline but can be easily detected looking at the bundle and is simple to remove. We can indeed perform a simple analysis on principal streamlines direction to clean the tract and exclude streamlines whose properties differ from the one of the reference tract. Looking at the tracts, it is then possible to chose between the preferred version of the tract. This post-processing phase is in any case automatic and optional.

5.7.1 Principal direction and tortuosity

Many fiber bundles have a dominant principal direction (also called first principal direction), that is, their course follow a preferred direction with respect to the others. For instance, the corticospinal tract (CST) has a superior-to-inferior first principal direction since it starts in cortical areas of the brain and goes down into the spinal cord. If we extract the first principal direction of the reference streamlines, we can compare it to the first principal direction of our obtained streamlines and eliminate the ones that show a different behavior (Figure 5.11). At this purpose, the three principal directions of each streamline, called principal components, are computed using PCA (Principal Component Analysis). Basically this technique assumes the direction with the highest variance to be the first principal direction and the amount of variance retained by each principal component is measured by the so-called eigenvalue. Thus the principal component with the highest eigenvalue is the first principal direction. Knowing the dominant direction of the reference streamlines it is possible to clean the model eliminating the streamlines that have a different first principal direction, or that have a smaller eigenvalue.

A further correction could be made comparing the streamlines tortuosity, defined as a measure of how many turns and twist the streamlines performs during his course, between our and the reference tract. In particularly we firstly used the arc-chord ratio (ACR), the ratio between the the length of the streamline and the distance between its endpoints. The ACR is equal to 1 for a straight line and is infinite for a circle, thus the higher the ACR value, the higher the tortuosity. The ACR is a degree of how much a streamline has a U-shape and allows their elimination from our tract if they are too different from the reference tract. However, it does not accounts for the winding, which is a measure of the turning angle between consecutive segments of a streamline. Computing this other measure contributes to the bundle cleaning.

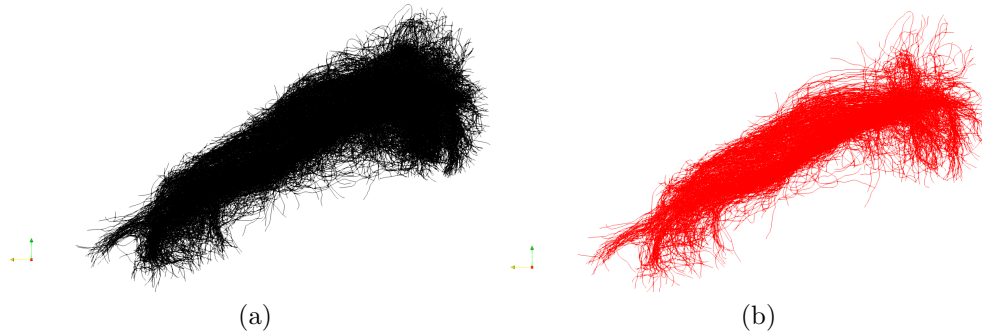


Figure 5.11: ILF uncleaned (a) and cleaned (b) streamlines using principal direction

Contrary to expectations, we obtained bundles that were too clean and, in the end, composed by just some hundreds of streamlines. That was mainly caused by the tortuosity cleaning. The reason is that our streamlines are composed by on average 100 points while TractSeg streamlines have, on average, more or less 25 points. This strong difference was causing the winding to have very different values from the reference and thus to exclude too many streamlines. Finally, since the initial idea was to use the TractSeg reference just as an initial hint on the bundle location and general shape and not to faithfully rely on someone else model, we decided not to perform the tortuosity cleaning because it would have led to the application of too selective constraints. We instead maintained the principal direction cleaning since it gives just a general and proper measure of the streamlines geometry. It can in any case be undone to allow the user to choose the preferred model.

Chapter 6

Tracts modelling

This chapter contains the list of all modelled bundles. Each section describes a different tract and has two paragraphs. The first paragraph contains the anatomical definition found in literature while the second one the explication of the reference structures used.

It should be noted that the number of segmented structures at our disposal is sometimes not sufficient to write a proper definition and other structures different from the ones found in literature have to be used. Moreover, it may happen that the classical definition leads to the creation of a too wide space that has to be reduced using other reference structures.

A summary of all tracts and definitions can be found in tables [6.1](#), [6.2](#) and [6.3](#) at the end of the chapter. The definitions in red have been used in the beginning to model the tracts, but after an analysis of their impact on the final result (See Table [8.2](#)) we concluded that they can be removed without causing a change in the final output.

In the last page of this chapter, Figure [6.1](#) shows all the obtained tracts.

6.1 Arcuate Fasciculus (AF)

The arcuate fasciculus [\[54\]](#) is a nerve tract that connects the lateral temporal cortex with the frontal cortex, arching around the Sylvian fissure. It can be divided into three segments according to the area they connect: an anterior indirect segment, a posterior indirect segment and a direct segment. The anterior indirect segment connects the ventral portion of the precentral gyrus and the posterior part of pars opercularis to the supramarginal gyrus. The posterior indirect segment links the posterior middle temporal gyrus to the angular gyrus. Finally, the direct segment includes the nerve fibers that directly goes from the anterior termination of the anterior indirect segment to the dorsal termination of the posterior indirect segment, thus connecting the ventral portion of the precentral gyrus and the posterior part of the pars opercularis to the middle and inferior temporal gyrus.

The segmentations at our disposal are not detailed as the ones described in the definition found in literature. For example, the precentral gyrus is not segmented in its ventral and dorsal portion and including the whole structure in the definition would lead to consider a huge quantity of fibers that do not belong to the definition, thus making the detection of the anterior indirect segment hard. Moreover,

we encountered difficulties in modelling the posterior indirect segment since the angular gyrus is not present in the segmentations. We tried to replace it using the most similar closest gyrus, which is the supramarginal gyrus, but this resulted in unsatisfactory results. The best option was to include the three segments in a single definition comprehensive of all the areas. We used the inferior temporal gyrus as posterior termination and the caudal-middle frontal gyrus as anterior termination. The latter lies indeed just above the pars opercularis and allows to include the fibers whose terminations are in the ventral portion of the precentral gyrus and in the posterior part of pars opercularis. Finally, the Sylvian fissure, also known as lateral sulcus, separates the frontal and parietal lobes superiorly from the temporal lobe below [55]. Since we do not dispose of fissure segmentations but we want to preserve only the fibers that arches around it, we used as exclusion structure the putamen. It turned out to be too big since it leads to the exclusion of an excessive number of fibers but it was the best compromise to exclude unwanted fibers around the Sylvian fissure.

6.2 Anterior Thalamic Radiation (ATR)

Thalamic radiations [56], also known as thalamocortical pathways, are nerve fibers that connect the thalamus to the cerebral cortex. They are divided in different fasciculi according to their direction inside brain. The Anterior Thalamic Radiation (ATR), also called thalamofrontal fasciculus, connects, as the name suggests, the thalamus with the frontal pole of the brain. In particular it connects the anterior and medial lateral nuclei of the thalamus to the cortex of the frontal pole.

In our definition, at first a big space in between the anterior part of thalamus and the frontal pole is created. Then some reference structures that lie close to this space, like the putamen, the caudal-anterior cingulate gyrus and the rostral-anterior cingulate gyrus are used to eliminate any fiber that from the thalamus does not go directly to the frontal pole. Finally, since the relations did not take into account the medial part of the thalamus, we used the caudate nucleus to include the fibers that start from this region.

6.3 Cingulate Fasciculus (CG)

The cingulate bundle is located above the corpus callosum. In particular, according to [61], it originates in the temporal pole, turns forming a “ring-like” belt around the corpus callosum and terminates in the orbital-frontal cortex.

The main structure we need to use to create the definition is, as we can see from literature, the corpus callosum. Unlikely this is not present in the segmentations at our disposal. We can however use a structure which is just above the corpus callosum and that follows pretty accurately his pathway, giving the name to the cingulate fasciculus. This is the cingulate gyrus and we have all its segmentations, from the rostral-anterior segment to the isthmus. We also exclude unwanted fibers that lie under the cingulate gyrus exploiting the putamen as reference structure.

6.4 Corticospinal Tract (CST)

The corticospinal tract is the major descending motor pathway and rules the movement of distal extremities. It can be divided in three parts according to whether they decussate or not in the medulla: the crossed lateral, the uncrossed lateral and the uncrossed anterior (ventral) CST. The crossed lateral segment is the largest one and constitute between 75% and 90% of the the CST fibers [57]. All the segments mostly originates in the precentral gyrus, continue through the centrum semiovale and descend in the posterior limb of the internal capsule, occupying the anterior portion of the posterior half for the most part of their course. The tract then enters the midbrain through the cerebral peduncle and course toward the medulla where the most part of them decussate [58].

In our query definition, we use the precentral gyrus as beginning region for the CST fibers and we consider all its inferior space since it contains the region crossed by the tract. This space below the precentral gyrus is however too wide and in order not to include unwanted fibers we exclude part of it using the caudate nucleus as reference structure. Finally, since fibers enter the internal capsule, thus they enter the region contained between the thalamus and the putamen, we exclude the area outside the internal capsule using the Putamen as reference. Since the definition tells us that the CST occupies the two-thirds of the posterior limb of the internal capsule, but in our segmentation we do not have such a structure, the only thing we can do is to consider the internal capsule in its entirety, leading to a tract that contains more streamlines than the one described in literature. Moreover, given that the tractogram has been obtained from dMRI volumes that stops at peduncles, we do not have any information on the medulla and we cannot distinguish between the three parts of the CST, thus we consider it as a single segment.

6.5 Fronto-pontine Tract (FPT)

The fronto-pontine tract arises from the frontal lobe and passes through the anterior limb of the internal capsule [11], until reaching and crossing the anterior one-third of the cerebral peduncle [59].

To create the definition of the fronto-pontine tract we use as starting region for the fibers the frontal pole and we consider all the area included between him and the internal capsule. Since the space is bigger than the region crossed by the tract, we introduce some constraints using other reference structures. In particular, we exclude all the area that directly surrounds the internal capsule but is is not directly connected with the frontal pole, as well as all the region that is inferior to the internal capsule and anterior to the peduncles, where the fibers enter to continue their path until the nuclei of the pons. As for the CST, since we do not have a segmentation for the internal capsule but we have to recreate it has a combination of relations between the thalamus and the putamen, we are obliged to consider all the fibers that cross the internal capsule and not just the ones that pass in the anterior limb, as it would be required by the FPT definition. However, since we impose as starting region the frontal pole, we are able to exclude the majority of unwanted streamlines but some unwanted fibers might remain.

6.6 Inferior Cerebellar Peduncle Fasciculus (ICP)

The ICP is known as the spinocerebellar tract and is the set of afferent fibers that goes from the spinal cord, through the peduncles, to the cerebellum.

During the writing of the definition, since the use of the cerebellum structures was not possible, we used the closest superior structures as upper bounds for the wanted region, namely the inferior temporal gyrus and the lingual gyrus. Since these structures are clearly located far above from the superior part of the cerebellum, we excluded from the space, by means of the pallidum, the region that lies between the superior part of the cerebellum and these structures to not consider unwanted fibers. The fibers going through the peduncles are considered just using the inferior relations with the inferior temporal gyrus and lingual gyrus.

6.7 Inferior Longitudinal Fasciculus (ILF)

The inferior longitudinal fasciculus connects the occipital lobe with the anterior temporal lobe, with branches with the fusiform gyrus, the middle temporal gyrus, the lingual gyrus and a minor link with the cuneus [60].

We translated the definition in query language using the temporal pole as anterior termination and the lateral occipital gyrus as posterior termination, which lies close to the cuneus. We used the middle temporal gyrus and the fusiform gyrus as constraints to both reduce the dimension of the space to one crossed by the tract and to possibly consider the branch of the bundle in these areas. A further constraint represented by the Hippocampus was necessary to limit the space in the wanted region.

6.8 Superior Longitudinal Fasciculus (SLF)

As said in [62] the SLF is an association fiber tract composed by three separate components, according to the areas they connect. They link frontal and opercular areas with the superior-parietal lobe (SLF I), the angular gyrus (SLF II) and the supramarginal gyrus (SLF III). The AF discussed earlier is considered to be the fourth component of the SLF (SLF IV).

6.8.1 Superior Longitudinal Fasciculus I (SLF I)

The SLF I originates from the medial and dorsal parietal cortex and terminates in the dorsal and medial part of the frontal lobe [62].

According to the definition, we firstly generated a big space that extends from the superior frontal gyrus to the superior parietal gyrus and then we applied some constraints to reduce it to the path that directly connects the frontal with the parietal gyri.

6.8.2 Superior Longitudinal Fasciculus II (SLF II)

SLF II is located just above the insula. It extends from the angular gyrus to the caudal–lateral prefrontal regions [62].

In our definition, we firstly included the space which goes from the angular gyrus to the prefrontal regions using the inferior-parietal gyrus and the rostral-middle-frontal one. Then we reduced the space dimensions with secondary relations and excluded the region under the insula.

6.8.3 Superior Longitudinal Fasciculus III (SLF III)

The SLF III begins in the supramarginal gyrus and ends in the ventral premotor and prefrontal areas, also known as Brodmann areas 6 (part of precentral gyrus), 44 (pars opercularis) and 46 (middle third of middle frontal gyrus and rostral inferior frontal gyrus) [62].

Our definition imposes the tract to begin in the inferior parietal gyrus, just above the supramarginal gyrus to consider also the streamlines that crosses the supra-marginal structure. Instead, Brodmann areas (BAs) are not segmented. They are usually formed by just some parts of the parcellations, like BA6 which is composed by just one part of the precentral gyrus, thus using the corresponding segmented parcellation in its entirety would lead to wrong results. To tackle this difficulty we decided to create an initial big space using the inferior parietal gyrus and then to apply different constraints with the surrounding structures to adapt the region to the one crossed by the tract and to include in the definition the not segmented BAs.

6.9 Summary tables

The following tables contains the list of all the modelled tracts, their classical definition found in literature, the source of that definition and our query definition. To simplify the visualization of the query definitions in the tables, the word "aperure=" is omitted from the relations and only the corresponding value is displayed. For the same reason, the "_of" term is neglected (e.g. the relation "right_of" is abbreviated in "right").

Tract list			
Name	Reference article	Anatomical definition	Query definition
AF	Bernard et al. [54]	Connects the ventral portion of the precentral gyrus and the posterior part of pars opercularis to the middle and inferior temporal gyrus	between(ctxlhcaudalmiddlefrontal, ctxlhinferiortemporal) and not left(LeftPutamen, 0.01) and not right(LeftPutamen, 0.4)
ATR	Kakou et al. [56]	Connects the anterior and medial lateral nuclei of the thalamus to the cortex of the frontal pole	(anterior(LeftThalamusProper, 0.1) and not anterior(ctxlhfrontalpole, 0.6) and not inferior(LeftPutamen, 0.3) and not right(wmlhcaudalanteriorcingulate, 0.45) and not right(wmlhrostralanteriorcingulate, 0.45)) or (posterior(LeftCaudate, 0.1) and not posterior(LeftThalamusProper, 0.5))
CG	Wu et al. [61]	Located above the corpus callosum. Originates in the temporal pole, turns forming a “ring-like” belt around the corpus callosum and terminates in the orbital-frontal cortex	(proximity(ctxlhsthmuscingulate) or proximity(ctxlhcaudalanteriorcingulate) or proximity(ctxlhrostralanteriorcingulate)) and not right(LeftPutamen, 0.1)
CST	Almasri [58]	Originates in the precentral gyrus, continues through the centrum semiovale and descends in the posterior limb of the internal capsule. Enters the midbrain through the cerebral peduncle and course into the medulla	inferior(ctxlhprecentral, 0.01) and not inferior(LeftPutamen, 0.1) and not left(LeftPutamen, 0.1) and not right(LeftCaudate, 0.3)

Table 6.1: Tracts definitions (Part I)

Tract list			
Name	Reference article	Anatomical definition	Query definition
FPT	Jellison et al. [11] and Ture et al. [59]	Arises from the frontal lobe and passes through the anterior limb of the internal capsule, until reaching and crossing the anterior one-third of the cerebral peduncle	(left(LeftThalamusProper, 0.5) and right(LeftPutamen, 0.5) and not anterior(wmlhfrontalpole, 0.5) and not posterior(ctxlhsthmscingulate, 0.4) and not right(ctxlhcaudalantteriorcingulate, 0.4)) and not (inferior(LeftAmygdala, 0.6) and left(LeftAmygdala, 0.5)) and not(inferior(LeftAmygdala, 0.6) and anterior(LeftAmygdala, 0.5))
ICP	Mendoza [63]	Begins in the cerebellum and runs through the peduncles	right(wmlhinferiortemporal, 0.5) and inferior(wmlhlingual, 0.1) and anterior(wmlhlingual) and not posterior(LeftPallidum, 0.05)
ILF	Herbet et al. [60]	Connects the occipital lobe with the anterior temporal lobe, with branches with the fusiform gyrus, the middle temporal gyrus, the lingual gyrus and a minor link with the cuneus	(anterior(ctxlhlateraloccipital, 0.2) and posterior(ctxlhtemporalpole, 0.2)) and not inferior(ctxlhfusiform, 0.1) and not inferior(ctxlhmiddletemporal, 0.05) and not right(LeftHippocampus, 0.3)
SLF I	Makris et al. [62]	Originates from the medial and dorsal parietal cortex and terminates in the dorsal and medial part of the frontal lobe	(posterior(wmlhsuperiorfrontal) or anterior(wmlhsuperiorparietal)) and not inferior(wmlhposteriorcingulate, 0.4) and not anterior(wmlhfrontalpole, 0.65) and not posterior(ctxlhcuneus, 0.35) and not left(ctxlhprecentral, 0.01)

Table 6.2: Tracts definitions (Part II)

Tract list			
Name	Reference article	Anatomical definition	Query definition
SLF II	Makris et al. [62]	Located above the insula. It extends from the angular gyrus to the caudal-lateral prefrontal regions.	anterior(ctxlhinferiorparietal, 0.1) and posterior(ctxlhrostralmiddlefrontal, 0.1) and not left(LeftThalamusProper, 0.16) and not right(ctxlhinsula, 0.2) and not left(ctxlhinsula, 0.1) and not (ctxlhtransversetemporal, 0.4) and not inferior(ctxlhparsoptoculic, 0.1)
SLF III	Makris et al. [62]	Begins in the supramarginal gyrus and ends in the ventral premotor and prefrontal areas, also known as Brodmann areas 6, 44 and 46	(anterior(ctxlhinferiorparietal, 0.05) and superior(ctxlhsuperiortemporal, 0.1)) and not left(wmlhsuperiorfrontal, 0.01) and not left(LeftThalamusProper, 0.01) and not superior(ctxlhposteriorcingulate, 0.4)

Table 6.3: Tracts definitions (Part III)

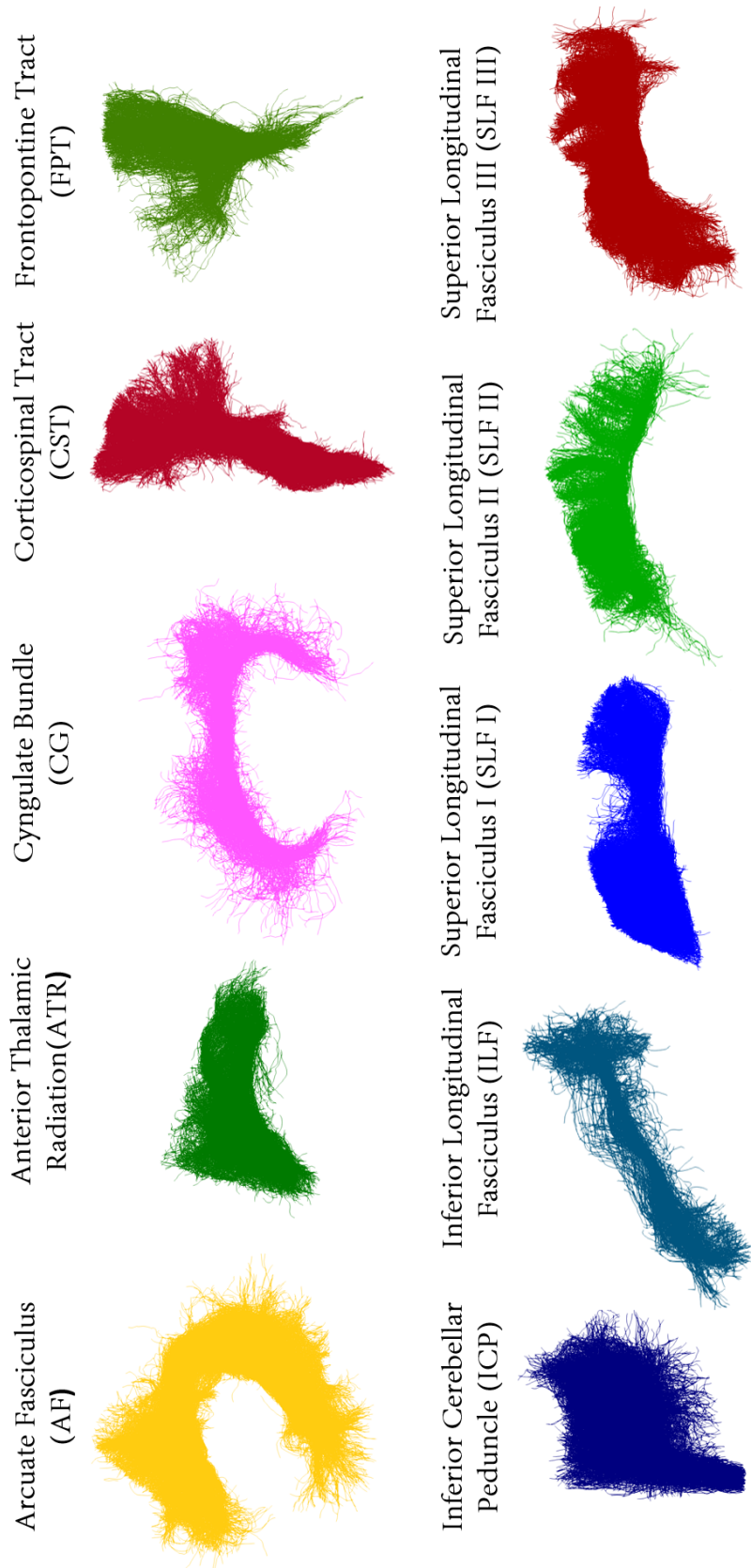


Figure 6.1: All the 10 segmented tracts

Chapter 7

FiberExtractor

FiberExtractor is the base algorithm that includes all the previous steps and is able to evaluate all the tract definitions, to extract the corresponding fiber bundles and to merge them in a unique model. The final volume contains all the segmented tracts, represented with a different color to allow an easy visualization. We created two version of this extraction algorithm, one for training and another for test purposes. The training version aims to find the best extraction threshold for each tract using TractSeg bundles as reference model. The test version, uses the best threshold found to extract the wanted bundles, without exploiting TractSeg model.

One modification have been made to the steps cited in the previous chapters, in order to speed up the process and to ensure an acceptable execution time for what concerns tracts extraction and merging. It has been proved that this modification does not affect accuracy but dramatically decreases the computation time and costs needed. The general pipeline remains thus the same (fuzzy spaces generation and tracts extraction), with the add of a final tool that merges all bundles in a single volume.

7.1 Tracts extraction: fuzzy score simplification

To speed up the process, fibers extraction is performed in parallel. All tracts are extracted at the same time, without the need of waiting for one extraction to finish before beginning the next one. This parallel processing allows to obtain all the tracts with a single click and decreases the time needed by a factor of 7 or 8 with respect to a serial approach, but some bottlenecks may still be present due to the big amount of processed data. In particular, we found an heavy slowdown when applying the fuzzy space to the whole tractograms. The aim was to give a fuzzy value to each streamline of the tractogram in order to extract, according to a threshold, only the ones that better fit the current anatomical definition, but the huge amount of fibers was requiring 30 minutes just for this step. The solution is to split the fuzzy space application in multiple steps:

1. Computation of tractogram clusters and centroids
2. Application of the fuzzy space to the tractogram centroids
3. Selection of a restricted number of streamlines

4. Application of the fuzzy space to the restricted group
5. Selection of the streamlines that give the best dice score

The first step consists in computing the tractogram clusters using Quickbundle and in finding their centroids (Figure 7.1 (b)). The fuzzy space is then applied only to these centroids and the ones whose fuzzy value does not respect the current threshold are discarded, together with the clusters they belong to. On the contrary, the centroids that respect the threshold are preserved as well as their clusters and the corresponding streamlines. In this way, we applied the fuzzy space to just few hundreds of centroids (instead of hundreds of thousands fibers) and we ended up with a number of streamlines that is much less than the ones of the initial tractogram. This first part can be seen as a “reduction process” that is used to get a restricted number of streamlines (Figure 7.1 (c)) to which apply again the fuzzy space. The same fuzzy space is indeed applied to the remaining streamlines, their fuzzy value is calculated and the ones whose value is bigger than the threshold are preserved and constitute the wanted fiber tract (Figure 7.1 (d)). The result is the fiber tract extracted in a much faster way.

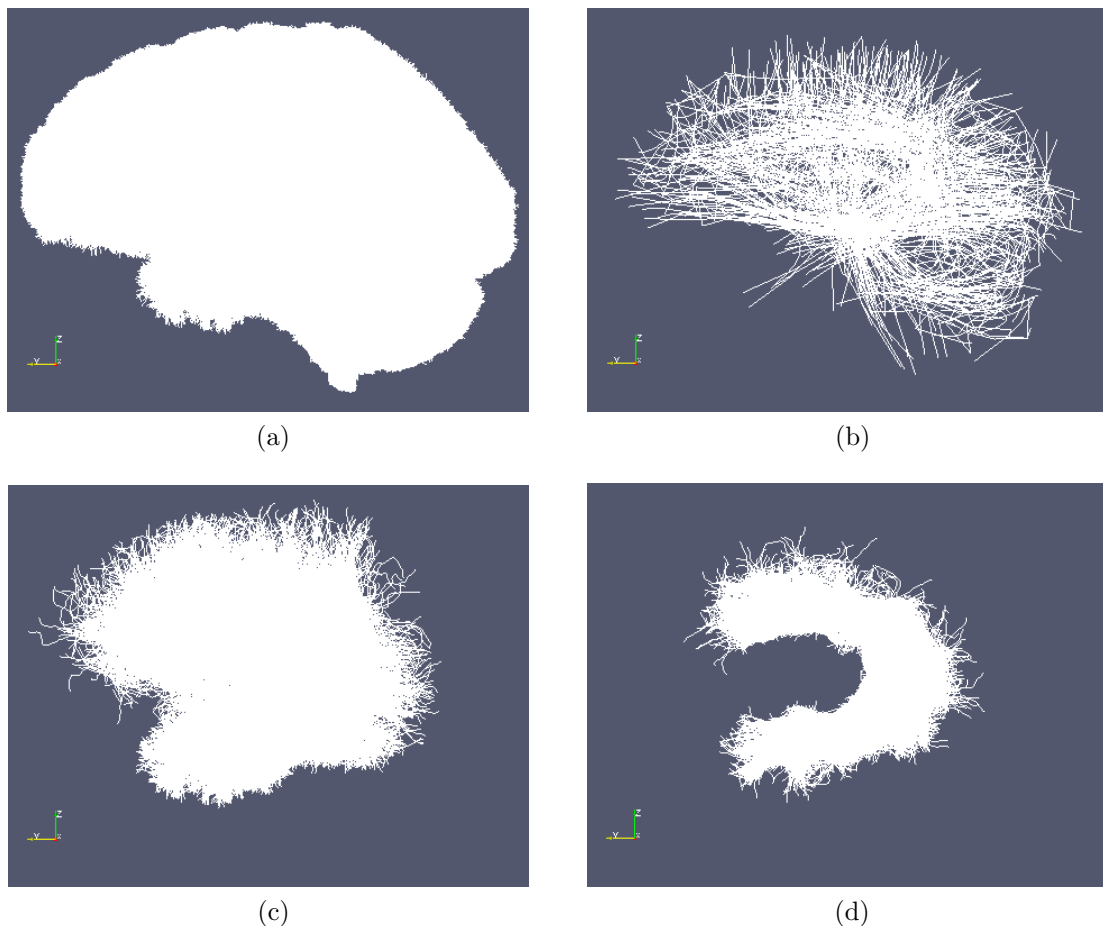


Figure 7.1: Extraction of the left hemisphere Arcuate Fasciculus. From the tractogram (a), we compute its centroids (b), we preserve the corresponding streamlines that respect the current threshold (c) and we extract the fiber tract (d).

The clustering parameters (12 points, 20 mm) are in this case less stringent

than the ones presented in [section 5.4.2](#), since centroids are used here just to get a restricted number of streamlines. This allows to have a quick cluster computation and, at the same time, it preserves accuracy since the wanted tract is then extracted from the restricted streamlines.

The steps are repeated for all the threshold range and the dice score is computed for each extraction. Finally, the fiber tract that gives the best dice score is given in output. The whole process is carried out in parallel, thus at the same time, for all of ours 10 tracts.

The time needed for the extraction of 10 tracts, trying 7 different thresholds for each bundle during the training process, is 11 minutes per subject. This duration does not include the time needed to create the corresponding fuzzy spaces since it is very variable, depending on the number of used structures and their dimension and depending on the number of tracts one wants to extract. Including the time for fuzzy spaces generation, the whole time is 1 hour per subject. In any case, the advantage is that tracts definitions have been written on the basis of the anatomical knowledge, thus they are valid for *any* healthy adult subject. There is no need to rewrite the definitions when extracting the bundles for a new subject, even if the user is free to add any new definition or to change the existing ones. What is required is instead the definitions evaluation that lead to the creation of the corresponding fuzzy spaces. Definitions do not change across subjects but their fuzzy spaces do, since they refer to parcellations which are proper of each subject. The fuzzy spaces have thus to be computed for each subject.

7.2 Tracts merging and VTK to OBJ conversion

Once all the tracts have been extracted, they are saved in separate files so that they can be individually visualized. FiberExtractor provides also a tool that merges all tracts in a single volume, in order to give the user an overall view of white matter connections. Each tract is saved in the volume with a different color to facilitate its identification ([Figure 7.2](#)).

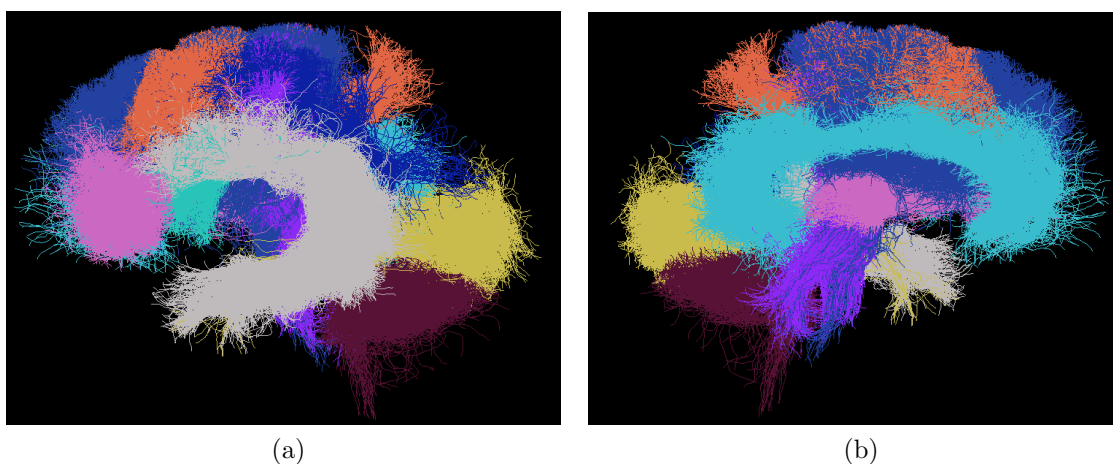


Figure 7.2: Side views of the 10 left hemisphere segmented tracts

The individual files and the volume containing all the segmented tracts have a

“vtk” extension, a popular data file format that can be loaded in softwares used in medical field, like 3DSlicer, to visualize the stored model. The limit is that this kind of file can store just one-dimensional structures like lines, whose visualization would be improved and made more realistic using a 3D model. For this reason, FiberExtractor provides a further tool capable of transforming one-dimensional lines into 3D cylinders, whose radius can be freely chosen by the user. The output are two files, an “obj” that contains the model and “mtl” file that contains the information on color, luminosity, reflectivity and transparency of each bundle. The “obj” is the standard 3D image format and is usually found in combination with the “mtl” material properties given to the model. They can be loaded and exported by a wide number of editing softwares.

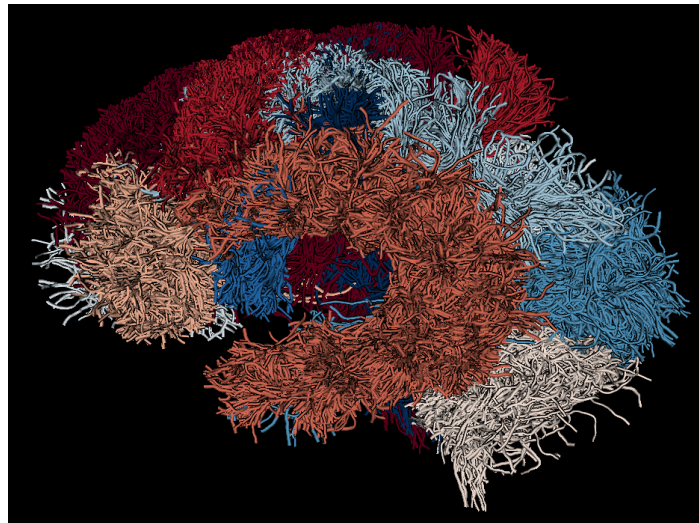


Figure 7.3: 3D rendering of the 10 tracts

A software that can be of particular interest for our purposes is Blender: we can give to each bundle a different degree of transparency, so that it is possible to analyze each tract individually but also to look at its relationship with the surrounding tracts.

7.3 Implementation of a 3DSlicer extension

3DSlicer is an open source software widely used in the medical field for image processing and three-dimensional visualization [64]. It is equipped with a large number of extensions that apply to many necessities, from whole heart segmentation from CT images to neurosurgical planning. In this thesis, 3DSlicer have been extensively used for visualization purposes. The great potential of this software is that it allows a certain degree of customization, and users with programming skills can decide to create their own extensions and to integrate them in the software architecture. This avoids the use of different softwares and helps to maintain the work in a compact environment.

For this reason, and as an example, we decided to create a plug-in to perform the VTK to OBJ conversion of individual tracts. The code has been written in python using an object oriented approach and then included in the software functionalities. It generates a user-friendly interface which is very intuitive and easy to use, where

the user has just to drag and drop the VTK file he wants to convert (Figure 7.4). The extension computes the conversion and saves the OBJ file in the same directory of the input file. This is a largely more human approach than the classical use of the command line to pass the parameters and launch the execution of a script. The idea will be then to transfer the whole algorithm for fiber extraction in a single 3DSlicer user-friendly plug-in.

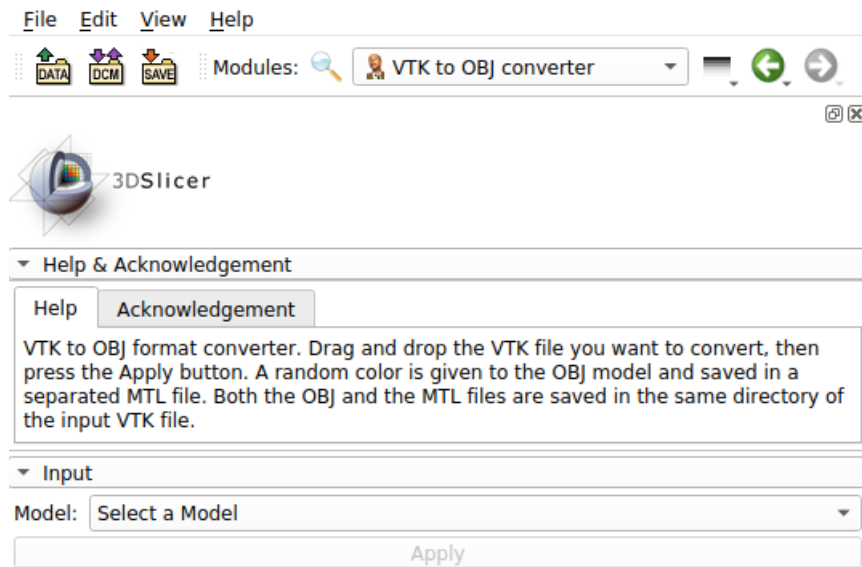


Figure 7.4: Screenshot of the functional part of the implemented 3DSlicer plug-in.

Part V

Results and discussion

Chapter 8

Results

8.1 Important relations

When writing an anatomical definition, one can use as many relations as he wants. However, as we have seen, limiting the number of used parcellations to the essential ones can importantly reduce the execution time. In order to understand which were the fundamental relations for our definitions, that is the ones without which the dice score would fall to unacceptable values, we analyzed the impact of each relation on the final result. We have removed one relation at a time and evaluated the resulting definition. The dice score was calculated for each evaluation and the fundamental relation was identified. Table 8.2 and Table 8.3 show the impact of each relation on the evaluated anatomical definitions. The relations in red are the ones whose removal speeds up the process without losing accuracy.

Before coming to conclusions, we have to remember that the convex hull method used to compute the dice score between our tracts and the reference ones has one important limitation. It is not capable to detect concavities, thus a binary mask with a U shape is not considered as an open mask but it is seen as a filled mask. The U shape is approximately seen as a filled O (Figure 8.1). This means that the convex hull approach gives the same dice score both for a U and a filled O, even if the latter contains many more streamlines than the U mask. We partially solved this problem creating fuzzy spaces that actually have U shapes for fibers with concave shapes, like the Arcuate Fasciculus (AF). In this way we are sure that, even if the convex hull approach will calculate a dice score between two O masks, in that masks they will be contained only streamlines with a U shape and in the concave region there will be no streamline. The erroneous filling won't thus have a big impact on the dice score computation. In any case, such an error can easily be detected looking at the result and it is sufficient to add a "not" relation to solve the problem.

In addition to the lack of a ground truth, the convex hull limitation imposes us to consider the dice score not as a real indicator of the representation of reality, but just as a suggestion of the goodness of a definition. Just for this analysis on important relations, the fact that some partial definitions have a higher dice score than the original one, does not necessarily mean that they provide a better output. A visual check is still necessary to assess the correctness of the result.

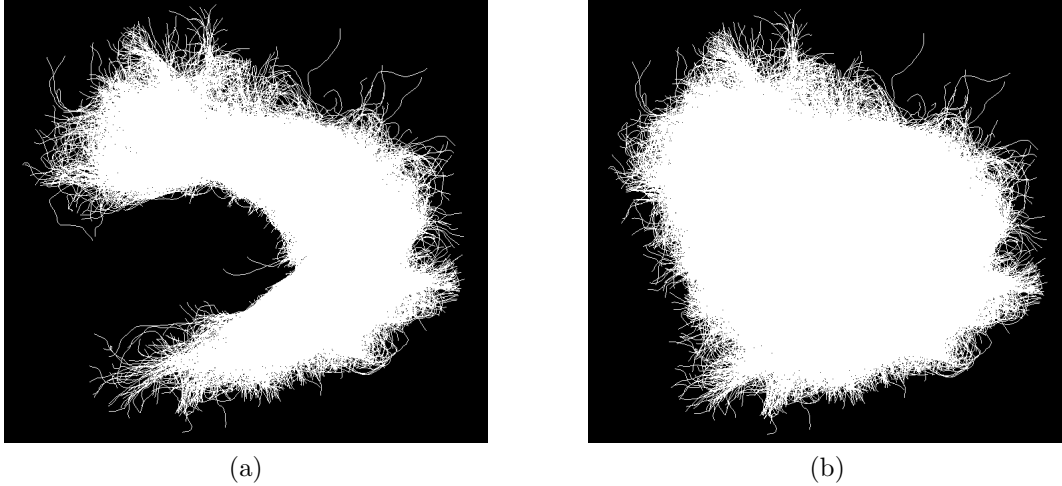


Figure 8.1: Limitation of the convex hull approach in dice calculation: the technique gives the same dice score for both sets of streamlines. The problem has been solved creating fuzzy spaces with U shapes for concave fibers. In this way we are sure that, even if the masks are accidentally filled, they only contains the streamlines shown in (a) and not the ones shown in (b).

However, during the “important relations” analysis, the removal of some parcellations does not guarantee the creation of a U fuzzy space and issues in dice score calculation may be present. For example, testing the partial definitions on the AF, we found that the first two dice scores correspond to reality while the third one is incorrect. It creates a O shape like the one in Figure 8.1 (b), giving him a wrong dice score. We can thus conclude that for the AF, the relation *between(ctxlhcaudalmiddlefrontal, ctxlhinferiortemporal)* is the fundamental one and its removal would cause a falling of the dice score. We could remove the relation *not right(LeftPutamen, 0,4)* and still maintaining an acceptable dice value, but since we do not want to trade speed for accuracy, we can say that for the AF all the used relations are important to reach a good final score.

Relations impact		
Name (Original Dice)	Removed relation	Dice
AF (0.83)	<i>between(ctxlhcaudalmiddlefrontal, ctxlhinferiortemporal)</i>	0.46
	<i>not right(LeftPutamen, 0.4)</i>	0.8
	<i>not left(LeftPutamen, 0.01)</i>	0.82
ATR (0.81)	<i>anterior(LeftThalamusProper, 0.1)</i>	0.23
	<i>not anterior(ctxlhfrontalpole, 0.6)</i>	0.76
	<i>not inferior(LeftPutamen, 0.3)</i>	0.74
	<i>not right(wmlhcaudalanteriorcingulate, 0.45)</i>	0.80
	<i>not right(wmlhrostralanteriorcingulate, 0.45)</i>	0.78
	<i>not posterior(LeftThalamusProper, 0.5)</i>	0.41
	<i>posterior(LeftCaudate, 0.1)</i>	0.43

Table 8.1: Table showing the resulting dice score when we remove a certain relation from the original anatomical definition of a tract (Part I)

Relations impact		
Name (Original Dice)	Removed relation	Dice
CG (0.82)	proximity(ctxlhisthmuscingulate)	0.69
	proximity(ctxlhcaudalanteriorcingulate)	0.71
	proximity(ctxlhrostralanteriorcingulate)	0.76
	not right(LeftPutamen, 0.1)	0.82
CST (0.76)	inferior(ctxlhprecentral, 0.01)	0.21
	not inferior(LeftPutamen, 0.1)	0.66
	not left(LeftPutamen, 0.1)	0.7
	not right(LeftCaudate, 0.3)	0.79
FPT (0.64)	left(LeftThalamusProper, 0.5)	0.55
	right(LeftPutamen, 0.5)	0.37
	not anterior(wmlhfrontalpole, 0.5)	0.64
	not posterior(ctxlhisthmuscingulate, 0.4)	0.57
	not right(ctxlhcaudalanteriorcingulate, 0.4)	0.64
	not inferior(LeftAmygdala, 0.6)	0.61
	not left(LeftAmygdala, 0.5)	0.64
	not inferior(LeftAmygdala, 0.6)	0.27
not anterior(LeftAmygdala, 0.5)	0.64	
ICP (0.72)	right(wmlhinferiortemporal, 0.5)	0.72
	inferior(wmlhlingual, 0.1)	0.2
	anterior(wmlhlingual)	0.75
	not posterior(LeftPallidum, 0.05)	0.64
ILF (0.7)	anterior(ctxlhlateraloccipital, 0.2)	0.6
	posterior(ctxlhtemporalpole, 0.2)	0.26
	not inferior(ctxlhfusiform, 0.1)	0.73
	not inferior(ctxlhmiddletemporal, 0.05)	0.78
	not right(LeftHippocampus, 0.3)	0.64
SLF I (0.74)	posterior(wmlhsuperiorfrontal)	0.45
	anterior(wmlhsuperiorparietal)	0.56
	not inferior(wmlhposteriorcingulate, 0.4)	0.42
	not anterior(wmlhfrontalpole, 0.65)	0.66
	not posterior(ctxlhcuneus, 0.35)	0.7
	not left(ctxlhprecentral, 0.01)	0.7

Table 8.2: Table showing the resulting dice score when we remove a certain relation from the original anatomical definition of a tract (Part II)

Relations impact		
Name (Original Dice)	Removed relation	Dice
SLF II (0.77)	anterior(ctxlhinferiorparietal, 0.1)	0.53
	posterior(ctxlhrostralmiddlefrontal, 0.1)	0.73
	not left(LeftThalamusProper, 0.16)	0.77
	not right(ctxlhinsula, 0.2)	0.72
	not left(ctxlhinsula, 0.1)	0.77
	not left(ctxlhtransversetemporal, 0.4)	0.77
	not inferior(ctxlhparsopercularis, 0.1)	0.78
SLF III (0.76)	anterior(ctxlhinferiorparietal, 0.05)	0.72
	superior(ctxlhsuperiortemporal, 0.1)	0.65
	not left(wmlhsuperiorfrontal, 0.01)	0.66
	not left(LeftThalamusProper, 0.01)	0.74
	not superior(ctxlhposteriorcingulate, 0.4)	0.69

Table 8.3: Table showing the resulting dice score when we remove a certain relation from the original anatomical definition of a tract (Part III)

For what concerns the Anterior Thalamic Radiation (ATR), the fundamental relations are the first one and the last two. All the others ones are important and contribute to have a good dice score, except for the *not right(wmlhcaudalanteriorcingulate, 0,45)*. The removal of this relation has a minimum impact on the dice score and causes negligible changes in tracts visualization. It is thus possible to remove that parcellation from the definition and speed up its evaluation.

In the Cingulate fasciculus (CG) the last exclusion relation *not right(LeftPutamen, 0.1)* can be removed. Unlike AF, the use of *proximity* relations already ensures that no streamline is present in the concavity and the last parcellation is redundant, thus it can be neglected.

In CST definition we should not remove the last relation, even if the final dice score is higher than the original one.

Considering the Fronto-pontine Tract (FPT), we can remove the third and fifth relations, namely *not anterior(wmlhfrontalpole, 0,5)* and *not right(ctxlhcaudalanteriorcingulate, 0,4)*, since they do not modify neither the dice score, neither they add or eliminate streamlines. On the contrary, the last relation removes some fibers but has the same dice score of the original definition, thus it cannot be deleted.

The analysis showed that the first relation of ICP, *right(wmlhinferiortemporal, 0.5)* does not add information to the final result and can thus be removed. The third relation, *anterior(wmlhlingual)* provides a better dice score. A visual check of the output revealed, however, that the global shape of the tract is lost in case of removal of this relation. In addition, further tests showed that the increase of the aperture parameter from 0.1 to 0.2 in the second relation *inferior(wmlhlingual, 0.1)*, highlighted in blue, would decrease the dice score but would allow a better global

shape visualization. This last changing should thus be considered to improve the final visual output.

Looking at the Inferior Longitudinal Fasciculus (ILF), it seems that the third and the fourth relations could be removed, since they improve the dice score. This is indeed true but, visualizing the result, we see that the output tracts fit very well the reference bundles all long the central region but they are less accurate at the extremities. We conclude that no relation should be removed. We prefer a more raw result with a good diffused accuracy than bundles whose accuracy is really high in some focused regions but that are not precise in others.

All relations are important in SLF I definition . However we saw that, even if it gives a smaller dice score, the relation *not posterior(ctxllhcuneus, 0.35)* should be removed so that streamlines that were not present in the original definition can be added.

According to visual check of SLF II results, we can remove the fifth relation *not left(ctxlhinsula, 0.1)* since its elimination does not change the final result. On the contrary, we cannot remove the third and last two relations, even if their dice scores are the same of the original one or slightly superior, since they remove wanted streamlines or introduce undesired ones.

Finally, in last tract SLF III, all relations are important and should not be removed to guarantee a good result.

8.2 Training and test

To test the correctness of an anatomical definitions and to see if the use for one single threshold is suitable for tracts extraction, we split the 105 subjects dataset into a 85 subjects training set and a 20 subjects test set. The training set is used to find the thresholds that give the highest dice scores. In this training step we use a range of thresholds for each bundle and we select the one which gives the best result, using TractSeg bundles as reference tracts. The mean values with their standard deviations are reported in the second and third column of Table 8.4.

The ideal condition would be to obtain a threshold whose standard deviation is as small as possible and that gives a high dice score. In this way, applying the threshold to the test subjects, we would be sure to obtain bundles with good values, close to the ones of the training. On the contrary, a high standard deviation in the training threshold would not guarantee to obtain a good result in the test process. A high dispersion means that the threshold may perfectly fit for some subjects but may be inadequate for others.

We expect thus to find similar test dice scores to the ones of the training for thresholds with small standard deviations. Likewise, we expect to find worst mean dice scores in test subjects whose threshold has a high standard deviation.

Results			
Tract	Training Threshold	Training Dice	Test Dice
AF	0.95 ± 0.02	0.79 ± 0.04	0.77 ± 0.03
ATR	0.92 ± 0.02	0.82 ± 0.03	0.82 ± 0.02
CG	0.96 ± 0.01	0.77 ± 0.04	0.75 ± 0.05
CST	0.87 ± 0.04	0.75 ± 0.06	0.75 ± 0.04
FPT	0.64 ± 0.03	0.63 ± 0.05	0.61 ± 0.08
ICP	0.81 ± 0.03	0.73 ± 0.05	0.65 ± 0.13
ILF	0.85 ± 0.05	0.67 ± 0.12	0.64 ± 0.07
SLF I	0.99 ± 0.01	0.75 ± 0.04	0.73 ± 0.08
SLF II	0.94 ± 0.04	0.73 ± 0.06	0.69 ± 0.09
SLF III	0.97 ± 0.06	0.72 ± 0.09	0.72 ± 0.08

Table 8.4: Mean and standard deviation for threshold and dice score of the training and test set

As we can see from the results table, for example, the high dispersion of the standard deviation in SLF III threshold leads to even higher dispersion in dice values, with average training dice of 0,79 that can reach peaks of 0,81 as well as bad results as 0,61. The result is quite the same for test subjects. On the contrary, small threshold standard deviations and good dice scores allow the achievement of good results, like in ATR, where the mean dice score ranges from 0.79 to 0,85 for the training set and from 0,80 to 0,84 for the test set. There are then surprisingly results as ICP, in which the standard deviation of the training threshold is slower than other tracts but lead to worst test dice score standard deviations, making the mean dice value to jump from terrible results (0,52) to acceptable ones (0,78). And even more interesting is the small training threshold standard deviation of SLF I, which leads to very high dispersion in test dice scores. This is due to the fact that, when writing the anatomical definitions, a lot of cortical and subcortical parcellations were missing, forcing us to use different structures that sometimes weakened the definitions. Especially for these tracts, the use of a single threshold is counterproductive and may produce good results as well as unacceptable ones. The generalization process of using an individual threshold value can thus be achieved for those tracts for which they exists the needed parcellations or good alternatives of them, that is for AF, ATR, CG and CST. For the others, we should use a range of thresholds and then visually check the results to choose the best output, or integrate the parcellation atlas with new segmented structures.

Given the fuzzy spaces, finding the best threshold, calculating the dice score and extracting the 10 tracts from a tractogram takes approximately 10 minutes per training set subject. The segmentation process for test subjects takes instead 90 seconds per subject when only one threshold values is used.

8.3 Fuzzy vs WMQL

We used WMQL to segment the same 10 bundles, exploiting their definitions, for the 20 test subjects. We computed the mean and the standard deviation of the dice score. We then compared the results with the ones obtained with our method, using a single threshold, and listed them in Table 8.5.

Dice score		
Tract	Our Dice	WMQL Dice
AF	0.77 ± 0.03	/
ATR	0.82 ± 0.02	0.38 ± 0.04
CG	0.75 ± 0.05	0.50 ± 0.06
CST	0.75 ± 0.04	0.36 ± 0.04
FPT	0.61 ± 0.08	/
ICP	0.65 ± 0.13	/
ILF	0.64 ± 0.07	0.75 ± 0.06
SLF I	0.73 ± 0.08	0.38 ± 0.06
SLF II	0.69 ± 0.09	0.51 ± 0.06
SLF III	0.72 ± 0.08	0.30 ± 0.07

Table 8.5: Disce scores obtained using our method and WMQL

In WMQL, FPT and ICP definitions were not provided, thus their segmentation has not been taken in consideration. The AF have not been segmented since WMQL definition relies on computation of other tracts that, in our turn, we do not have segmented yet. For all other bundles, our method seems to give better results than WMQL, except for ILF segmentation, in which WMQL has better outputs. Visually checking the extracted bundle, however, we have noticed that WMQL actually provides better results also for CG and sometimes also for CST. The so low dice score is due to the fact that WMQL approach extracts bundles which are very noisy and contains much more streamlines that should not be present, with respect to the reference TractSeg model (Figure 8.2. The CG global shape is however more complete than in our model. Furthermore, in the reference model of CST, there is one long extremity which is missing and dramatically lowers the WMQL dice score. The CST extracted with WMQL is sometimes better than ours, other times it is worst: the only way is to visually check the result.

In conclusion, our model gives better outputs than WMQL in case of ATR, SLF I, SLF II and SLF III. It is worst when extracting CG and ILF. Instead, CST is a borderline case for which, depending on the subject, one methods overcomes the other. No data were provided by WMQL for FPT and ICP, possibly for the difficulties in creating their definition. AF was not segmented since it relied on other tracts that we do not have segmented yet.

One important issue is that WMQL was consuming too many computer resources when trying to extract the bundles and the use of our cluster was needed. On the contrary, our method for fibers extraction was not affected by this problem.

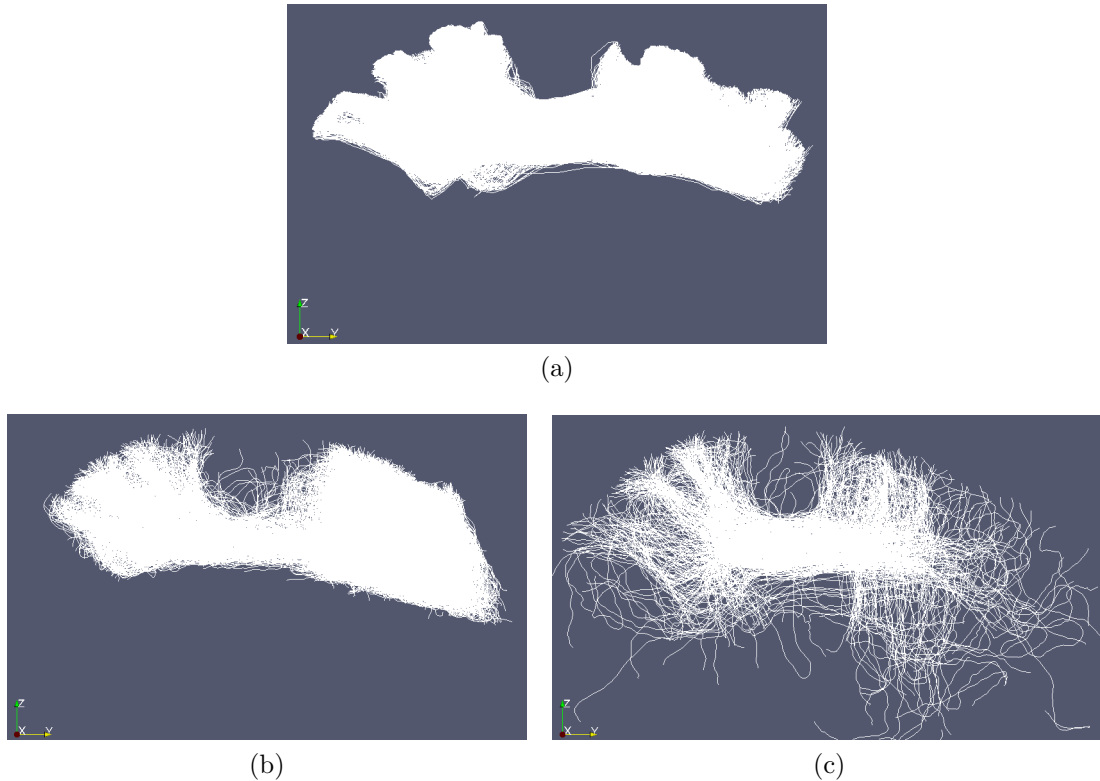


Figure 8.2: Left SLF I in TractSeg reference bundle (a), extracted with our method (b) and using WMQL (c).

8.4 Future developments

As we have seen, the convex hull approach used for dice score computation does not account for concavities in binary masks. Even if we added specific spatial relations in tracts definitions to be sure that no streamline was present in that concavities and that the dice score error was minimized, a different solution for dice calculation can provide more precise results. A future improvement will be to create a “concave” hull method, able to generate 3D meshes for both the reference and the extracted tracts and to compute the union and the intersection of the two meshes.

Another future development will be to create an interactive tool that allows an user to visually choose the desired result. We would like to load in a visualization window the tractogram where, to each streamline, it is associated the corresponding fuzzy value of the current definition, and to use a slider to progressively eliminate fibers with low degree of membership, until reaching the desired output. The elimination results should be visible in real-time when moving the slider.

Finally, since if we consider the whole process almost the entire time consumption is given by the fuzzy spaces generation, and given that different definitions sometimes share one or more common relations, an improvement would be to first compute all the relations and then to assemble them in the wanted definitions. In this ways, if one relation is repeated multiple times among different tracts definitions, its fuzzy space is computed only once, instead of a number of times equal to the number of its repetitions.

8.5 Conclusions

We saw that, nowadays, the most used segmentation technique is manual segmentation. However, it is a very slow approach and it is non-exploitable for datasets which contain a big amount of subjects. The development of supervised learning methods improved accuracy, but their slowness and the fact that they usually rely on hyperparameters that do not have anatomical meaning, makes their use to be difficult by medical personnel. A very interesting approach was introduced by WMQL with the purpose of using a near-to-english language to establish spatial relations between cortical and subcortical structures, as well as between different tracts, to extract the wanted bundles. This technique creates however fixed bounding boxes that dramatically limit segmentation accuracy, since tracts definitions are usually inaccurate.

We developed a novel approach, based on fuzzy sets theory, with the aim to improve accuracy extraction by modeling the intrinsic vagueness common to every tract definition. We combined cortical and subcortical parcellations to create spatial relationships useful to tract segmentation. The relations were merged in anatomical definitions. We then generated the corresponding fuzzy spaces, whose regions with the highest membership degrees were the ones crossed by the wanted bundle, and applied them to subjects tractograms. We extracted the desired tract according to a threshold that was previously fixed following the results of a training process. However, the lack of some important brain parcellations made the use of a single threshold to be counterproductive for some tracts and multiple thresholds were used for certain bundles. Tracts segmentation is thus reproducible, but the generalization that aims to use a single threshold lowers the segmentation accuracy and, as just said, for certain tract the use of more than one threshold is suitable.

We also merged the tracts into a single model to give a global representation and represented them as 3D cylinders to have a more real model. A 3DSlicer plug-in was also implemented to convert file format in an extension readable by common 3D creation softwares like Blender. The latter can be used for example to visualize and give transparency to some tracts, in order to study their relationship with the surrounding bundles or with a potential lesion (that can be for example manually segmented and added to the model).

We saw that our method provides better results than WMQL for 4 (ATR, SLF I, SLF II, SLF III) of the 10 tracts, while it is worst for 2 bundles (CG, ILF) and no comparison has been possible for other 3 tracts (AF, FPT, ICP). The remaining tract, CST, is a borderline case which sometimes is better segmented using our method, sometimes using WMQL approach. The creation of our novel approach makes it possible to use the two methods in a complementary way, so that one can be used instead of the other when one of two fails. It is still valid the fact that WMQL creates fixed bounding boxes whose result cannot be changed, while we can always improve our result choosing another threshold or finding better anatomical definitions. Moreover, WMQL produced memory errors that we did not find using our approach.

The power of our novel approach comes also from the fact that all algorithms have been optimized to reduce resources and time consumption, so that the anatomical definitions evaluation and the and the tracts segmentation can be performed on everyday computers. In particular, once the fuzzy spaces have been evaluated, the segmentation is performed in a really small time. Using one single threshold, the segmentation of 10 tracts for a single subjects takes only 90 seconds. All steps, from fuzzy spaces generation, to training, to tracts extraction and dice computation can be performed on an ordinary machine. The whole process, for a single subject, takes on average 1 hour.

Bibliography

- [1] J. Topping, “Investigations on the theory of the brownian movement,” *Physics Bulletin*, vol. 7, pp. 281–281, 10 1956.
- [2] D. L. Bihan, “The ‘wet mind’: water and functional neuroimaging,” *Physics in Medicine and Biology*, vol. 52, pp. R57–R90, mar 2007.
- [3] P. Mukherjee, J. Berman, S. Chung, C. Hess, and R. Henry, “Diffusion tensor mr imaging and fiber tractography: Theoretic underpinnings,” *American Journal of Neuroradiology*, vol. 29, no. 4, pp. 632–641, 2008.
- [4] E. Stejskal and J. Tanner, “Spin diffusion measurements: Spin echoes in the presence of a time-dependent field gradient,” *JCP*, vol. 42, pp. 288–292, 01 1965.
- [5] O. Dietrich, A. Biffar, A. Baur-Melnyk, and M. Reiser, “Technical aspects of mr diffusion imaging of the body,” *European Journal of Radiology*, vol. 76, no. 3, pp. 314–322, 2010.
- [6] S. Mori and J. Zhang, “Principles of diffusion tensor imaging and its applications to basic neuroscience research,” *Neuron*, vol. 51, pp. 527–39, 10 2006.
- [7] T. Huisman, “Diffusion-weighted and diffusion tensor imaging of the brain, made easy,” *Cancer imaging : the official publication of the International Cancer Imaging Society*, vol. 10 Spec no A, pp. S163–71, 10 2010.
- [8] P. W. Schaefer, P. E. Grant, and R. G. Gonzalez, “Diffusion-weighted mr imaging of the brain,” *Radiology*, vol. 217, pp. 331–345, 11 2000.
- [9] P. Marcon, K. Bartusek, and M. Cap, “Measurement of dwi and dti images of isotropic and anisotropic materials by using nmr methods,” *Progress in Electromagnetics Research Symposium*, 01 2012.
- [10] P. Mukherjee, J. Berman, S. Chung, C. Hess, and R. Henry, “Diffusion tensor mr imaging and fiber tractography: Theoretic underpinnings,” *American Journal of Neuroradiology*, vol. 29, no. 4, pp. 632–641, 2008.
- [11] B. J. Jellison, A. S. Field, J. Medow, M. Lazar, M. S. Salamat, and A. L. Alexander, “Diffusion tensor imaging of cerebral white matter: A pictorial review of physics, fiber tract anatomy, and tumor imaging patterns,” *American Journal of Neuroradiology*, vol. 25, no. 3, pp. 356–369, 2004.

- [12] S. Mori, “Chapter 9 - three-dimensional tract reconstruction,” in *Introduction to Diffusion Tensor Imaging* (S. Mori, ed.), pp. 93 – 123, Amsterdam: Elsevier Science B.V., 2007.
- [13] S. Mori and J.-D. Tournier, “Introduction to diffusion tensor imaging: And higher order models: Second edition,” *Introduction to Diffusion Tensor Imaging: And Higher Order Models: Second Edition*, pp. 1–126, 09 2013.
- [14] P. Macey, M. Thomas, and L. Henderson, “Dti-based upper limit of voxel free water fraction,” *Heliyon*, vol. 4, p. e00700, 07 2018.
- [15] B. Jeurissen, A. Leemans, J.-D. Tournier, D. Jones, and J. Sijbers, “Investigating the prevalence of complex fiber configurations in white matter tissue with diffusion mri,” *Human brain mapping*, vol. 34, p. 2747–2766, 11 2013.
- [16] J.-D. Tournier, F. Calamante, D. Gadian, and A. Connelly, “Direct estimation of the fiber orientation density function from diffusion-weighted mri data using spherical deconvolution,” *NeuroImage*, vol. 23, pp. 1176–85, 12 2004.
- [17] J.-D. Tournier, F. Calamante, and A. Connelly, “Robust determination of the fibre orientation distribution in diffusion mri: Non-negativity constrained super-resolved spherical deconvolution,” *NeuroImage*, vol. 35, pp. 1459–72, 06 2007.
- [18] D. Essen, K. Ugurbil, E. Auerbach, D. Barch, T. Behrens, R. Bucholz, A. Chang, L. Chen, M. Corbetta, S. Curtiss, S. Della Penna, D. Feinberg, M. Glasser, N. Harel, A. Heath, L. Larson-Prior, D. Marcus, G. Michalareas, S. Moeller, and E. Yacoub, “The human connectome project: A data acquisition perspective,” *NeuroImage*, vol. 62, pp. 2222–31, 02 2012.
- [19] K. Ugurbil, J. Xu, E. Auerbach, S. Moeller, A. Vu, J. Duarte-Carvajalino, C. Lenglet, X. Wu, S. Schmitter, P.-F. Van de Moortele, J. Strupp, G. Sapiro, F. De Martino, D. Wang, N. Harel, M. Garwood, L. Chen, D. Feinberg, S. Smith, and E. Yacoub, “Pushing spatial and temporal resolution for functional and diffusion mri in the human connectome project,” *NeuroImage*, vol. 80, 05 2013.
- [20] D. Van Essen, S. Smith, D. Barch, T. Behrens, E. Yacoub, and K. Ugurbil, “The wu-minn human connectome project: an overview,” *NeuroImage*, vol. 80, 05 2013.
- [21] V. Nath, C. Hansen, P. Parvathaneni, J. Blaber, Y. Gao, P. Neher, D. B. Aydogan, Y. Shi, M. Ocampo-Pineda, S. Schiavi, A. Daducci, G. Girard, M. Baraković, J. Rafael-Patino, D. Romascano, G. Rensonnet, M. Pizzolato, A. Bates, and B. Landman, “Limits to anatomical accuracy of diffusion tractography using modern approaches,” *NeuroImage*, vol. 185, 10 2018.
- [22] B. Kreilkamp, B. Weber, M. Richardson, and S. Keller, “Automated tractography in patients with temporal lobe epilepsy using tracts constrained by underlying anatomy (tracula),” *NeuroImage: Clinical*, vol. 14, 01 2017.

- [23] A. Voineskos, N. Lobaugh, S. Bouix, T. Rajji, D. Miranda, J. Kennedy, B. Mul-sant, B. Pollock, and M. Shenton, “Diffusion tensor tractography findings in schizophrenia across the adult lifespan,” *Brain : a journal of neurology*, vol. 133, pp. 1494–504, 03 2010.
- [24] J. Fitzsimmons, M. Kubicki, K. Smith, G. Bushell, R. Estepar, C.-F. Westin, P. Nestor, M. Niznikiewicz, R. Kikinis, R. McCarley, and M. Shenton, “Dif-fusion tractography of the fornix in schizophrenia,” *Schizophrenia research*, vol. 107, pp. 39–46, 12 2008.
- [25] C.-H. Wu, T.-J. Hwang, Y. Chen, Y. Hsu, Y. Lo, C.-M. Liu, H.-G. Hwu, C. Liu, H. Ming, Y.-L. Chien, C. Chen, and W.-Y. Tseng, “Altered integrity of the right arcuate fasciculus as a trait marker of schizophrenia: A sibling study using tractography-based analysis of the whole brain,” *Human Brain Mapping*, vol. 36, 11 2014.
- [26] S.-H. Lee, J.-P. Coutu, P. Wilkens, A. Yendiki, H. Rosas, and D. Salat, “Tract-based analysis of white matter degeneration in alzheimer’s disease,” *Neuro-science*, vol. 301, 05 2015.
- [27] M. Daiyanu, M. Mendez, V. Baboyan, Y. Jin, R. Melrose, E. Jimenez, and P. Thompson, “An advanced white matter tract analysis in frontotemporal dementia and early-onset alzheimer’s disease,” *Brain imaging and behavior*, vol. 10, 10 2015.
- [28] A. Bartsch, A. Biller, and G. Homola, *Presurgical Tractography Applications*, pp. 531–567. 12 2014.
- [29] L. O’Donnell, Y. Suter, L. Rigolo, P. Kahali, F. Zhang, I. Norton, A. Albi, O. Olubiyi, A. Meola, W. Essayed, P. Unadkat, P. Ciris, W. Wells, Y. Rathi, C.-F. Westin, and A. Golby, “Automated white matter fiber tract identification in patients with brain tumors,” *NeuroImage: Clinical*, vol. 13, 11 2016.
- [30] H. Zakaria, S. Haider, and I. Lee, “Automated whole brain tractography affects preoperative surgical decision making,” *Cureus*, vol. 9, 09 2017.
- [31] S. Wakana, A. Caprihan, and M. e. a. Panzenboeck, “Reproducibility of quan-titative tractography methods applied to cerebral white matter,” *NeuroImage*, vol. 36(3), pp. 630–644, 07 2007.
- [32] M. Catani and M. Thiebaut de Schotten, “A diffusion tensor imaging tractog-raphy atlas for virtual in vivo dissections,” *Cortex; a journal devoted to the study of the nervous system and behavior*, vol. 44, pp. 1105–32, 06 2008.
- [33] B. Fischl, “Freesurfer,” *NeuroImage*, vol. 62, pp. 774–781, 08 2012.
- [34] D. Wassermann, M. Nikos, Y. Rathi, M. Shenton, R. Kikinis, M. Kubicki, and C.-F. Westin, “The white matter query language: A novel approach for describ-ing human white matter anatomy,” *Brain Structure and Function*, vol. 221, 12 2015.

- [35] Z. Ding, J. C Gore, and A. Anderson, "Classification and quantification of neuronal fiber pathways using diffusion tensor mri," *Magnetic resonance in medicine : official journal of the Society of Magnetic Resonance in Medicine / Society of Magnetic Resonance in Medicine*, vol. 49, pp. 716–21, 04 2003.
- [36] L. O'Donnell, A. Golby, and C.-F. Westin, "Fiber clustering versus the parcellation-based connectome," *NeuroImage*, vol. 80, pp. 283–289, 04 2013.
- [37] L. e. a. O'Donnell, "A method for clustering white matter fiber tracts," *AJNR. American journal of neuroradiology*, vol. 27(5), pp. 1032–1036, 05 2006.
- [38] L. Jonasson, P. Hagmann, J. Thiran, and V. Wedeen, "Fiber tracts of high angular resolution diffusion mri are easily segmented with spectral clustering.," *Proceedings of 13th Annual Meeting ISMRM, Miami*, p. 1310, 2005.
- [39] I. Corouge, G. Gerig, and S. Gouttard, "Towards a shape model of white matter fiber bundles using diffusion tensor mri.," *2004 2nd IEEE International Symposium on Biomedical Imaging: Macro to Nano*, vol. 1, pp. 344–347, 04 2004.
- [40] S. Zhang and D. H. Laidlaw, "Dti fiber clustering and cross-subject cluster analysis," *The International Society for Magnetic Resonance in Medicine*, 2004.
- [41] L. O'Donnell and C.-F. Westin, "Automatic tractography segmentation using a high-dimensional white matter atlas," *IEEE transactions on medical imaging*, vol. 26, pp. 1562–75, 12 2007.
- [42] E. Visser, E. Nijhuis, J. Buitelaar, and M. P Zwiers, "Partition-based mass clustering of tractography streamlines," *NeuroImage*, vol. 54, pp. 303–12, 01 2011.
- [43] J. Wasserthal, P. Neher, and K. Maier-Hein, "Tractseg - fast and accurate white matter tract segmentation," *NeuroImage*, pp. 239–53, 05 2018.
- [44] O. Ronneberger, P. Fischer, and T. Brox, "U-net: Convolutional networks for biomedical image segmentation," *LNCS*, vol. 9351, pp. 234–241, 10 2015.
- [45] Y. Xia, U. Turken, S. L. Whitfield-Gabrieli, and J. D. Gabrieli, "Knowledge-based classification of neuronal fibers in entire brain," *Medical Image Computing and Computer-Assisted Intervention*, pp. 205–212, 2005.
- [46] I. Bloch, "Fuzzy relative position between objects in image processing: A morphological approach," *IEEE Trans. Pattern Anal. Mach. Intell.*, vol. 21, pp. 657–664, 07 1999.
- [47] I. Bloch and A. Ralescu, "Directional relative position between objects in image processing: A comparison between fuzzy approaches," *Pattern Recognition*, vol. 36, pp. 1563–1582, 07 2003.
- [48] I. Bloch, "Fuzzy spatial relationships for image processing and interpretation: A review," *Image and Vision Computing*, vol. 23, pp. 89–110, 02 2005.

- [49] A. Delmonte, “Segmentation of white matter tractograms using fuzzy spatial relations,” Master’s thesis, Politecnico di Torino, 2018.
- [50] A. Delmonte, C. Mercier, J. Pallud, I. Bloch, and P. Gori, “White matter multi-resolution segmentation using fuzzy set theory,” Ap 2019.
- [51] G. Theaud, J.-C. Houde, A. Boré, F. Rheault, F. Morency, and M. Descoteaux, “Tractoflow: A robust, efficient and reproducible diffusion mri pipeline leveraging nextflow & singularity,” *bioRxiv*, 2019.
- [52] E. Garyfallidis, M. Brett, M. Correia, G. Williams, and I. Nimmo-Smith, “Quickbundles, a method for tractography simplification,” *Frontiers in Neuroscience*, vol. 6, p. 175, 2012.
- [53] A. A. Taha and A. Hanbury, “Metrics for evaluating 3d medical image segmentation: analysis, selection, and tool,” *BMC Medical Imaging*, vol. 15, 2015.
- [54] F. Bernard, I. Zemmoura, A. Minassian, J.-M. Lemee, and P. Menei, “Anatomical variability of the arcuate fasciculus: a systematical review,” *Surgical and Radiologic Anatomy*, vol. 41, pp. 889–900, Aug 2019.
- [55] S. S. Idowu OE and A. K., “Morphometry, asymmetry and variations of the sylvian fissure and sulci bordering and within the pars triangularis and pars operculum: an autopsy study,” *Journal of Clinical and Diagnostic Research*, Nov 2014.
- [56] K. Medard, K. Fulbert, N. O. Dominique, S. M. Alban, P. Johann, and V. Stéphane, “Microanatomy of thalamic radiations,” *International Journal of Human Anatomy*, vol. 1, pp. 27–36, 2017.
- [57] S. H. Jang, “The corticospinal tract from the viewpoint of brain rehabilitation,” *Journal of Rehabilitation Medicine*, vol. 46, pp. 193–199, 2014.
- [58] O. Almasri, “An essay on the human corticospinal tract: History, development, anatomy, and connections,” *Neuroanatomy*, vol. 10, pp. 1–4, 01 2011.
- [59] U. Ture, M. Yasargil, A. Friedman, and O. Al-Mefty, “Fiber dissection technique: Lateral aspect of the brain,” *Neurosurgery*, vol. 47, pp. 417–26, 09 2000.
- [60] G. Herbet, I. Zemmoura, and H. Duffau, “Functional anatomy of the inferior longitudinal fasciculus: From historical reports to current hypotheses,” *Frontiers in Neuroanatomy*, vol. 12, p. 77, 2018.
- [61] Y. Wu, D. Sun, Y. Wang, Y. Wang, and S. Ou, “Segmentation of the cingulum bundle in the human brain: A new perspective based on dsi tractography and fiber dissection study,” *Frontiers in Neuroanatomy*, vol. 10, p. 84, 2016.
- [62] N. Makris, D. N. Kennedy, S. McInerney, A. G. Sorensen, R. Wang, J. Caviness, Verne S., and D. N. Pandya, “Segmentation of Subcomponents within the Superior Longitudinal Fascicle in Humans: A Quantitative, In Vivo, DT-MRI Study,” *Cerebral Cortex*, vol. 15, pp. 854–869, 12 2004.
- [63] J. E. Mendoza, *Spinocerebellar Tracts*, pp. 2357–2358. 2011.

- [64] A. Fedorov, R. Beichel, J. Kalpathy-Cramer, J. Finet, J.-C. Fillion-Robin, S. Pujol, C. Bauer, D. Jennings, F. Fennessy, M. Sonka, J. Buatti, S. Aylward, J. Miller, S. Pieper, and R. Kikinis, “3d slicer as an image computing platform for the quantitative imaging network,” *Magnetic resonance imaging*, vol. 30, pp. 1323–41, 07 2012.
- [65] E. Garyfallidis, *Towards an accurate brain tractography*. PhD thesis, 05 2012.